Neutronics and Photonics Design for CTR Blanket and Shields

M.A. Abdou

July 1973

UWFDM-67

FUSION TECHNOLOGY INSTITUTE

UNIVERSITY OF WISCONSIN

MADISON WISCONSIN

Neutronics and Photonics Design for CTR Blanket and Shields

M.A. Abdou

Fusion Technology Institute
University of Wisconsin
1500 Engineering Drive
Madison, WI 53706

http://fti.neep.wisc.edu

July 1973

UWFDM-67

Neutronics and Photonics Design for CTR Blankets and Shields

by

M. A. Abdou
and
C. W. Maynard

July 1973

FDM 67

Nuclear Engineering Department
University of Wisconsin
Madison, Wisconsin

Preface to FDM-66 and FDM-67

The contents of the FDM-66 and FDM-67 reports are parts of a Ph.D. thesis entitled, "Calculational Method for Nuclear Heating and Neutronics and Photonics Design for CTR Blankets and Shields" by M. A. Abdou under the supervision of Professor C. W. Maynard.

To facilitate the distribution of the FDM reports, the contents of the thesis is divided into two parts. FDM-66 contains Chapters 1, 2, and 3. These chapters deal with the calculational methods for nuclear heating and are self-contained. Chapters 4, 5, and 6 are the contents of FDM-67. Chapter 4 is an investigation of discrete-ordinates calculational models for fusion neutronics and photonics. Chapter 5 deals with the nuclear design of blanket and shield. The thesis conclusions and recommendations are given in Chapter 6.

Although each of the two FDM reports are self-contained, cross reference by chapter is frequently made. Therefore, the pages are numbered consecutively throughout the two reports. The list of references and table of contents are given, however, in each report.

Table of Contents

Chapter 4

Discrete-Ordinates Calculational Model For Fusion Neutronics and Photonics

4.1 Introduction

In neutronics and photonics analysis of fusion reactor blankets and shields the basic problem is calculation of "response" rates. A response rate generally takes the form

$$R = \int_{\vec{P}} \Sigma_R(\vec{P})\psi(\vec{P})d\vec{P} \qquad (4.1)$$

where $\Sigma_R(\vec{P})$ is the response function, $\psi(\vec{P})$ is the angular flux, and $\vec{P}$ represents a point in the phase space. The previous chapters were devoted to calculating Σ_R's of interest; namely, neutron and gamma kerma factors and group cross sections by reactions. An adequate calculational model for determination of ψ in the blanket and shield is investigated in this chapter.

The angular flux, ψ, is obtained from a solution of the Boltzman transport equation:

$$L\psi = S \qquad (4.2)$$

where L is the Boltzman operator and S is the external source. Since exact analytic solution to general transport theory problems is not possible a numerical solution of equation (4.2) with the concomittant necessity of introducing some approximations is the only way to predict neutron and photon transport. Currently, the most widely used techniques for solving the Boltzman equation are the Monte Carlo method for one-, two-, and three-dimensional and the Discrete-Ordinates method for one-, and two-dimensional problems. The choice between the two methods is governed largely by the geometry of the nuclear system. For one-dimensional problems, the discrete-ordinates method is preferred on the ground of low computational cost, for three-dimensional problems there is no

practical method other than Monte Carlo, and for two-dimensional problems each of the two methods has its own merits and drawbacks.

In this stage of fusion reactor design, the view is that steady-state fusion reactors will be either cylindrical or toroidal in geometry with some possible variations foreseen in practical designs of full-scale reactors. The cylinder is conceived to have a large height-to-diameter ratio with large plasma diameters anticipated. The toroidal geometry is expected to have a large aspect (major-to-minor diameter) ratio of about 3 for Tokamak-type devices and roughly 200 or greater for theta-pinch reactors with the major diameter so large that the curvature can be neglected in neutronics calculations. Full-scale reactors will employ feed pipes, divertors and several other necessary access regions. Therefore, a very accurate neutronics and photonics analysis of a full-scale reactor design wil have to be carried out eventually in three-dimensional geometry. From the neutronics point of view, the access regions built into fusion blankets and shields will have the effects of 1 - having regions of low nuclide density from which neutrons and photons can stream out of the system affecting the neutron economy, energy deposition and multiplication, and requiring shields somewhere near the outer ends of the ducts; and 2 - increasing parasitic absorption of neutrons by neutron collisions in the access regions walls. However, due to the lack of substantial detailed information about access regions at present, two- or three-dimensional transport calculations are not justified--at least for survey studies--in terms of the reliability and usefulness of the results obtained compared to the computing machine time consumed. Even as our knowledge deepens and expands and we become more sophisticated

in building necessary detailed complications into the design of the fusion systems, one-dimensional neutronics models will always be required in carrying out the first iteration in optimization studies and survey analysis. Therefore, a one-dimensional model is employed for transport calculations in the rest of this work. The calculations are essentially reactor model-independent. In other words, a stylized fusion reactor consisting of cylindrical annuli will be used; and the calculational results are considered to be applicable whether the cylinder is the center section of a mirror machine or is wrapped into a torus.

In fusion reactors with magnetic confinement schemes, the blankets and shields have unique chacteristics that are not frequently met in other areas of nuclear work. The fusion shell (blanker and shield) has a strong volumetric neutron source in vacuum on one end and a superconducting magnet cryogenically cooled at about 4°K on the other end. To reduce the heat load into the refrigeration system to a reasonable limit, the neutron and gamma fluxes must be attenuated by a factor of about 10^6. In addition, the neutrons are born as roughly a delta function in energy space and only at one end of the blanket and therefore the error in predicting the neutron flux in the first few mean free paths in the upper energy group propagates rapidly to lower energy groups and deeper regions of the blanket and shield. Therefore, CTR blankets and shields represent deep penetration problems which have the characteristics that low-order approximations will usually predict poor results. In the following, an attempt is made to find out the order of approximations adequate for predicting reasonably accurate neutronics and photonics results without excessive costs. The approximations studied here are source form and

geometry, anisotropy of scattering, angular quadrature and spatial mesh spacing for both neutrons and photons for the discrete-ordinates method.

Before proceeding to a discussion of results a few words about the nuclear data used in the calculations presented in this chapter is in order. Most of the investigation carried out in this chapter for assessing adequate approximations for flux determination was carried out before the ENDF/BIII data was available to the author. Therefore, most of the calculations presented in this chapter were carried out using ENDF/BII data. The neutron heating rates were also calculated using the kerma factors given in reference 7 because the MACK program discussed in the previous chapters was not developed at that time. While there is a change in the absolute magnitude of the parameters calculated here when ENDF/BIII data is used, e.g. Nb(n,2n), the relative magnitude of the results predicted by the various approximations do not change. Therefore, repeating these calculations would not change the conclusions derived here nor add anything new to our understanding of the problems investigated. Therefore, we present the results calculated from ENDF/B2 with a special note in each table to that effect. Results in tables given in this chapter without a note about the source of data are derived from ENDF/B3. All other calculations presented everywhere in this thesis except this chapter were carried out using ENDF/B3 data (unless otherwise indicated) with the partial group cross sections and neutron kerma factors generated with the MACK program.

4.2 Neutron Source Distribution

The nearly monoenergetic neutron source is essentially isotropic because the ions are nearly isotropically distributed; and so little of the available momentum of the products is needed to balance the initial momentum, that the neutrons would be virtually isotropic regardless of the ion distribution. The source intensity is proportional to the square of the ion density and to the cross section which in the temperature range of interest for practical applications is essentially linear in the temperature. The equations governing the spatial distribution of these quantities are the energy and particle conservations and Maxwell's equations. This system of coupled equations can only be solved numerically or by rather drastic simplifying assumptions. It has been shown [36] that plausible source spatial distributions take the form

$$S(r) = S_o\left[1 - \left(\frac{r}{r_p}\right)^{\alpha}\right]^{\beta} \qquad (4.3)$$

where α is two for slabs and cylinders and 5/2 for toroidal geometry and β is one for neo-classical and two for Bohm diffusion [37]. The radius r_p at which the ion density and neutron source become zero is fixed by a system of magnet windings which divert any ions beyond this radius out of the central reactor region. In any event, from the point of view of the neutron source r_p is a parameter.

Our interest here is to investigate the sensitivity of the neutronics results to the neutron source distribution and more specifically to the parameters α, β and r_p in equation 4.3. This problem represents one of several cases in which it is machine time consuming to carry out the survey or sensitivity study by direct transport calculations and other approaches should be followed if possible. One of these alternatives is

through the use of the adjoint which is the solution of the adjoint Boltzman equation:

$$L^*\psi^* = S^* \tag{4.4}$$

where L^* is the Boltzman operator and S^* is the adjoint source. The following relation is known to hold for appropriate choice of boundary conditions [25]

$$<\psi^*,S> = <\psi,S^*> \quad . \tag{4.5}$$

This equation represents another approach for calculating the response rate in equation 4.1 if S^* is chosen as the desired response function. Therefore, if the effect of changing the neutron source distribution on a particular result is required one needs only to evaluate the integral $<\psi^*,S>$ for each distribution S. This requires solving equation 4.4 with S^* as the response function of interest only once. However, we are interested here in finding out the sensitivity of several neutronics results, e.g. neutron energy deposition, helium and hydrogen production, tritium production, leakage, etc., to various forms of the source distribution. This requires a solution of the adjoint Boltzman equation for each response function. Therefore, such an approach can obviously be more expensive than the direct solution if the number of neutronics results of interest exceed the number of variations to be made in the source distribution. Since this is the case here another approach is discussed next. Incidentally, gamma energy deposition and leakage are the only two results of interest in photonics studies and therefore the use of the above method is very efficient in investigating the sensitivity of these results for changes in neutron flux spectra and gamma

production cross sections.

The most important neutronics results in CTR reactors are affected most by high energy neutrons. Almost all the (n,2n), helium and hydrogen production in all proposed structural CTR materials are induced by neutrons of energies above 8 MeV. As seen in the last chapter, this high energy range, 8 to 14 MeV contributes a large fraction of the neutron heating. In addition, about 85% of Li^7 tritium production is induced by neutrons above 8 MeV. This high energy range is also of great concern because neutrons in this energy range have the strangest deep penetration power and the most adverse effects on the cryogenic system and the radiation stability of the magnet. Furthermore, any error in determining the fluxes at such high energies propagates to lower energies. Due to the smoothness of the neutron cross sections at such high energies and for other reasons discussed in the previous chapter, six energy groups (the first six groups in table 3.4) are adequate for accurate spectrum determination in this range. Direct transport calculation with these six groups is relatively inexpensive and provides the most important information needed here. The calculations given below are based mostly on a standard fusion reactor blanket model adopted for benchmark and cross sections formed at the International Working Sessions on Fusion Reactor Technology held at Oak Ridge in June 1971 [42]. This standard blanket is shown schematically in figure 4.1.

Table 4.1 shows the influence of the neutron source distribution on helium and hydrogen production and atom displacement in the structural material, tritium production and atom displacement in the structural material, tritium production in Li^7, neutron heating, and leakage. The

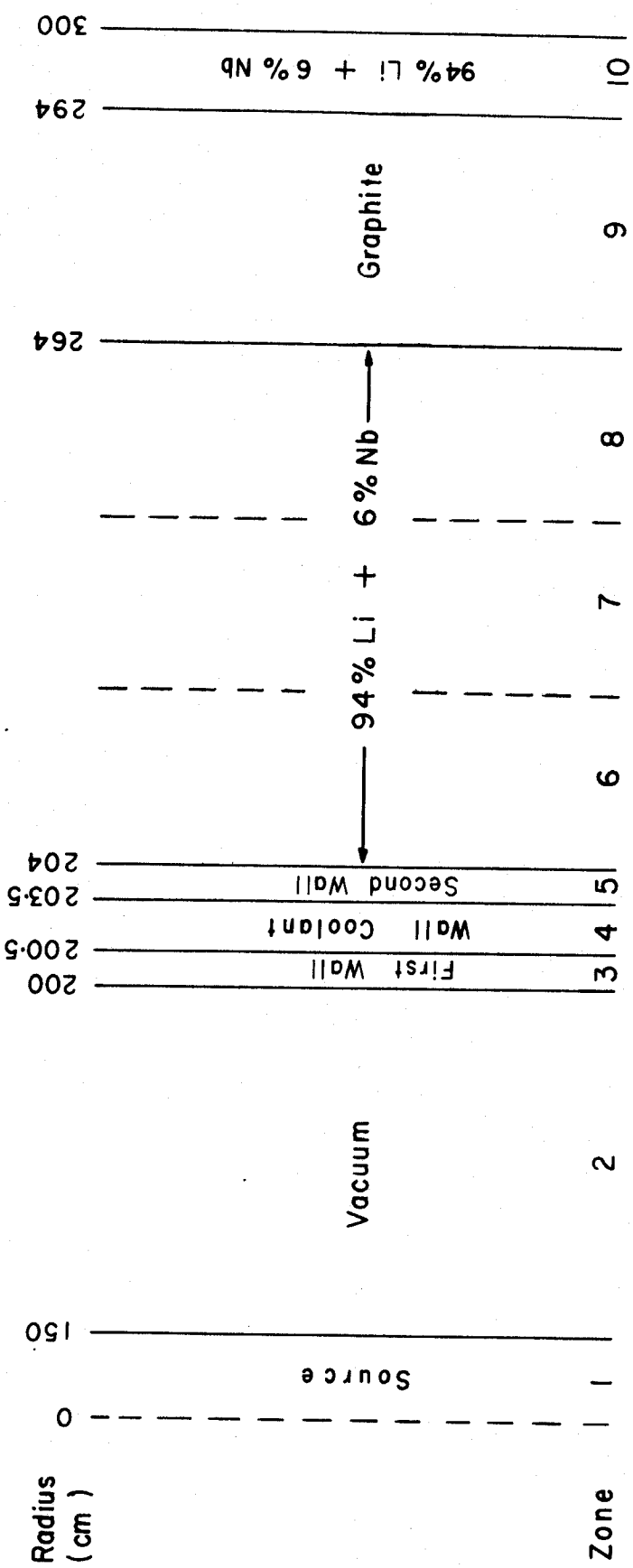

Figure 4·1 Schematic of Standard Blanket for Benchmark Calculation

results of table 4.1 show that the reaction rates in the inner regions are lowest for (parabolic)^2, higher for (parabolic), and highest for a uniform source distribution and the reverse is true in the outer regions. The results can be understood in terms of the fraction of source neutrons close to the cylinder axis and the direction of incidence on the first wall. Define χ as the angle between the projection of direction of neutron incidence on the first wall on a plane perpendicular to the cylinder axis and the normal to the first wall (see figure 4.2) at the surface of the first wall. The larger χ, the more interaction a neutron undergoes for the same distance along the direction perpendicular to the first wall. A line isotropic source represents the extreme case in which θ_i for all source neutrons is zero and hence the neutrons suffer fewer collisions in the first few regions and the fraction of neutrons above 8 MeV for an isotropic line source carried away from the inner regions of the blanket is higher than for any of the other three source distributions.

For the same source distribution, the average χ for the source neutrons increases as the ratio $\frac{r_p}{r_w}$ increases. Table 4.2 shows the effect of the plasma and wall radii. As expected from the above discussion, the larger the ratio $\frac{r_p}{r_w}$, the larger the reaction rates in the first few zones and the smaller the leakage.

The change in the reaction rates due to changing the source distribution is small and is generally within 1 to 2% for (parabolic)^2, parabolic, and uniform distributions. Since the thickness of the first wall is much less than one mean free path for neutrons of such high energy, the reaction rates in the first wall are generally more sensitive to

Table 4.1 Neutron Source Distribution Results for Cylindrical Geometry (S_{12} and P_3 approximations)

(Results normalized to unit neutron source)

Source Form	Zone	Volumetric (parabolic)^2	Volumetric parabolic	Volumetric uniform	Line isotropic
Niobium $(n,\alpha)\times10^4$	3	4.42	4.46	4.56	3.57
	5	3.01	3.04	3.09	2.77
	T[a]	15.01	15.07	15.20	14.40
Niobium $(n,p)\times10^3$	3	1.46	1.47	1.50	1.18
	5	1.01	1.01	1.03	0.93
	T[a]	5.07	5.09	5.13	4.77
Niobium Displacement (DPA/n. sec)$\times5\times10^{20}$	3	3.74	3.77	3.86	3.03
	5	2.62	2.64	2.69	2.40
Li^7 tritium production	4	0.062	0.062	0.064	0.054
	6	0.214	0.214	0.210	0.220
	7	0.085	0.084	0.082	0.093
	8	0.034	0.034	0.0327	0.039
	T[b]	0.395	0.395	0.394	0.404
Neutron Heating rate in watts$\times10^{14}$	3	0.81	0.81	0.83	0.65
	4	15.78	15.90	16.27	13.77
	5	0.55	0.56	0.57	0.51
	6	52.40	52.47	52.60	53.05
	7	19.82	19.60	19.19	22.01
	8	7.79	7.67	7.41	8.97
	T[b]	95.95	95.82	95.58	97.94
Right boundary Leakage$\times10^4$	T[c]	37.8	35.97	34.4	43.3

a - sum over all zones (for neutrons above 8 MeV)

b - sum over breeding zones (for neutrons above 8 MeV)

c - sum for outgoing neutrons above 8 MeV

This table based on ENDF/B II data

Table 4.2 Effect of Plasma and Wall Radii on Response Rates

(uniform source, S_{12},P_3)

(Results Normalized to a Unit Neutron Source)

Wall Radius r_w (meters) / Plasma Radius r_p (meters)	Zone	2 line source	2 0.1	2 1.5	8 7.5
Niobium (n,α) × 10^4	3	3.57	4.33	4.56	4.92
	5	2.77	2.95	3.09	3.24
	T[a]	14.1	14.8	15.2	15.6
Neutron Heating Rate in watts × 10^{14}	3	0.65	0.79	0.83	0.89
	4	13.77	15.45	16.27	17.28
	5	0.51	0.54	0.57	0.59
	T[b]	97.94	96.10	95.94	94.90
Leakage × 10^4	T[c]	43.3	38.3	34.4	28.2

a. sum over all zones (for neutrons above 8 MeV)

b. sum over breeding zones (for neutrons above 8 MeV)

c. sum for neutrons above 8 MeV (assuming no reflection)

This table based on ENDF/B II data

variations in the source form than all other regions. Table 4.1 also shows that Li^7 (n,n'α)t reaction is less sensitive than other reactions. The neutron leakage decreases by about 5% when the $(\text{parabolic})^2$ distribution is replaced with parabolic and about 9% when replaced by uniform neutron source distribution. Since the exact neutron source distribution is not well known it suffices to use a distribution source something resembling a parabola. However, in the rest of this work a uniform source distribution will be employed in order to save on spatial mesh.

4.3 Neutron Source Geometry Effects and Cylinder - Slab Comparison

As discussed above, cylindrical geometry is the best one-dimensional approximation to almost all proposed fusion reactor designs. As the plasma radii are large for most designs, the approximating of the cylindrical geometry by slab geometry has frequently been used [38, 39 & 40] in neutronics and photonics analysis. The CTR blanket, however, has a rather unique situation since the neutron source occupies the central vacuum section of the cylinder and is surrounded by a source free blanket. The first wall is particularly important from heat removal and radiation damage points of view. Since any variation in the geometry of the neutron source will produce its largest effect in the first wall region a great deal of care must be exercised in introducing any approximation about the source distribution and geometry. The effect of approximating the cylindrical by slab geometry on the neutronics and photonics results of the blanket is investigated next.

For cylindrical geometry, the angular flux of the fusion neutrons outside the plasma central section can be shown to have the form:

$$\psi(r,\xi,\chi) = \frac{Sa}{2\pi\sqrt{1-\xi^2}}\sqrt{1-\frac{r^2}{a^2}\sin\chi}$$

$$\text{for} \quad \sqrt{1-\frac{a^2}{r^2}} \leq \cos\chi \leq +1 \; ; \qquad (4.3.1)$$

$$\text{and} \quad = 0 \qquad \text{otherwise}$$

$$\text{where} \quad a < r < r_w \; .$$

The cylindrical coordinate system is shown in figure 4.2 and the cylinder axis is taken as the $\hat{z}$ axis. a is equal to the plasma radius, r_p, and S is the source strength for a uniform distribution. r is the projection of $\vec{r}$ on the plane normal to the $\hat{z}$ axis, ξ is equal to $\vec{\Omega}\cdot\hat{z}$.

$\vec{\Omega}$ is a unit vector in the direction of the neutron motion and χ is the angle between the planes formed by the $\vec{\Omega}$ and $\hat{z}$ vectors and by the $\hat{z}$ and $\hat{r}$ vectors. For convenience we define the parameter d_c for any region as the distance the neutron has to travel in this region if it makes no collision. Obviously, the larger the parameter d_c for a neutron entering a region the greater the probability of interacting the the neutron can undergo in the region. From equation 4.3.1 the angular flux at the vacuum face, r_w, of the first wall depends on r_w, r_p, ξ and χ. ψ and d_c for the first wall increase as ξ increases. For fixed ξ, d_c for neutrons entering the first blanket increases as χ increases. As the ratio $\frac{r_p}{r_w}$ gets smaller the maximum value of χ decreases and the reaction rates in the first wall become smaller as confirmed numerically in table 4.2. For an isotropic line source, χ is zero for all source neutrons. Hence, this source form produces smaller reaction rates and higher leakage for the first wall than other source distributions as was discussed in the last section.

ψ approaches infinity as ξ approaches one for all source distributions due to the assumption that the cylinder is infinite in the direction of its axis. Since ψ increases rapidly as ξ increases, the reaction rate in the first mean free path in the blanket is very sensitive to the order of angular quadrature when the discrete-ordinates method is used. In addition, continous angle-Monte Carlo and discrete-ordinates results are expected to agree only for high order S_n. For finite cylinders and high order S_n the singularity of ψ in the neighborhood of $\xi = 1$ is eliminated by neglecting the portion of the source neutrons that stream out of the vacuum region and do not enter the blanket. For toroidal geometry,

all source neutrons enter the blanket but due to the vacuum gap between the plasma and the first wall none of the neutrons enter the blanket with a direction tangential to the first wall. Removal of the strict one-dimensional singularity can be achieved by properly adjusting the angular distribution of the source.

In slab geometry, the neutron angular distribution is assumed to have azimuthal symmetry and the angular flux in the vacuum gap outside the plasma region has the form:

$$\begin{aligned} \psi(x,\mu) &= \frac{S\,a}{2\pi\mu_s} && \mu_s > 0 \\ &= 0 && \mu_s < 0 \\ &= \infty && \mu_s = 0 \quad ; \end{aligned} \tag{4.3.2}$$

where a is half the width of the plasma region, μ_s is the cosine of the angle between the neutron direction and the x axis which is perpendicular to the first wall. S is the number of neutrons emitted per unit volume per sec. in the plasma region for a uniform neutron source. It should be noted, however, that the angular dependence of the angular flux at the vacuum face of the first wall for slab geometry is independent of the spatial distribution of the neutron source, the plasma width and the size of the vacuum gap. A more important observation about the difference between slab and cylinder geometries for CTR blankets can be seen by comparing the angular distribution of the source neutrons at the first wall. In slab geometry, the angular flux increases as θ_s increases for any azimuthal angle. This means that the angular flux of the incident source neutrons in slab geometry is most peaked in the directions for

which the parameter d_c (defined above) is greatest. In cylindrical geometry, however, the case is different. The behavior of the angular flux is the same as in slab for the ξ dependence only. However, for fixed ξ, the angular flux decreases as χ increases. Furthermore, the angular flux is zero for χ greater than a limit shown in equation 4.3.1. In other words, for fixed ξ in cylindrical geometry, the angular flux of the source neutrons at the first wall is largest in the directions for which the parameter d_c is smallest. Hence, the number of interactions in the inner regions of the blanket is larger in slab than in cylindrical geometry. The higher the number of interactions in the inner blanket regions the lower the leakage from these regions and the smaller the number of neutron interactions in the outer region.

Table 4.3 shows the most important neutronics results for cylindrical and slab geometries for the standard blanket of figure 4.1. Table 4.3 shows that the slab representation overestimates all the neutronics results in the first wall by about 70%, and in the second wall by about 17%. As expected, the slab representation underestimates the neutronics results in the outer regions. The neutron leakage from the slab for neutrons above 8 MeV is 50% lower than the leakage from the cylindrical blanket. Table 4.3 also shows the results for an isotropic shell source in slab geometry. In the isotropic shell source, the number of neutrons entering the walls for which the parameter d_c is large is smaller than that for a volumetric source in slab geometry and larger than that for a uniformly distributed source in cylindrical geometry. The results for the isotropic shell source are closer to the cylindrical results, but the difference is still large enough to make it necessary to use cylin-

Table 4.3 Slab - Cylinder Comparison (Reference Design of Figure 4.1)

(S_8,P_3)

(Results normalized to a unit neutron source)

Geometry Source		Cylinder Volumetric Uniform	Slab Volumetric Uniform	Slab Shell Isotropic
Niobium $(n,\alpha) \times 10^4$	3	4.61	7.77	5.27
	5	3.14	3.68	3.32
	T[a]	15.28	18.4	16.02
Niobium $(n,p) \times 10^3$	3	1.52	2.56	1.74
	5	1.05	1.23	1.11
	T[a]	5.16	6.17	5.41
Niobium Displacement (DPA/n. sec) $\times 5 \times 10^{20}$	3	3.90	6.53	4.45
	5	2.73	3.20	2.89
Li^7 tritium production	4	0.065	.089	.071
	6	0.214	.193	.214
	7	0.081	.057	.074
	8	0.0325	.020	.028
	T[b]	0.393	.361	.387
Neutron Heating Rate in watts $\times 10^{14}$	3	0.84	1.41	0.96
	4	16.54	22.84	18.07
	5	0.52	0.68	0.61
	6	52.39	47.03	52.30
	7	19.04	13.18	17.30
	8	7.34	4.51	6.27
	T[b]	99.28	87.62	94.07
Leakage $\times 10^4$	T[c]	33.75	17.6	26.1

a - sum over all zones (for neutrons above 8 MeV)

b - sum over breeding zones (for neutrons above 8 MeV)

c - sum for outgoing neutrons above 8 MeV

ENDF/B II data used in obtaining these results

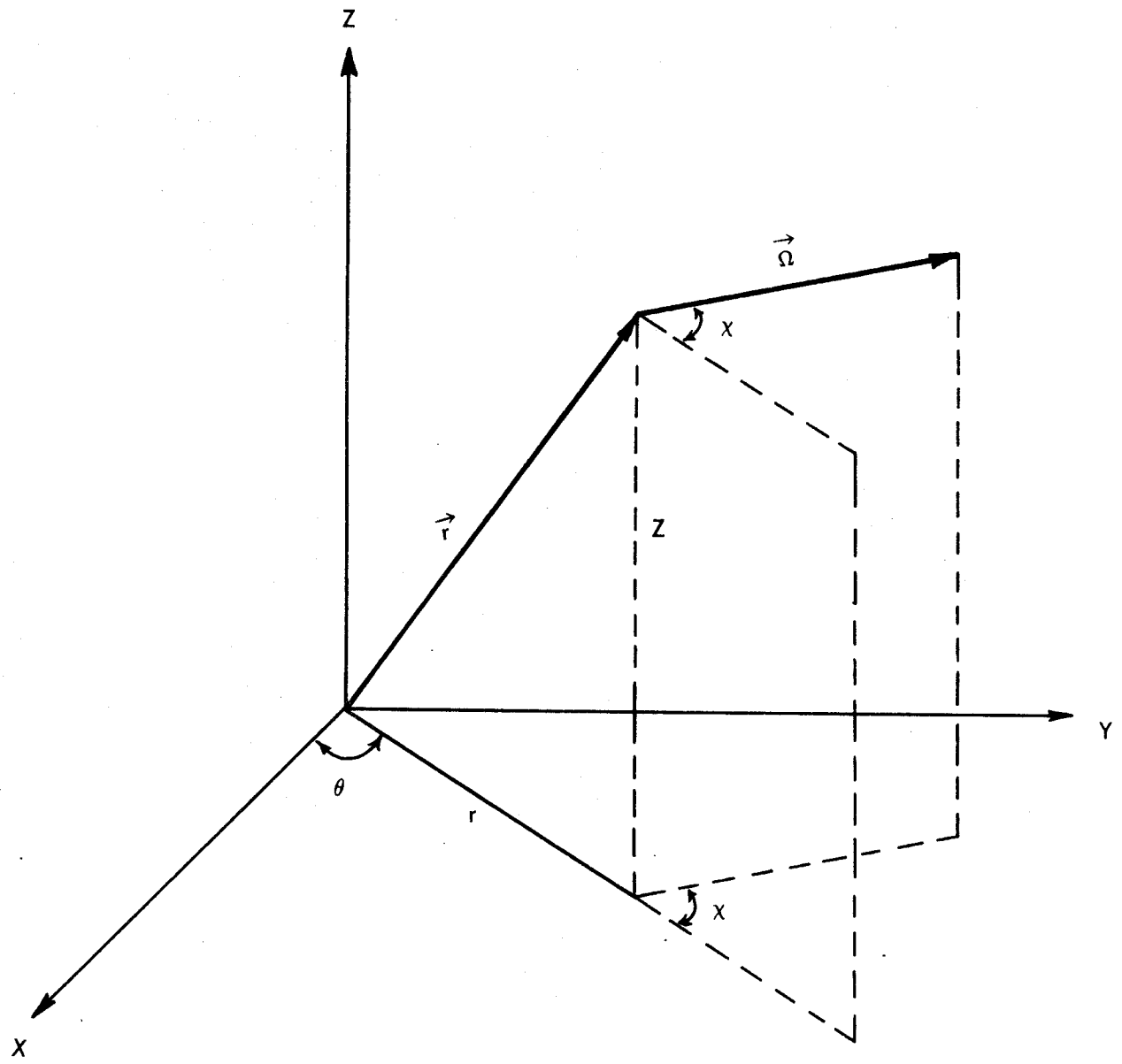

FIG. 4·2 Cylindrical Coordinate System

rical geometry.

Table 4.4 shows the effect of the slab approximation on the neutronics results for the entire energy range from zero to 14 MeV for both blanket and shield of the reference design discussed in the last chapter and shown schematically in figure 3.19. The results in this table are obtained using ENDF/B III data and the neutron kerma factors of the present work. The transport calculations were carried out with the S_4, P_3 approximations. As will be shown shortly the error in using the slab approximation increases with the order of the S_n approximation and hence the actual difference between the slab and cylinder results is much larger than that shown in table 4.4.

All reactions given by zone in table 4.4 are in units of reactions per one fusion neutron and hence the comparison between slab and cylinder includes also the 1/r effect (i.e. volume change with r per unit area normal to r) of the cylindrical geometry.

The results in table 4.4a show, as expected, that the difference between slab and cylinder neutronics results is generally smaller for the entire energy range zero to 14 MeV than for the 8 to 14 MeV range. The total tritium production from natural lithium is the least affected among the various neutronics results by changes in geometry. The Li^7 $(n,n'\alpha)t$ reaction is important in the high energy range and the cross section increases as the energy decreases from 15 down to about 8 MeV then decreases at lower energies. Therefore, the shift in the spectrum toward lower energies when the slab representation is used does not greatly affect the Li^7 $(n,n'\alpha)t$ reaction rate. Tritium production in Li^6 occurs mostly below about 2 MeV (i.e. below the threshold for the Li^7 $(n,n'\alpha)t$ reaction).

Table 4.4 Slab - Cylinder Comparison for Reference Design of Fig. 3.19

Table 4.4a - Geometry Effects on Response Rates (S_4,P_3)

(Results normalized to a unit neutron source)

Geometry source distribution	Zone	(A) Cylinder Uniform Vol.	(B) Slab Volumetric	% Difference $\frac{B-A}{A} \times 100$
Neutron Heating in MeV per fusion neutron	3	1.2759 (+5)	1.5691 (+5)	22.972
	4	6.2493 (+6)	6.6704 (+6)	6.738
	5	1.8745 (+6)	1.7504 (+6)	-6.620
	6	1.5469 (+6)	1.3972 (+6)	-9.677
	7	3.5603 (+5)	2.4804 (+5)	-30.332
	10	1.3948 (+4)	9.946 (+3)	-28.692
	14	5.6934 (+2)	2.868 (+2)	-49.626
	16	4.2807 (+0)	1.8186 (+0)	-57.516
Li^7 (n,n'α)t	4	3.5662 (-1)	3.7391 (-1)	4.848
	5	7.92 (-2)	6.5438 (-2)	-10.236
	6	4.7759 (-2)	3.5858 (-2)	-24.919
	T_7	4.8358 (-1)	4.7521 (-1)	-1.731
Li^6 (n,α)t	4	3.8974 (-1)	4.2456 (-1)	8.934
	5	1.8168 (-1)	1.8582 (-1)	2.279
	6	1.8787 (-1)	1.8454 (-1)	-1.773
	T_6	7.5929 (-1)	7.9492 (-1)	4.693
Nb (n,α)	3	9.4473 (-4)	1.1749 (-3)	24.363
Fe (n,α)	7	5.6426 (-3)	3.3974 (-3)	-37.387
B^{10}(n,α)	8	8.4946 (-2)	7.0127 (-2)	-17.445
B^{10}(n,α)	17	3.0526 (-7)	1.2419 (-7)	-59.317

Table 4.4 Slab - Cylinder Comparison for Reference Design of Fig. 3.19

Table 4.4b - Geometry Effects on Neutron Energy Leakage

(Results normalized to a unit neutron source)

	(A)	(B)	% Difference
Geometry source distribution	Cylinder Uniform Volumetric	Slab Volumetric	$\frac{B - A}{A} \times 100$
Zone	MeV per 1 fusion neutron	MeV per 1 fusion neutron	
2	14.208	14.208	0.0
3	11.208	10.879	-5.458
4	4.263	3.236	-24.091
5	2.662	1.888	-29.076
6	1.656	1.108	-33.092
7	6.202 (-2)	3.846 (-2)	-34.988
8	1.629 (-2)	9.188 (-3)	-43.597
9	4.336 (-3)	2.229 (-3)	-48.593
10	1.173 (-3)	5.516 (-4)	-52.975
11	3.215 (-4)	1.389 (-4)	-56.796
12	8.877 (-5)	3.537 (-5)	-60.155
13	2.458 (-5)	9.072 (-6)	-63.092
14	6.812 (-6)	2.334 (-6)	-65.737
15	1.886 (-6)	6.010 (-7)	-68.134
16	5.244 (-7)	1.558 (-7)	-70.290
17	1.630 (-7)	4.652 (-8)	-71.460

A neutron slowed down past 2 MeV in the lithium region does not have much chance other than getting absorbed in Li^6. Since the $Li^7(n,n'\alpha)t$ reaction rate does not change significantly the change in the $Li^6(n,\alpha)$ reaction is also relatively small.

Table 4.4a shows that the heating rate in the first wall is higher for slab than for cylindrical geometry by about 23% for the S_4 approximation. We will see shortly that this difference is sensitive to the order of the S_n quadrature and increases as higher S_n are used. The difference in the heating rate increases in the outer regions of the blanket and shield because of the dual effect of changes in the neutron spectrum and the 1/r effect in cylindrical geometry. While the energy deposition in the shield region may not be important from an energy recovery point of view, it is necessary to have a reasonable estimate of the heating rate in the shield regions for the purpose of designing an appropriate cooling system. The slab representation underestimates the neutron heating in the shield by about 50%.

Table 4.4b shows the energy leakage by zone for both slab and cylinder. The slab model consistently underestimates the energy leakage. The difference increases monotonically with distance from the first wall and the energy leakage to the cryogenic system is underestimated in the slab representation by more than 70%.

It is concluded, therefore, that cylindrical geometry should be used in one-dimensional CTR neutronics studies unless only the order of magnitude of the results is of interest.

4.4 Effects of Scattering Anisotropy

Since the D-T neutrons have high energies, anisotropy of the scattering has important effects on neutron transport. As is well known, the differential scattering cross section is usually approximated by a truncated Legendre polynomial expansion in the scattering angle,

$$\sigma(\mu_0) = \sum_{l=0}^{L} \sigma_l \, p_l(\mu_0) \qquad (4.4.1)$$

where μ_0 is the cosine of the scattering angle and L is chosen sufficiently large to adequately describe the anisotropy of the angular distribution. An adaquate value of L for CTR blankets is discussed next.

Table 4.5 shows the important neutronics results as a function of L for the standard blanket of figure 4.1. This series of calculations was carried out for the P_0 through the P_8 approximations for slab and cylindrical geometries. The results show that convergence is achieved by P_5. However, table 4.5 shows that results obtained using P_3 are adequate to better than 1% accuracy. The results also show that increasing the order of anisotropy retained in the scattering increases the streaming tendency and lowers the heating and reactions in the inner blanket regions.

Table 4.5 Neutron Scattering Anisotropy (order of P_n)

(cylindrical geometry, S_{16})

(Results normalized to a unit neutron source)

Scattering order	Zone	P_0	P_1	P_2	P_3	P_4	P_5
Niobium $(n,\alpha) \times 10^4$	3	6.015	4.568	4.558	4.548	4.549	4.540
	4	1.709	1.340	1.325	1.329	1.328	1.328
	5	3.836	3.137	3.068	3.085	3.080	3.082
	6	4.402	4.288	4.185	4.199	4.199	4.199
	7	1.000	1.459	1.481	1.469	1.472	1.472
	8	0.235	0.507	0.554	0.546	0.546	0.547
	T*	17.198	15.304	15.178	15.183	15.181	15.175
Li^7 tritium production $\times 10^2$	4	8.321	6.403	6.335	6.352	6.349	6.350
	6	22.948	21.967	21.441	21.517	21.514	21.517
	7	5.65	8.207	8.271	8.215	8.227	8.228
	8	1.399	3.087	3.323	3.284	3.285	3.286
	10	0.007	0.039	0.051	0.051	0.051	0.051
	T*	38.324	39.703	39.422	39.419	39.426	39.433
Neutron Heating in watts $\times 10^4$	3	1.099	0.834	0.832	0.830	0.830	0.828
	4	20.962	16.302	16.122	16.168	16.159	16.163
	5	0.704	0.575	0.562	0.565	0.564	0.565
	6	55.723	53.831	52.540	52.723	52.717	52.724
	7	13.162	19.157	19.376	19.230	19.261	19.264
	8	3.177	6.929	7.514	7.418	7.420	7.424
	9	0.628	2.010	2.500	2.491	2.484	2.485
	10	0.015	0.081	0.109	0.096	0.110	0.110
	T*	95.47	99.717	99.554	99.520	99.546	99.563
	GRP						
System Leakage $\times 10^4$	1	1.336	5.302	9.084	9.806	9.791	9.788
	2	0.720	5.557	9.174	9.462	9.426	9.429
	3	0.498	4.225	6.097	6.109	6.094	6.097
	4	0.488	3.421	4.307	4.270	4.267	4.268
	5	0.397	2.183	2.522	2.512	2.510	2.511
	6	0.428	1.973	2.224	2.222	2.221	2.221
	T[c]	3.866	22.661	33.408	34.381	34.308	34.315

* sum over all zones for neutrons above 8 MeV

c sum over outgoing neutrons of energies above 8 MeV

This table is based on ENDF/B II data.

4.5 Order of S_n Angular Quadrature

The next problem posed is the order required of the angular quadrature for the S_n method. It has been established [41] that the inherent approximations in the S_n method are adjustable such that these approximations do not materially affect the desired solution. Practical limitations, however, prohibit using the finest energy, spatial, and angular mesh. Since the number, M, of angles in one-dimensional cylindrical geometry is equal to $n(n + 4)/4$ where n is the order of the quadrature used and the computation (CPU) time increases linearly with the number of angles, the cost of computation increases roughly as n^2 for high order S_n. Therefore, it is highly desireable to find the smallest order of quadrature that provides the desired accuracy.

Table 4.6 shows the effect of the order of angular quadrature on the important neutronics results for the standard blanket of figure 4.1. The results are given for both slab and cylindrical geometry. A uniformly distributed volumetric source and the P_3 approximation were employed in both cases. The spatial mesh was chosen with a step size of $1/8\Sigma_t$ in all cases which is fine enough to essentially eliminate the effect of the spatial mesh on the accuracy of the results. The cylinder results in table 4.6 show that as the order of approximation is increased the flux anisotropy is treated more adequately and it becomes more forward peaked resulting in decreased reactions in the first zones. In the following discussion it is assumed that the S_{16} results represent the "exact results" and the accuracy of the lower order S_n is quoted relative to the S_{16} results. The results of S_4 overpredict the neutronics resuts in the first zone by about 7 to 10%, overestimates the neutron heating in the

Table 4.6 Order of S_n Approximation

(Results normalized to a unit neutron source)

Geometry / Order of S_n	Zone	Cylinder S_4	Cylinder S_8	Cylinder S_{12}	Cylinder S_{16}	Slab S_4	Slab S_8	Slab S_{16}
Niobiu $(n,\alpha)\times10^4$	3	4.819	4.609	4.567	4.548	6.148	7.771	8.178
	4	1.439	1.360	1.338	1.329	1.772	1.881	1.848
	5	3.320	3.141	3.096	3.085	3.931	3.682	3.547
	6	4.126	4.172	4.189	4.199	4.139	3.719	3.698
	7	1.351	1.454	1.466	1.469	0.970	0.992	0.991
	8	0.521	0.540	0.545	0.546	0.317	0.326	0.326
	T*	15.585	15.282	15.209	15.183	17.280	18.375	18.591
Niobium $(n,p)\times10^3$	3	1.590	1.519	1.505	1.499	2.029	2.556	2.687
	4	0.478	0.452	0.444	0.441	0.589	0.625	0.614
	5	1.109	1.049	1.034	1.030	1.315	1.233	1.188
	6	1.412	1.426	1.432	1.435	1.421	1.280	1.272
	7	0.480	0.516	0.520	0.521	0.350	0.356	0.356
	8	0.190	0.198	0.199	0.120	0.118	0.121	0.121
	T*	5.263	5.163	5.139	5.130	5.823	6.172	6.239
Niobium Displacement (dPa/n.sec)$\times5\times10^{20}$	3	4.081	3.899	3.862	3.845	5.204	6.528	6.855
	5	2.881	2.726	2.687	2.676	3.413	3.205	3.090
Li^7 tritium production $\times 10^2$	4	6.865	6.492	6.392	6.352	8.452	8.955	8.802
	6	21.206	21.389	21.468	21.517	21.435	19.352	19.235
	7	7.588	8.135	8.201	8.215	5.653	5.719	5.708
	8	3.124	3.248	3.277	3.284	1.983	2.026	2.022
	T*	38.837	39.314	39.389	39.419	37.551	36.079	35.795
Neutron Heating in watts $\times10^{14}$	3	0.879	0.841	0.833	0.830	1.122	1.415	1.489
	4	17.492	16.535	16.273	16.168	21.536	22.840	22.444
	5	0.608	0.576	0.567	0.565	0.720	0.675	0.650
	6	51.879	52.391	52.598	52.723	52.219	47.029	46.755
	7	17.726	19.036	19.197	19.230	12.963	13.187	13.165
	8	7.069	7.336	7.403	7.418	4.397	4.507	4.500
	9	2.508	2.453	2.483	2.491	1.351	1.348	1.347
	10	0.115	0.108	0.109	0.096	0.059	0.057	0.057
	T*	98.277	99.275	99.464	99.520	94.40	96.80	95.30
Leakage $\times10^4$	T[c]	36.919	33.752	34.258	34.381	18.012	17.604	17.575

* sum over all zones (for neutrons above 8 MeV)
c sum over outgoing neurtons above 8 MeV

This table is based on ENDF/B II data

last zone by more than 20%, and underestimates the neutron heating, tritium and charged particle productions in zones 6,7, and 8. S_8 provides better than 5% accuracy almost everywhere in the blanket. A 5% accuracy was also found to be obtainable with S_6 provided that an adequate spatial mesh is used.

As is well known, the accuracy of the discrete ordinate solution does not necessarily improve by increasing the order of angular quadrature alone or decreasing spatial mesh size alone. Studies were carried out in the present work as to adequate mesh spacing for a given angular quadrature and conformed to a rule that an adequate mesh for any region resulted if the steps were $1/\Sigma_t N$ where N is the order of S_n used and Σ_t is the largest total cross section in any group for the mixture in that region. Following this rule guarantees improvement of the accuracy of the solution as N is increased. It was also found that the calculations in groups corresponding to energies lower than a few KeV could be performed in lower approximations without degradation of the quality of the neutronics results. This is very convenient since Σ_t increases rapidly for most materials in this lower energy range and applying the above rule at such low energies would require a very fine spatial mesh.

Gamma Calculational Model

An adequate model for neutronics calculations was discussed above. A calculational model for photonics is investigated below.

The effects of scattering anisotropy was done in slab geometry for economy using S_{16}. Convergence is not greatly affected by geometry. The results of interest in photonics are energy deposition and leakage. The system employed for the calculations is that of figure 4.1. The boundary condition or albedo is reflecting in this series and a set of results in selected blanket regions for anisotropy through P_n with n from zero to seven is shown in Table 4.7. These results are converged by P_3. However in the problem studied here P_1 doesn't give bad results and one strongly suspects that a transport corrected P_0 would be satisfactory. However, the combination of an isotropic and distributed source cause very low order approximations to work well in this instance. Experience with other gamma flux problems indicates that a P_3 treatment would be prudent even though the above results would allow less. The last column in table 4.7 gives the P_7 results but with a void boundary condition. The only results that are affected in a major way are near the tight boundary as would be expected. Table 4.8 shows the same general results for a void at the right boundary in two lower order S_N calculations for both slab and cylindrical geometries. The S_6 slab results are within 1% of the S_{16} results and compare very favorably with the last column of the preceeding table indicating that S_6 is adequate as is P_3 anisotropy. However, the cylindrical and slab result differ enough even here to require the cylindrical model; further the S_4-P_0 results are inadequate with respect to the leakage and other results near the right boundary.

Table 4.7 Gamma Scattering Anisotropy Convergence

(21 energy groups, slab S_{16}, 1 photon/sec)

Order of P_n Zone	P_0	P_1	P_2	P_3	P_4	P_6	P_7	P_7[a]
3[b]	8.0597	7.9087	7.9432	7.9297	7.9342	7.9324	7.9316	7.9240
4	2.7702	2.7180	2.7297	2.7257	2.7271	2.7268	2.7267	2.7238
5	7.0977	6.9699	6.9960	6.9876	6.9902	6.9895	6.9894	6.9814
6	12.0342	11.874	11.8916	11.8923	11.8906	11.8917	11.8925	11.8686
7	6.0468	6.0767	6.0542	6.0656	6.0615	6.0626	6.0627	6.0245
8	3.0105	3.1059	3.0828	3.0894	3.0885	3.0886	3.0885	3.0184
9	2.5544	2.9073	2.8667	2.8695	2.8697	2.8695	2.8695	2.3770
10	0.2470	0.2868	0.2903	0.2884	0.2888	0.2886	0.2886	0.1398
Lc	1.1515	1.5254	1.5742	1.5648	1.5670	1.5665	1.5664	1.2543

a. All cases except this carried out with a reflecting boundary condition on the right, while here a void condition is used
b. Heating rates in niobium (zones 3 - 8 and 10) and graphite (zone 9) are in watts × 10^{15}
c. Right boundary positive current × 10^3

Table 4.8 Slab - Cylinder Comparison For Gamma Transport Calculation

Order of Approximation	S_6, P_3		S_4, P_0	
Zone/Geometry	Cylinder	Slab	Cylinder	Slab
3[a]	7.25828	7.80623	7.36158	7.83919
4 (Nb)	2.53098	2.69892	2.57156	2.71759
4 (Li)	0.73625	0.78866	0.760072	0.80484
5	6.58181	6.95842	6.69689	7.03164
10	2.73871	2.36319	2.46407	2.12604
L[b]	1.57105	1.25367	1.03650	0.81425

a. Heating rates in watts $\times 10^{15}$

b. Right boundary leakage $\times 10^{3}$

CHAPTER 5

NUCLEAR DESIGN OF BLANKET AND SHIELD

5.1 Introduction

In chapter two, theoretical and computational methods were developed for calculating fluence-to-kerma factors which are necessary for determining nuclear heating. With the MACK program developed, a library of multigroup kerma factors and group cross sections by reaction was generated, as described in chapter three, using weighting functions and a group structure appropriate for CTR systems. In chapter four, a discrete ordinates calculational model adequate for determination of the flux in fusion blankets and shields was investigated and the error in using the various approximations determined. With these developments, all response rates of interest in the blanket and shield can be calculated for any design and the neutronics and photonics analysis of the system becomes feasible. This chapter is devoted to an investigation of the neutronics and photonics design of the blanket and shield. Closely related aspects of the other areas of design are also examined.

In the following section, previous work in CTR neutronics is briefly summarized. In section 5.3, the nuclear data and computational methods used in deriving the results presented in this chapter are discussed. Section 5.4 defines the general requirements of the blanket and shield regions. The neutronics and photonics and related aspects of the design of the first wall, blanket, reflector, and shield are investigated in section 5.5. Based on the results of section 5.5, a complete blanket and shield design is proposed in section 5.6. Thesis summary and recommendations for future studies are given in the next chapter.

5.2 Previous Neutronics Work

A number of workers have studied the nuclear behavior of fusion reactor blankets. The work on fusion reactor problems had two marked stages. The early investigations by Impink [52], Homeyer [53] and Lontai [54] at the Massachusetts Institute of Technology in the early 1960's comprise the first stage of exploration. Later, more reliable data were available and better calculational methods for accurately predicting neutron and gamma transport, heat transfer, magnetic losses of circulating liquid metals across magnetic field, etc., were developed. This laid the basis for the second stage of deeper insight into the blanket problems. A good number of workers presented their efforts in several papers at the B.N.E.S. Conference [60-68] in 1969. A few other papers were also presented at the IAEA Fourth Plasma Physics and Controlled Nuclear Fusion [73] and at the International Working Session [74] at ORNL in June 1971. A more detailed literature survey can be found in reference 79.

Previous researchers were concerned mostly with the question of tritium breeding. The combined efforts of Impink [52] and Hameyer [53] evolved a blanket design consisting of: a - two cm. molybdenum first wall, b - 6.25 cm. flibe ($2LiF \cdot BeF_2$) coolant region, and c - a blanket region of 56 cm. consisting of 79% flibe plus 21% graphite. Tritium breeding ratios in the range 1.2 to 1.8 were deduced for this type of blanket and hence the feasibility of adequate tritium breeding was proved. Steiner [69] investigated two basic blanket designs in terms of tritium breeding and nuclear heating. The configuration of the two types is shown in figure 4.1. The first design employs lithium and the second employs flibe as the vacuum wall coolant; with lithium used to

cool the remainder of the blanket in both designs. Steiner showed that the tritium breeding ratio is adequate in both cases and is about 9% higher for the first than for the second design. He also showed that the heating rate in the first wall increases by about 50% when the first wall lithium coolant is replaced by flibe. Similar conclusions were reached by other workers using different calculational methods and alternative blanket configurations.

5.3 Nuclear Data and Computational Techniques

In the following, a brief documentation is given of the nuclear data and computer programs used in deriving the results presented shortly.

The basic quantities to be calculated in nuclear design are of the form of "response" rates. These require a knowledge of the flux and the response functions. Determination of the flux is performed by transport codes which require the following nuclear data: a - neutron multigroup cross sections, b - gamma multigroup cross sections, and c - gamma production cross sections. The response functions of interest here are: 1 - cross sections for the reactions of interest, e.g. (n,α), (n,p), (n,t), $(n,n'\alpha)$, ... etc., 2 - displacement cross sections, and 3 - neutron and gamma kerma factors.

The ANISN [11] computer program was employed in all neutron and photon transport calculations. Although the technique of using a coupled neutron-gamma transport calculation is efficient and convenient, some important information about gamma production is "practically lost" in this method. In addition coupled calculations complicate the severe problem of data storage on the computer. An alternative technique was employed. The neutron transport calculations were run first for the purpose of determining the neutron flux which was then stored on tape. This part of the calculation was performed with the appropriate routines from the ANISN program which was then overlayed and the program LINK was automatically brought into the machine. The program LINK was written by the author for the present work and it performs two tasks: 1 - Using the RESPONSE library described shortly and the flux stored from the

neutron transport calculations, LINK calculates all desired response rates such as tritium, helium, and hydrogen production, atom displacements, and neutron heating., 2 - After step 1 is completed the RESPONSE library was "Free'd" and the gamma production cross section file was assigned. The program LINK then calculates the gamma production source by energy group and spatial interval in ANISN Format (17*). Furthermore, the program performs some additional functions such as the calculation of the spatial distribution of the energy of the secondary gamma production by each material in the system. With the gamma production source (17*) stored, the program LINK is overlayed and ANISN is brought in again to perform the gamma transport calculations which is the final step in the calculations for a design. This approach has largely eliminated the problem of machine storage in addition to providing more necessary detailed information which could not have been obtained without considerable difficulty otherwise. The UNIVAC-1108 computer at Madison Academic Computing Center was used in all but a few of the series of calculations given in this chapter.

The neutron multigroup cross sections (transfer matrices) were obtained from the DLC-2D [31] data package. This data was generated from ENDF/B III with the SUPERTOG program [16] in the one-hundred group structure shown in table 3.4 using a 1/E weighting function. For the purpose of this work, this data was collapsed into the 46 group structure shown in table 5.1 using a typical blanket spectrum. The gamma multigroup cross sections were generated with the MUG program [8] in the 43 group structure shown in table 3.5.

The gamma production cross sections for H-1, Be-9, N-14, O-16, Na-23, Al-27, K, Fe, and Pb were generated from ENDF/B III with LAPHFOR [81] which is a revision of the program LAPHANO [82]. The resonance cross sections required by LAPHANO and LAPHFOR were calculated for Na-23 and Fe with the MACK program. Vanadium gamma production cross sections were also generated with LAPHFOR from a recent ORNL evaluation [27]. Photon production cross sections for Li-6, Li-7, Nb, and C-12 were obtained from data in reference 7 which were generated with the POPOP4 program [83,84]. It was shown in chapter 3 that these gamma production cross sections for Li-6, Li-7, Nb, and C-12 suffer from large uncertainties. For a blanket of 50 cm consisting of 95% natural lithium and 5% structure, the total energy of the gammas produced by lithium is roughly 30% of the total energy of photons produced in the blanket. The latter is only about one-third of the total gamma energy production produced in the 1 cm first wall, the 50 cm blanket, and the 20 cm stainless steel reflector region. Furthermore, the total gamma heating in such systems is about 30 to 40% of the total nuclear heating. Therefore, 20 to 30% error in the lithium gamma production data has the effect of changing the nuclear heating by only about 1 to 2%. This is fortunate since lithium is used in all the designs presented in this chapter. For systems employing niobium in the first wall, the error in the total nuclear heating due to a 20% error in the energy of gamma production by niobium is about 4 to 5%. However, the error in the nuclear heating in a niobium first wall is roughly the same as the error in the niobium secondary photon production. In a system consisting of a 1 cm. first wall, a 40 cm. blanket of 95% Li plus 5% structure, followed by 25 cm. reflecting region of graphite, the total energy of the secondary

photons produced by C-12 is only about 4% of that produced in the system. Hence, 20 to 30% uncertainty in the data for C-12 gamma production has little effect on the total nuclear heating in the system.

The fluence-to-kerma factors and group cross sections by reaction were generated for all materials from ENDF/B III with the MACK program as described in chapter 3. The derived data were then arranged in a library, called RESPONSE, which has a format convenient for use with existing transport codes. For each material, there is a "response" table in ANISN cross section table format. Each position in the response table corresponds to a specific response function, e.g. (n,2n) cross section, kerma factor for (n, charged particles) reaction type, total kerma factor, etc. The RESPONSE library has proved extremely useful in evaluating all the response rates of interest here. A brief description of the RESPONSE library is given in Appendix D. The library has been placed at the Radiation Shielding Information Center (RSIC) at ORNL for distribution.

Radiation damage to CTR materials, particularly the first wall, currently represents a major feasibility problem. Rates of charged particles production and atom displacement are the most important neutronics results since they constitute the basic input to radiation damage studies. Such results are presented and compared for the important CTR materials in the following sections. Helium, hydrogen and tritium productions are calculated with the (n,α), (n,n'α), (n,n'2α), (n,n'3α), (n,p), (n,n'p), (n,t) and (n,n't) cross sections obtained from the RESPONSE library discussed above. The displacement cross sections were also included in the RESPONSE library for the refractory metals and stainless steel. Some

comments on atom displacement and displacement cross sections are given below.

Among the effects of neutron irradiation on metals is the displacement of the material's atoms from their original lattice positions. The atomic displacements produce point defects which may cluster into defect loops and harden the materials. These point defects may also cluster and remain as voids resulting in swelling and an increase in creep rates. The number of atom displacements is a measure of the radiation-induced changes in the physical properties of materials [86,87]. The number of displacements per atom, dpa, is defined to be

$$\text{dpa} = \int \phi(E)\, \sigma_d(E) dE$$

where $\phi(E)$ is the neutron flux and $\sigma_d(E)$ is the displacement cross section at incident neutron energy E and is given by

$$\sigma_d(E) = \sum_i \sigma_i(E) \int_{E_d}^{T_{max}} P_i(E,T)\, \nu(T) dT$$

where $\sigma_i(E)$ is the cross section for reaction i at incident neutron energy E, $P_i(E,T)$ is the normalized probability that a reaction i induced by a neutron of energy E will produce a primary knock-on atom (PKA) of kinetic energy T. $\nu(T)$ is the number of displacements per PKA and is usually derived from theoretical models [85-90]. $\nu(T)$ is inversely proportional to E_d, where E_d is the effective displacement energy for the material. Accurate values of E_d are not known for most materials. Most of the displacement cross sections currently available in the literature include only elastic and inelastic scattering [85]. Doran [88] added the contribution of the (n,2n) and (n,γ) reactions in addition to elastic

and inelastic scattering for stainless steel and tantalum. His displacement cross sections [91] are used in this work. Almost all displacement cross sections currently available have an accuracy not better than 50% because of 1) the neglect of the contribution from important reactions such as (n,α) and (n,p), 2) employing several simplifying assumptions in the solution of the kinematics equations, and 3) large uncertainties in the parameters E_d and $\nu(T)$. Hence, all dpa values calculated in the following section have this uncertainty.

5.4 General Description and Requirements of Blanket and Shield

As mentioned earlier, reactors operating on the D-T cycle and using magnetic confinement are the type considered in this work. However, since about 50% of the neutrons produced in the D-D cycles are 14 MeV, most of the neutronics and photonics results derived here apply equally well, except for a normalization factor, to D-D reactors.

A schematic of a fusion reactor is shown in figure 5.1. The plasma is confined to a region of radius r_p by superconducting magnets cryogenically cooled to about 4°K. In a D-T reactor, 17.6 MeV of energy is released per fusion reaction in the form of an alpha particle and a neutron with average kinetic energies of 3.5 and 14.1 MeV, respectively. In systems utilizing magnetic confinement schemes, most of the alpha particles will be trapped by the magnetic field.. The plasma region, however, is nearly vacuum as far as the neutrons are concerned and they escape freely. These 14 MeV neutrons represent the source of recoverable energy in this power producing system. The neutrons therefore must be slowed down converting their kinetic energy into heat in a region surrounding the plasma. This region is called the blanket. Since tritium is not available in nature, at least a tritium atom per fusion reaction must be produced through nuclear reactions in the blanket. Lithium is the only material with adequate potential for tritium production and hence it must be present in one form or another in the blanket. Lithium is also a good neutron moderator and heat transfer coolant and therefore it can perform the three basic functions of neutron slowing down, transporting the heat generated in the blanket into the "conventional" part of the plant and tritium production. Being a liquid metal, lithium

flowing in a magnetic field of about 100 KG requires excessive pumping power unless the flow pattern is very carefully designed [92-94]. Employing flibe (LiF·BeF) as a coolant in a lithium moderator or as both coolant and moderator has also been proposed [6,7 & 11] because of the low electrical conductivity of this molten salt.

While lithium is excellent for tritium regeneration and heat removal, its moderating power below a few MeV is low and is roughly one-third of that for graphite. Therefore, it is desirable to use other materials such as graphite or stainless steel in the reflector region (see figure 5.1).

The first surface seen by the neutrons is subjected to severe radiation damage and heating from Bremsstrahlung, synchrotron, and neutron radiation and charged particles bombardment. The first wall material therefore must be radiation-resistant and have a low coefficient of expansion and high thermal conductivity. Some amount of structure is required in the blanket and is likely to be (but not necessarily so) of the same material as the first wall.

About 1000 KW of electric power is required to pump 1 KW of heat from 4°K to 300°K. Since the superconducting magnets are cryogenically cooled at about 4°K, it is extremely important to minimize energy deposition in the magnet. If only about .1% of the plant power output is to be spent for refrigeration requirements the 14 MeV neutrons must be attenuated in energy by a factor of 10^6. This factor is independent of (or at least insensitive to) the wall loading. Since the blanket region requirements are satisfied by roughly a factor of 10^2 attenuation an efficient shield has to be designed for the region between the blanket

and magnet.

The above discussion defines the general features and requirements of the blanket and shield region. In summary, the blanket and shield have three major functions: 1 - convert the kinetic energy of plasma neutrons into heat, 2 - breed tritium, and 3 - attenuate the neutrons to the permissible levels imposed by the magnet refrigeration system. A full-scale design of a fusion reactor system is a complex process involving a number of physics and engineering disciplines. The design is usually confronted with wide variety of conflicting requirements and therefore involves necessarily the familiar trade-offs between the various requirements. However, in the selection of reactor materials and design of the blanket and shield several stringent requirements must be carefully considered in addition to the three major functions discussed above. Among these requirements are

1 - low induced radioactivity and afterheat,

2 - minimum potential hazards to the public,

3 - reactor components, particularly the first wall, must have acceptable life under the severe radiation damage expected from high wall loadings dictated by economics considerations.

4 - compatibility of the various materials employed

5 - low cost per unit power output (relatively inexpensive materials, small inner magnet radius, modest maintainance requirements, etc.)

With the basic requirements to be satisfied in the blanket and shield design defined above we can now proceed to investigate the neutronics and photonics aspects of the nuclear design.

5.5 Neutronics and Photonics Design of Blanket and Shield

5.5.1 Introduction

This section is concerned with the nuclear design of the blanket and shield, and is organized into four parts: first wall and structural materials, main blanket region, reflector, and shield. For each region, a series of designs is investigated using the calculational techniques and nuclear data described earlier in section 5.3. It is helpful at this point to discuss and define some of the quantities and parameters used repeatedly in this section. Some of these were used previously in the literature, but the exact meaning of each parameter was not the same in all works.

The results presented here are based on one-dimensional cylindrical geometry. Hence, they are independent of the reactor type. However, the reactor is assumed to operate on the D-T cycle and utilizes a magnetic confinement scheme. The results are also not affected by plasma parameters except for a slight dependence on the plasma radius, r_p, and the first wall radius, r_w, as discussed below.

A quantity of importance in fusion reactors is the neutron wall loading. The neutron wall loading is defined as the total energy of the plasma neutrons transported into the first wall per unit time per unit surface area of the wall. Mathematically, the neutron wall loading, W_n, is defined as

$$W_n = E_0 J_{nw} \tag{5.1}$$

where E_0 is the average energy of fusion neutrons (= 14.06 MeV for D-T) and J_{nw} is the source neutron current to the first wall. A neutron

wall loading of 1 MW/m^2 corresponds to a neutron current of 4.43×10^{13} neutrons/cm^2 sec to the first wall. A similar quantity, W_r, can be defined for charged particles and radiation to the first wall. The total wall loading, W_T, is then

$$W_T = W_n + W_r \tag{5.2}$$

The neutrons undergo a variety of endothermic and exothermic reactions in the first wall and blanket. Hence, the recoverable energy, designated as E_{eff}, which is deposited in the first wall, blanket, and reflector may be greater or smaller than E_0. An effective Q-value for the system, designated as Q_b, is defined by the relation

$$E_{eff} = E_0 + Q_b \tag{5.3}$$

The total energy per unit time (i.e. power, P_{system}) produced in the system is then given by

$$P_{system} = [\ W_r + W_n(1 + Q_{eff}/E_0)\ ] \cdot A_w \tag{5.4}$$

where A_w is the total surface area of the first wall. An effective wall loading, W_{eff}, can also be defined as

$$W_{eff} = P_{system}/A_w \tag{5.5}$$

The fusion neutron current to the first wall, J_{nw}, is simply related to the plasma parameters. J_{nw} times A_w is equal to the total number, S'_{np}, of neutrons produced by the plasma per unit time. Since one neutron is produced per fusion reaction, this is also equal to the number of fusion reactions per unit time. The following relation can be written

$$S'_{np} = J_{nw}\, 2\pi r_w L \int_0^{r_p} R_p(r) r\, dr \qquad (5.6)$$

where we assumed the central cross section of the reactor to be perfectly circular, L is the reactor length in the direction of the cylinder, or toroidal axis, and $R_p(r)$ is the fusion rate per unit volume.

The normalization used in deriving the results presented in this chapter needs explanation. Since one-dimensional geometry was employed, all of the results and the source strength are taken per unit length in the unbounded direction. In all calculations, r_p was taken as 2.5 meters and r_w as 3.0 meters. The results are generally presented in two different ways. The first way is to tabulate the response rates (reaction rates, rates of neutron and gamma heating, etc.) by zone. The response rate given by zone is the spatial integral of the volumetric response rate over the volume of the zone. In this case, the results are normalized to one source neutron per unit time. These result can also be interpreted as the total response rate in the zone per unit surface area of the first wall per unit neutron current to the first wall including the 1/r effect of cylindrical geometry.

The other type of results is encountered in presenting the spatial distribution of the response rates, usually given in graphical forms, in units of response per unit volume per unit time. Here, the source strength, S_{np}, is again normalized to one fusion neutron per second per unit length in the unbounded direction but the response rate at every spatial point r is multiplied by $2\pi r$. Hence, the spatial distribution of the response rate is normalized to a unit neutron current density (i.e. $J_{nw} = 1\ n/cm^2 \cdot sec$) and corrected for the 1/r effect.

Because of the linearity of the Boltzman transport equation, the response rates are directly proportional to the neutron source strength

S_{np}, neutron wall current J_{nw}, or neutron wall loading W_n. Hence, all the results presented in this chapter can be easily renormalized to any desired source strength or neutron wall loading.

It should be noted that these choices of normalizing the results nearly eliminate the dependence on r_w. The response rate at a point r, when presented as described above, depends only on the ratio r/r_w. Hence, the dependence of the results given here on r_w is relatively weak.

All percentages of material compositions given are by volume unless otherwise indicated.

5.5.2 First Wall and Structural Materials

Several materials have been proposed for use as first wall and structural materials in the blanket. The strongest candidates are vanadium, niobium, molybdenum, and stainless steel. The first three are refractory metals and offer the most attractive high temperature characteristics for use in CTR systems. It is very likely that alloys such as Nb-1 Zr, V-20 Ti, or TZM alloys will be used rather than the pure metals. The neutronics and photonics results are usually not greatly affected by low concentrations of alloying materials.

The first wall and blanket structural material would preferrably meet the following requirements:

1 - Low nuclear heating in the first wall is highly desirable to ease the heat transfer problem, particularly with a liquid metal flowing in a strong magnetic field.

2 - Minimum induced radioactivity and afterheat.

3 - results in favorable effects on neutron economy and energy multiplication.

4 - minimum radiation damage (helium and hydrogen production, dpa, swelling, sputtering, etc.) allowing for acceptable life under high wall loadings dictated by the economics of the system.

5 - compatibility with the coolant.

6 - easy fabrication.

7 - reasonable cost.

Molybdenum is generally rejected on the ground of extreme difficulty [59 & 99] in fabrication. Further, the nuclear data for charged particle and secondary photon production in Molybdenum is not known to a reasonable accuracy. Therefore, molybdenum is excluded in the following discussion.

The choice of the thickness of the first wall involves considerations of thermal stresses, buckling stresses, corrosion and sputtering in addition to neutronics effects. Figure 5.2 shows a reference design for which a series of calculations were made varying the thickness of the first wall. Table 5.2 compares the neutronics results for .5, 1.0, and 2.0 cm niobium first walls. As expected, the total number of (n,2n), (n,α) and (n,p) reactions in the first wall increases with thickness. The tritium production increases in Li-6 and decreases in Li-7 with the net result that the tritium breeding ratio decreases as the first wall thickness is increased. This result differs in its implication from the Impink conclusion [52] that the tritium breeding is a maximum for molybdenum wall thickness of 2.0 cm. The fact that the tritium breeding ratio decreases as the wall thickness is increased can be explained as

follows. The main competition at high energy is between Nb(n,2n), inelastic scattering in Nb and $Li^7(n,n'\alpha)t$ reactions. Source neutrons undergoing inelastic scattering in niobium emerge with an average kinetic energy of 2.4 MeV. Therefore, most of these neutrons are below the threshold for the $Li^7(n,n'\alpha)t$ reaction. The average kinetic energy per neutron emerging from (n,2n) reaction induced by a 14 MeV neutron is about 1.5 MeV. Hence, a very small fraction of these neutrons can induce $Li^7(n,n'\alpha)t$ reactions. Although two neutrons are produced per (n,2n) reaction, the $Li^7(n,n'\alpha)t$ reaction is preferable from a total tritium production point of view. The probability that each of the two neutrons of the (n,2n) reaction gets absorbed in the $Li^6(n,\alpha)t$ reaction is less than unity. On the other hand, for each $Li^7(n,n'\alpha)t$ reaction, a tritium atom is produced in addition to a neutron. This neutron has almost the same probability for inducing a $Li^6(n,\alpha)t$ reaction as the average probability per neutron from the (n,2n) reaction. Therefore, the presence of materials with high (n,2n) cross sections in a natural lithium blanket does not increase the tritium breeding ratio. This result is applicable only to materials with relatively high (n,2n) thresholds such as niobium, vanadium, molybdenum and iron. The average energy per neutron emerging from $Be^9(n,2n)$ reactions is more than twice that from Nb(n,2n) or V(n,2n) reactions with a good fraction of these neutrons well above the threshold for the $Li^7(n,n'\alpha)t$ reaction. Hence, the presence of beryllium with lithium does increase the tritium breeding ratio as will also be shown shortly for several designs.

Vogelsang [101] showed that for typical fusion systems, doubling times shorter than a year are obtainable with tritium breeding ratios

of about 1.05. Allowing for 10% loss of neutrons due to parasitic absorption in and streaming out of the access regions, a tritium breeding ratio of 1.15 in one-dimensional model calculations is adequate. Therefore, increasing the first wall thickness to 4.0 cm does not lower the breeding ratio below a satisfactory level.

The main conclusion that can be derived from the above results (see table 5.2) is that no neutronically unacceptable effects arise from using a first wall thickness somewhere between 0.0 and 4.0 cm. Hence, the designers are free to chose the optimum wall thickness satisfying the thermal and buckling stresses, corrosion, blistering, and sputtering. This will vary from one material to another. Previous work [92 & 99] has found that a 0.25 to 1.0 cm wall thickness would satisfy these requirements for stainless steel and niobium.

The most difficult question in the nuclear design of fusion reactors is the design of the first wall. Several materials have been proposed. To compare the various responses for these materials, a series of neutronics and photonics calculations were made for the configuration of figure 5.3 with the first wall and structural materials as vanadium, niobium, and stainless steel. All the designs in this chapter are given three digit identification numbers. Here, the identification numbers are 301 for niobium, 302 for vanadium, and 303 for stainless steel first walls and structure designs. The calculations were run for the configuration shown in figure 5.3 with an additional 20 cm region of 70% Pb plus 30% B_4C and outer albedo boundary condition obtained from complete blanket and shield calculations given later. It was found that the neutronics and photonics results in the first seven zones in figure 5.3 are

insensitive to the composition of the shield. The results in zone 8 are not appreciably affected by the rest of the shield if it is followed by roughly 20 cm of the actual shield composition.

Figures 5.4 and 5.5 compare the spatially dependent helium and hydrogen production for niobium, vanadium, and stainless steel in designs 301, 302, and 303, respectively. The normalization of the graphical and tabulated results was discussed earlier in the introduction for this section. Figures 5.4 and 5.5 show that helium and hydrogen production are highest in stainless steel, lower in vanadium, and the lowest in niobium. Table 5.6 summarizes all the important results for the three structural materials and it shows that helium production in a stainless steel wall is more than 13 times that in niobium and is about 4.3 times that in a vanadium wall. These ratios are roughly the same for the structure in the various blanket zones. Hydrogen is produced with the ratio 1:1.67:7.8 in the three materials with stainless steel the highest and niobium the lowest. This difference in helium and hydrogen production is mainly due to differences in (n,α) and (n,p) cross sections as shown in figures 5.10 and 5.11.

Figure 5.6 compares the spatially dependent dpa (displacements per atom) in the three structural materials. In the first wall, the dpa is the smallest in vanadium, slightly higher in niobium and highest in stainless steel. The number of displacements per atom decreases roughly exponentially and more rapidly in niobium than in vanadium. For 1 MW/m^2 neutron wall loading (i.e. fusion neutron, J_{nw}, to the first wall of 4.43×10^{13} neutrons/$cm^2 \cdot sec$) each atom is displaced about 15 times each year in niobium and vanadium and about 20 times each year in stainless

steel.

Figure 5.12 shows that the (n,2n) cross section is relatively small in iron, higher for vanadium, and highest for niobium. The number of nuclides per unit volume however, is largest for stainless steel, and smallest for niobium but the relative order of the (n,2n) reaction rate in three materials in the first wall and blanket zones follows the relative order of the cross section. Although the (n,2n) reaction rate in niobium is higher and the threshold is lower than in vanadium the tritium breeding ratio is larger in blankets with vanadium structure than with niobium. Inelastic scattering in stainless steel and niobium is more effective in slowing the neutrons down past the $Li^7(n,n'\alpha)t$ reaction than in vanadium. Furthermore the radiative capture reaction rate, although small, in niobium is about 10 times that in vanadium.

The neutron and gamma heating rates for designs 301, 302, and 303 are summarized by zone in tables 5.3 through 5.5. The spatially dependent heating rates are given in figures 5.7 through 5.9 for the three designs. A comparison of heating rates in the three designs is also included in table 5.6. These results show that the total heating rate in niobium is about 2.3 times that in a vanadium and 1.2 times that in a stainless steel first wall. The gamma energy production and gamma energy deposition in the three materials are in the same order as the total nuclear heating, but the neutron heating is highest in stainless steel, lower in vanadium, and lowest in the niobium wall. The relative magnitude of the neutron heating in the three materials follows the relative magnitude of the neutron kerma factors as previously discussed (see figures 3.15 and 3.16 in chapter 3). The gamma production is the largest in niobium because of the large inelastic scattering. The gamma

energy depostion is also the highest in niobium because it has the largest atomic number and secondary gamma source among the three materials. The comparison of the total energy deposition in the system for the three designs shows that using niobium increases the useful power by about 1.1 MeV per fusion reaction over a stainless steel and by 1.0 MeV over a vanadium system. This is a nontrivial gain since it represents an increase in the system power output by about 6 to 7%. Vanadium is also slightly better than stainless steel in this regard. The origin of the better energy production with niobium than with either stainless steel or vanadium is the reaction Q-values

Reaction	Vanadium	Niobium	Fe^{56}
(n,2n)	-11.0545	-8.8199	-11.2040
(n,α)	-2.047	+4.9452	+0.322
(n,p)	-1.678	+0.692	-2.919
(n,γ)	+7.3085	+7.2304	+7.6415

for reactions in which conversion of mass into kinetic energy or vice versa occurs as can be seen from the above table (Q-values are listed in units of MeV).

There are two other important considerations in the comparison of structural materials. These are induced radioactivity and the associated afterheat and void formation and the associated creep. Investigations by others [70, 72, 76, 97 and 98] in decay heating in fusion systems show that a - for a 1000 MW(th) fusion reactor with a niobium wall the decay power at shutdown is 6 MW, and b - stainless steel is worse, molybdenum

is slightly better, and vanadium is much better with the activation level about a factor of 10 lower than in the niobium system. Very little is known about irradiation behavior of most of the CTR materials under high energy neutron irradiation. Extrapolation of the data from material irradiation in fission spectra [96] and allowing a factor of 10 for the hardening of the spectrum in a fusion reactor shows the wall lifetime in almost all materials is limited to a fluence of less than 10^{22} nvt. Since for a 1 MW/m^2 neutron wall loading the fluence per year is about 2.8×10^{22} (there is roughly a factor of 2 between the neutron flux in the first wall and the neutron current to the wall). This means that the plant should be operated at a wall loading less than the 1 MW/m^2 favored by economics [99] and the first wall has to be replaced once every year. Reference 96 indicates that there is virtually no swelling up to 9×10^{22} nvt (fast fission neutrons) in the V-1% Ti alloy which indicates that it can be used in fusion reactors with 1 MW/m^2 or higher for a lifetime of 20 years.

The above discussion shows that no one material emerges as the best choice for the first wall and structure. Molybdenum is extremely difficult to fabricate. Stainless steel has an undesirably low melting point which reduces the plant thermal efficiency in addition to lower "energy multiplication" compared with niobium and vanadium. Hence, the choice seems to narrow down to niobium and vanadium. Niobium has a high melting point and high energy multiplication, but has the disadvantages of a large afterheat and a high heating rate in the first wall. V-1% Ti has the advantages of much better radiation damage characteristics, the lowest heating rate in the first wall, and the lowest afterheat among

the materials investigated above. A disadvantage of using vanadium instead of niobium is a reduction in energy production of about 1 MeV per fusion reaction as shown above but the possibility of operating the vanadium alloy under a higher wall loading than niobium improves significantly the economics of vanadium systems over those employing niobium.

5.5.3 Blanket region

In D-T reactors, 17.6 MeV is released in a fusion reaction compared with 200 MeV per fission reaction. In addition, all the useful energy in a fusion reactor must pass through one critical section and hence the wall loading seems to be limited to values lower than desired from an economics point of view. Furthermore, the capital cost of fusion reactors is likely to be higher than that of fission reactors [99] and low operating cost in fusion compared with fission reactors is not likely to compensate for the low energy produced per fusion reaction. Hence, ways of increasing the energy multiplication per fusion neutron must be investigated. Fission-fusion symbiosis has been proposed [54] for the purpose of increasing energy multiplication but the complicated safety and maintainance aspects in such systems is a strong disadvantage. The subject of increasing energy multiplication in fusion reactors deserves a separate detailed study. However, two concepts for improving the effective energy produced per fusion neutron are investigated next. Before proceeding into this discussion it should be noted that higher effective energy production values (22 to 30 MeV per fusion neutron) have been quoted in literature. Much lower values are calculated here. The main reason for the difference is that in the present work we use consistent and energy preserving sets of kerma factors and gamma production cross

sections while previous works employed kerma factors which are too large.

Natural lithium consists of 7.42% Li^6 and 92.58% Li^7. The dominant reaction in Li^7 is the $(n,n'\alpha)t$ which is important at high energy and has a Q-value of -2.467 MeV. The most important reaction in Li^6 is the (n,α) which has a large 1/v cross section at low energy and a Q-value of +4.785 MeV. Both isotopes have other exothermic and endothermic reactions but these two dominate the total reaction rates. Therefore, the energy multiplication may be increased by enriching lithium (increasing the isotopic ratio of Li^6). To see the effect of enriching lithium on energy multiplication in the blanket, a series of neutronics calculations were carried out for the system shown in figure 5.3 with a vanadium first wall and structure. The isotopic ratio of Li^6 in lithium was increased from the natural abundance of 7.42% (design 401) to 15% in design 402, 30% in design 403 and 50% in design 404. For photonics calculations, the only change in the four problems is the gamma production source. Hence, gamma heating can be calculated by simple spatial and energy integration (actually discrete summation) of each source times the adjoint (for gamma kerma factors) as described in the last chapter. However even this integration is not necessary since the total energy of the gamma production source (in addition to neutron heating) suffices for comparing the energy multiplication in the four problems. The total energy produced in the system (first wall, lithium blanket and reflector region; see figure 5.3) is given as a function of Li enrichment in table 5.8. The results show that the gain in energy multiplication as the Li^6 isotopic ratio is increased is only 0.06% for 15% Li^6, and 0.5% for 50% Li^6. Given the fact that isotopic enrichment is an expensive process, these results imply that the economics for lithium-enriched

systems may be worse than for systems operating with natural lithium. The reason for the increase in energy multiplication is small can be seen from table 5.9 which summarizes the rates of exothermic and endothermic reactions in Li^6 and Li^7. The reaction rates are compared in table 5.9 for the two cases of natural lithium (7.42% Li^6) and 30.0% Li^6 abundance in lithium. An increase in the $Li^6(n,\alpha)$ reaction rate by 0.1487 reactions per fusion neutron corresponds to a net gain of 0.7117 MeV. The (n,n')d high energy reaction in Li^6 is endothermic and increasing the Li^6 isotopic ratio in lithium results in an energy "loss" through this reaction. The net gain in Li^6 is 0.31 MeV. All reactions in Li^7 are endothermic and therefore decreasing the percentage of Li^7 in lithium results always in a decrease in the energy loss. Decreasing Li^7 from 92.58% to 70% reduces the energy loss and hence corresponds to a net gain of 0.48 MeV. Therefore, enriching lithium in Li^6 slightly increases the energy multiplication through a reduction in the energy loss in Li^7 and to a smaller extent through an increase in the energy gain in Li^6. It can also be seen from table 5.9 that increasing the Li^6 percentage increases the high energy endothermic reactions in vanadium, iron, chromium, and nickel with the net result of a loss in energy multiplication.

As a consequence of the above results, it is concluded that increasing the isotopic ratio of Li^6 in the lithium blanket does not significantly improve the economy of the system. While the number of $Li^6(n,\alpha)$ reactions can be made 1.0 or greater per fusion neutron with a gain of 4.786 MeV the effective Q-value for the blanket as shown above is only about 2 MeV. This is because the most important high energy reactions are endothermic with large Q-values in all the materials in the blanket.

If the 14 MeV neutrons are slowed down in a virtual material with only elastic scattering and the low energy neutrons are passed then in iron, vanadium, or niobium there is a gain per fusion neutron of 7 to 8 MeV from radiative capture. This is impractical, however. Another alternative is to multiply the number of neutrons through the (n,2n) reactions. Each neutron suffers an energy loss of about 9 MeV in niobium, 11 MeV in vanadium, 13 MeV in iron per (n,2n) reaction. Therefore, if the two neutrons are virtually absorbed in Li^6 the net result is still a loss of energy. The situation is different, however, with Be-9 since the (n,2n) reaction in this material has a Q-value of only -1.6 MeV which is smaller in magnitude than that for any other material. The possibility of improving the energy multiplication in the blanket through the use of Be-9 is investigated next.

Design 401 described earlier which is shown in figure 5.3 with vanadium as the first wall and structure was chosen for investigating the effect of adding beryllium to the blanket. The design was kept the same but an amount of beryllium equivalent to a 4 cm thick layer was homogenized with the first lithium region which is 20 cm of 95% natural lithium plus 5% vanadium and the new design was given the identification number 405. Design 406 is the same as design 405 except that the beryllium thickness was increased to 10 cm. Table 5.10 summarizes the effect of adding 4 cm and 10 cm of Be on the important reactions, heating, and secondary gamma energy production. The results show that the tritium breeding ratio in natural lithium increases from 1.46 in design 401 (no beryllium) to 1.68 in design 405 (4.0 cm Be) to 1.91 in design 406 (10.0 cm Be). The total energy production increases by 9.3% and 18.45% when

4.0 cm and 10.0 cm of Be, respectively, are added. The energy leakage to the shield was not added in all cases because this energy is generally not recoverable with high efficiency for power production. However, it is generally 0.02 to .07 MeV and does not affect any of the above results appreciably.

It is seen from the above results that adding 4 cm of beryllium increases the power output by about 10% which is large enough to offset the high cost of beryllium. Unless the cost of 4 cm of Be is greater than 9% of the total plant cost it is economical to use beryllium. As discussed earlier and from results to follow, the first wall, blanket, reflector, shield and magnet regions are of roughly 3.0 meters thickness. The average density of the materials in this region is about three times that of Be with an average cost that is uncertain at present but is somewhere between \$7/lb to \$15/lb [99]. The price of beryllium is high and uncertain too but has an estimated upper price of \$60/lb [100]. Therefore, the price of 4 cm Be is less than 3% of the total cost of the plant. Since the net gain in power is greater than 9%, it is economical to use beryllium. 10 cm of Be costs roughly 8% or less of the total plant cost but the power increases by about 18% with the net result of a lower cost per unit power. Although no detailed estimate of the cost per unit power was performed in this work, these qualitative arguments show that the benefits from using beryllium warrants future studies for assessing the various aspects associated with using beryllium such as toxicity and high helium production. Each (n,2n) reaction in beryllium is followed by the emission of two alpha particles and table 3.10 shows that for each fusion neutron 0.69 alpha particles are produced in a

beryllium layer 4.0 cm thick.

5.5.4 Reflector (Intermediate) Region

As shown from the above calculations, a lithium region of about 40 cm is adequate for satisfying the requirements of tritium regeneration. Most of the neutrons are also slowed down converting their kinetic energy into heat in this lithium region. However, the average kinetic energy of the neutrons streaming out of this region is roughly 7 MeV and the net energy leakage is about 1.5 to 2.0 MeV per source neutron. Clearly , this large amount of energy cannot be allowed to pass directly into and be "wasted" in the shield which must be operated at low temperatures. Therefore, an intermediate region between the lithium and shield regions is required to perform the following functions.

1 - moderates and reflects a large fraction of the neutrons back into the lithium region increasing the tritium production per unit volume and allowing a thinner lithium region to be employed,

2 - extracts nearly all the remaining kinetic energy from the neutrons thus increasing the recoverable energy and decreasing the energy leakage into the shield, and

3 - if possible - multiplies the energy production.

Obviously, the thickness of the lithium region can be increased to perform the above functions. However, this choice has the following disadvantages: 1 - the moderating power of lithium for fast neutrons is low and is roughly one-third of that for graphite and one-fifth of that for several heavy materials. Since it is essential to minimize the thickness of the blanket and shield as discussed shortly, it is highly desirable to use materials with high moderating power., 2 - Because

of the relatively low moderating power of lithium, increasing the lithium region lowers the tritium production per unit volume in the inner lithium regions with a net modest increase in the tritium breeding ratio. Both effects are undesirable because increasing the total tritium production beyond that required results in more tritium hazard and lower tritium concentration complicates the problem of tritium recovery., 3 - Increasing the lithium inventory increases the hazard of accidental potential energy release and 4 - Increasing the 40 cm lithium region into 60 cm increases the $Li^6(n,\alpha)$ reaction rate by only about 10%. Hence, the energy multiplication is not high to warrant an allowance for the difficulties given in 1, 2, & 3.

As a consequence, the thickness of the lithium region should be kept to a minimum that satisfies the tritium regeneration requirements and the lithium region should be followed by a better moderator, reflector, and energy multiplying material. Graphite has been widely used for neutron moderating applications and has also been proposed for use in fusion reactors. Iron, on the other hand, has considerably better neutron attenuation characteristics and the possibility of using it in the reflector region is explored here. In order not to perturb the magnetic field it is necessary that the materials employed be nonmagnetic. Hence, stainless steel which has more than 70% iron and is nonmagnetic should be used. Furthermore, the nickel and chromium contents of stainless steel are useful for covering the well known iron "windows" associated with the minima in its total cross section.

To bring up the salient points in comparing graphite and stainless

steel in the intermediate reflector region, the configuration of figure 5.13 is considered. The system consists of a 1 cm first wall, 40 cm of 95% Li plus 5% structure, 25 cm intermediate region, and a one-meter shield consisting of 50% Pb + 20% Fe + 30% B_4C. Calculations were carried out for three designs. The composition of the intermediate region is graphite in design 110, iron in design 112, and 50% Pb + 20% Fe + 30% B_4C in design 111. Iron was used in this series of calculations for the purposes of comparison but stainless steel does not change the results significantly as is shown later.

Tables 5.11 (a,b,c & d) and 5.12 compare the important neutronics and photonics results for the three designs. Table 5.11a shows the neutron heating by zone for the three materials. The neutron heating does not change appreciably in the first wall and the first 30 cm of the lithium region when graphite is replaced by iron. The neutron heating is lower in the 10 cm of lithium adjacent to the intermediate region when iron is used because of the higher (n,γ) reaction rates in iron compared with graphite. The neutron heating is lowest in this lithium region when the 50% Pb + 20% Fe + 30% B_4C mixture is employed in the intermediate region because in the presence of B^{10}, neutrons slowed down have little chance to escape absorption and be reflected back into the lithium region. In the reflector region, neutron heating is lowest for iron, higher for graphite and the highest for the mixture. Most of the reactions in graphite are elastic and $(n,n'3\alpha)$ while in iron a considerable fraction of the enrgy is converted to gammas as shown in table 5.11-c. Because of neutron absorption in the $B^{10}(n,\alpha)$ exothermic reaction, the neutron heating is highest in the lead-iron-boron carbide mixture.

Table 5.12 shows a summary of the results for the comparison between the three materials. Two important results can be deduced from table 5.12.

1 - The total recoverable energy per fusion neutron in design 112 (iron reflector) is higher than that for design 110 (graphite reflector) by 1.5 MeV. In other words, replacing graphite by iron increases the recoverable energy by 9.5%.

2 - The total (neutron plus gamma) energy leakage from the iron is about an order of magnitude lower than that from the graphite reflector.

3 - A mixture consisting of 50% Pb plus 20% Fe plus 30% B_4C is better than graphite in the reflector region from the energy attenuation and multiplication of recoverable energy points of view but iron is better than either. The tritium breeding ratio drops to 1.06, which is unacceptable in one-dimensional calculations, when this mixture is used. In addition, the heat generation in the reflector region is so high that it would be difficult to employ lead in this region because of its low melting point.

From the above results, iron is superior to graphite in the reflector region from both an energy multiplication, and a neutron and gamma attenuation point of view. In addition, graphite suffers from severe radiation damage [103], mainly dimensional changes, when irradiated to fluences higher than 10^{22} n/cm^2 but stainless steel has better radiation resistance at such fluences. Hence, stainless steel is superior to graphite in the reflector region. The only question remaining to be answered is the effect of cost considerations. Since no quality control is required in fabricating the stainless steel for this region, its cost

is roughly the same as that of graphite. In addition, the gain in energy multiplication would offset the increase in cost if stainless steel prices were higher. Furthermore, the stainless steel thickness required to perform the function of 25 cm graphite is roughly 9 cm. If the cost of 9 cm stainless steel were the same as 25 cm graphite there is still a benefit from using stainless steel since the shield and magnet volumes would be decreased by decreasing their inner radii.

5.5.5 Magnet Shield

If the neutrons and gammas streaming out of the blanket region are allowed to pass directly into the superconducting magnet, the total plant power output will not be sufficient to supply the power requirements of the refrigeration system. Hence, the need for a magnet shield is obvious. No quantitative design for the magnet shield has been previously investigated. The following discussion is devoted to the nuclear design of the magnet shield.

The shield is required to perform three major functions:

1 - reduces the nuclear radiation heating of the cryogenic coils to a permissible level to be defined shortly,

2 - reduces the radiation level to the superinsulation at the inner surface facing the shield in order that it may function properly without excessive radiation damage for a satisfactory lifetime ($\sim$20 years), and

3 - keeps the radiation to the magnet to the minimum allowed by a tolerable increase in the resistivity of the copper stabilizer and radiation damage to the superconductor for a satisfactory lifetime.

The energy attenuation required by the refrigeration system can be

determined by a compromise between its operating and capital cost, the shield cost, and the increase in the magnet cost if the shield thickness is increased. On the other hand, an increase in the resistivity of the copper stabilizer, radiation damage to the superconductor cannot be compromised beyond the tolerable level for the reactor lifetime. Therefore, a point of immediate interest is to see if the attenuation required by the refrigeration system is sufficient to satisfy the stringent requirements of the stabilizer, superconductor, and superinsulation. However, before this can be done we have to investigate first the various possible shielding materials and configurations and find out the energy attenuation coefficients obtainable.

Shield Composition

A considerable fraction of the neutrons leaking out of the blanket have kinetic energies above a few MeV. A basic requirement therefore of the shielding material is to have a large attenuation coefficient for high energy neutrons. Inevitably, this has to be a material of moderate or large mass number since inelastic scattering is the most efficient mechanism for reducing the energies of high energy neutrons. Furthermore, light materials such as water, LiH, and lithium have small total cross sections at high energies compared with heavy materials as shown in figure 5.14a. In order not to complicate the graph by the detailed resonance structure of the cross section, the average cross section in 100 energy intervals was plotted in figure 5.14 versus the midpoint energy for each interval. Stainless steel and lead have relatively large total cross section above 3 MeV and the average secondary neutron

energy per inelastic collision at 14 MeV is 2.2 and 2.5 MeV in lead and iron, respectively. Both materials are available, relatively inexpensive, and a great deal of knowledge about their characteristics exists. Below the inelastic threshold, however, these materials are no longer effective and a light material should be present. Borated water is efficient (see figure 5.14b) and is almost cost free. However, the presence of water in the same system with a high-temperature liquid metal increases significantly the hazard of accidental energy release. Graphite is an alternative choice. In addition, to minimize the gamma emission from radiative capture reactions, it is essential to use a sufficient amount of B^{10} which has a large (n,α) cross section for low energy neutrons and is associated with only soft gamma (.5 MeV) emission (compared with a strong line at 7.6 MeV in the capture gamma ray spectrum for iron). Boron carbide (B_4C) has been used in control rod applications in fission reactors [110] and seems to represent an excellent choice for neutron moderation and absorption at low energies. With the theoretical density, B_4C has a high content of B^{10} of 0.0217 atoms/cm^3. No significant radioactive decay products are formed in B_4C irradiation but helium production is significantly large. However, if B_4C is used in the shield with only 80% of the theoretical density, the swelling problem due to the excessive helium production can be tolerated. Boral (50% B_4C and 50% Al) is another good choice.

Based on the above discussion, a mixture of stainless steel and boron carbide, or of lead and B_4C, or a combination of the three materials are reasonable choices and further investigation is needed to find

the optimum composition and shield depth for an overall low cost. For this purpose, a fixed composition and configuration of the blanket coupled to a shield for which the parameters are to be varied as shown in figure 5.15 is considered. Based on the results presented earlier in this section, the blanket consists of a 1 cm first wall, 42 cm of 95% Li plus 5% structure, 20 cm stainless steel, and 7 cm of 95% Li plus 5% structure. The first wall and blanket structure is niobium in the following calculations but the results in the shield are insensitive to this choice. The extra 7 cm of lithium at the outer face of the reflector region was introduced to meet the cooling requirements of the reflector and inner regions of the shield. As a preliminary criteria, the attenuation required in the blanket and shield should be roughly 10^6. From the previous results for design 112, this requirement can be satisfied by roughly 70 cm of stainless steel plus boron carbide following the blanket described above. As a starting point, figure 5.15 in which the blanket is followed by a one meter shield was considered as a reference design for investigating the various aspects of the shield design. Four cases for the composition of the shield were considered; 70% SS plus 30% B_4C (design 114), 70% Pb plus 30% B_4C (design 115), 35% SS plus 35% Pb plus 30% B_4C (design 116), and 100% SS (design 117) where percentages are by volume. Neutronics and photonics calculations were carried out for the four designs. It was shown in chapter 4 that the convergence of the discrete ordinates results for such system are achieved by S_8 and that S_4 overestimates the leakage by 10 to 15%. In order to reduce the cost for these calculations, S_4 was used. The comparison is not significantly affected by the difference between S_4 & S_8. As in all

other calculations in this chapter, P_3 and cylindrical geometry were employed. Before proceeding into a discussion of the results, a few words about "terminology" is in order.

The energy deposition in the magnets by neutrons and photons streaming out of the shield increases, in general, with the neutron and photon energies. Hence, it is appropriate in comparing the performance of the various shield compositions to compare the "energy" rather than the "number" attenuations. The net neutron energy leakage at the right boundary for a spatial zone is defined as the total energy of the neutrons streaming out (to the right) of the zone minus the total energy of the neutrons entering the zone at the right boundary. Mathematically, the neutron energy leakage, L_{nE}, at a zone boundary is then given by

$$L_{nE} = \int E_n \, J_{no}(E_n) \, dE_n \cdot 2\pi r_o$$

and in multigroup representation,

$$L_{nE} = \sum_g E_{ng} \, J_{nog} \cdot 2\pi r_o \qquad (5.8)$$

where $J_{no}(E_n)$ is the neutron current density for neutrons of energy E_n at the outer (right) boundary for the zone. The current density here is the net current density (i.e. $J = J^+ - J^-$). The subscript g denotes an energy group and J_{nog} is the neutron current density in the group. E_{ng} is the midpoint energy for group g and $2\pi r_o$ is the surface area at the zone outer boundary per unit length in the unbounded direction. A similar term is defined for photons with the subscript γ replacing n. The total energy leakage, L_{TE}, is the sum of neutron and photon energy leakage, i.e.

$$L_{TE} = L_{nE} + L_{\gamma E} \tag{5.9}$$

The average kinetic energy for the neutron leakage at the outer boundary is defined as

$$\bar{E}_n = \frac{\sum_g E_{ng} J_{nog}}{\sum_g J_{nog}} \tag{5.10}$$

with a similar term for the gammas.

We will assume that L_{nE} , $L_{\gamma E}$, and L_{TE} vary exponentially with the spatial variable within the shield (it will be shown shortly that, to an excellent approximation, this is indeed so within a region of uniform composition), i.e.

$$L_{nE}(r) = L_{nE}(o)\ e^{-\mu_n r} \tag{5.11a}$$

$$L_{\gamma E}(r) = L_{\gamma E}(o)\ e^{-\mu_\gamma r} \tag{5.11b}$$

$$L_{TE}(r) = L_{TE}(o)\ e^{-\mu r} \tag{5.11c}$$

Each μ is called the energy attenuation coefficient for the appropriate type as indicated by the subscript or by no subscript for the total. The energy attenuation coefficient, A_f, for a distance of width r_2-r_1 is defined as

$$A_f = \frac{L_{TE}\ (r_2)}{L_{TE}\ (r_1)} \tag{5.12}$$

with a similar term for neutrons and photons. All the results are usually quoted here per fusion neutron (14 MeV) unless otherwise indicated. The above symbols and definitions will be employed in the tables

and text to follow.

The parameters $\bar{E}_n$, $\bar{E}_\gamma$, L_{nE}, $L_{\gamma E}$ and L_{TE} are shown for each zone in designs 114 through 117 in tables 5.13 through 5.16. A comparison of gamma energy production is given in table 5.17. The energy leakage, L_{TE}, is plotted against the distance from the inner boundary of the shield for the four compositions in figure 5.16. Inspection of this figure reveals the following:

1 - L_{TE} varies exponentially with the spatial variable in the shield, to an excellent approximation, as assumed in equations 5.11. The energy attenuation coefficients, μ_n, μ_γ, and μ in the four designs are given in table 5.18.

2 - The total energy attenuation coefficient is equal to.1445 cm^{-1} for design 114, 0.1113 for design 115, .1283 for design 116, and .0902 for design 117.

3 - Comparison of L_{TE} for designs 114 and 117 shows that the presence of B_4C (or an alternative) is necessary. At the end of a one meter shield the total energy leakage in a 100% stainless steel shield is about two or less of magnitude higher than that in a shield consisting of 70% SS plus 30% B_4C. This is mainly due to two reasons. B_4C is better than SS in attenuating neutrons below about 2 MeV (see total cross sections in figure 5.14). In addition, in the absence of B^{10}, neutrons slowed down eventually gets absorbed in radiative capture reactions in stainless steel increasing the gamma energy production as can be seen from table 5.17. (see the comparison of the neutron flux in fig. 5.18)

4 - Comparison of designs 114, 115 and 116 shows that stainless steel has considerably better neutron attenuation characteristics than lead if

both are mixed with a fair amount of light material. (see fig. 5.16 & 5.17)

5 - Although lead is more efficient in attenuating gamma radiation, using stainless steel does not increase the gamma energy leakage (compare $L_{\gamma E}$ in tables 5.13 and 5.14) appreciably. Furthermore, table 5.18 shows that μ_γ is greater in stainless steel-B_4C than in Pb-B_4C mixtures. These results can be explained as follows. The photons in the shield came primarily from gammas produced in neutron interactions in the shield rather than penetration from the blanket. Stainless steel attenuates fast neutrons quickly in the first few mean free paths, thus the photons produced have a long distance in which to be absorbed. In addition, the gamma energy leakage in the outer regions is affected most by the gammas produced in these regions. The secondary gamma production in deeper regions of a SS-B_4C shield is significantly lower than that in the same regions of the Pb-B_4C shield (compare designs 114 & 115 in table 5.17).

Shield Thickness

Increasing the thickness of the shield increases its cost and the magnet cost but lowers the refrigeration power requirements. In the following, an attempt is made to find the optimum thickness that minimizes the cost for a given shield composition. For convenience, toroidal reactors are considered when a reference to reactor type is needed. For the most part, however, the results are fairly independent of the reactor type.

The total cost of the reactor as a function of the shield thickness is given by Total cost = magnet cost + shield cost + refrigeration cost + other fixed costs independent of the shield parameters .

Since the reactor is fairly uniform in the toroidal direction the cost can be stated per unit lenth in the toroidal direction. The above equation can be rewritten as

$$C_T = C_M + C_S + C_R + C_F \tag{5.13}$$

where the subscripts M, S, R, and F denotes magnet, shield, refrigeration, and fixed costs, respectively. All the C's are in dollars per unit length. An expression for each of these items as a function of the shield parameters is derived next.

a - Magnet Cost

The magnet cost is proportional to the energy stored in the magnetic field. This is a function of the strength, the major radius for the torus, R, and the inner radius, r_m, of the magnet. Since our concern is the dependence on the shield thickness, all these parameters except r_m are assumed fixed. Further, it is assumed that the magnet cost, C_M, varies with r_m to the power m, i.e.

$$C_M = a'_m \left(\frac{r_m}{r_{ref}}\right)^m \tag{5.14}$$

where r_{ref} is the inner radius of the magnet in a reference design.

$$C_M = a_m r_m^m \quad , \quad a_m = \frac{a'_m}{(r_{ref})^m} \tag{5.15}$$

$$r_m = r_b + t_s \tag{5.16}$$

where r_b is the outer radius for the blanket (inner radius for the shield). t_s is the shield thickness and is the parameter to be optimized.

b - Shield Cost

The cost is taken to be that of the material in the shield, i.e.

$$C_s = \pi(t_s^2 + 2r_b t_s)\cdot a_s \qquad (5.17)$$

where a_s is the cost of the shielding material in dollars per unit volume.

c - Refrigeration Cost

As a first approximation, the operating cost of the refrigeration is ignored. Its effect on the optimum shield thickness will be discussed later. The refrigeration capital cost is estimated [104 & 106] to be \$6000 per watt of thermal load and it decreases with the capacity as follows

$$C_r = 6000\ P^{0.6} \qquad (5.18)$$

where P is the thermal load in watts. Considering only the nuclear heating, P is given by

$$P = 2\pi r_w \cdot W_n \cdot e^{-\mu_b t_b} \cdot e^{-\mu_s t_s} \qquad (5.19)$$

where r_w is the first wall radius, W_n is the neutron wall loading, μ_b and μ_s are the energy attenuation coefficients in the blanket and shield respectively, and t_b is the blanket thickness.

Thus

$$C_R = a_r e^{-0.6\mu_s t_s} \qquad (5.20)$$

where

$$a_r = 6000(2\pi r_w W_n e^{-\mu_b t_b})^{0.6} \tag{5.21}$$

Rewriting equation 5.13 in terms of the above parameters and minimizing C_T with respect to t_s, the optimum shield thickness, t_{so}, is found to be given by

$$t_{so} = \frac{1}{0.6\,\mu_s} \text{Log}_e \left(\frac{0.6\,\mu_s a_r}{m a_m (r_b + t_s)^{m-1} + 2\pi a_s (r_b + t_s)} \right) \tag{5.22}$$

Tables 5.19 and 5.20 tabulate the values of the optimum shield thickness for different values of the parameters in equations 5.13 through 5.22. The energy attenuation coefficient, μ_s, for the shield is taken as 0.1447 cm^{-1} (which is obtained from the results of design 114 for 70% SS + 30% B_4C) and 0.1113 cm^{-1} (which is obtained from design 115 for 70% Pb + 30% B_4C) in tables 5.19 and 5.20, respectively. In all cases in both tables, the value of $\exp(-\mu_b t_b)$ was taken as .007 which was found to represent the energy attenuation in the blanket in all of the designs 114 through 117 without any significant variation. The values of a'_m and r_{ref} in equation 5.14 were taken from Lubell's work [106] as \$70 × 10^6 and 5.6 meters, respectively. It was found that 50% change in this typical cost results in less than 5% change in the optimum shield thickness for the typical conditions of tables 5.19 and 5.20.

From equation 5.22 it is noted that the optimum shield thickness varies inversely with μ_s, m, a_m, r_b, and a_s and increases with the refrigeration coefficient, a_r. Except for μ_s, the dependence of t_{so} on these parameters is relatively weak due to the nature of the logar-

ithmic function. For example, inspection of both tables 5.19 and 5.20 shows that changing the dependence of the magnet cost on r_m in equation 5.14 from $m = 1$ to $m = 2$, changes t_{so} by only 3 to 8% depending on the other parameters. Doubling the wall radius (compare cases 1 & 7, and 4 & 8 in table 5.19; 1 & 5, and 4 & 7 in table 5.20) changes the optimum thickness of the shield by roughly 2%. The results show a relatively strong dependence of t_{so} on the wall loading. It is worth noting that if one assumes that a specified fraction of the power output is to run the refrigerators, the attenuation required is fairly independent of the wall loading.

In table 5.19 two prices for the stainless-B_4C mixture were used. The value a_s of .088 \$/cm^3 corresponds to \$6.4/lb for the mixture (effective density is 6.26 gm/cm^3). The other value of a_s is 0.035 and corresponds to \$2.55/lb of the mixture. The price for the lead-B_4C mixture was taken as 0.92 \$/lb.

Case number 5 in table 5.19 represents typical conditions for the reactor. The wall loading is 1 MV/m^2, μ is taken from transport calculations and the price of the shield and magnet are realistic. This case shows that for these conditions and for the blanket shown in figure 5.15 the total cost is minimized for a shield consisting of 70% SS + 30% B_4C by a thickness of 66.97 cm. The total cost in this case is 1.922×10^4 \$/cm and for a major radius of 12 meters is 144.8 million dollars. The corresponding case with the lead-B_4C mixture is case number 1 in table 5.20. The total price for a major radius of 12 meters is 128.42 million dollars. These prices do not include fixed costs (see equation 5.13). From these two cases, it is concluded that using the lead-B_4C mixture

saves 16 million dollars compared with the SS-B_4C mixture. Furthermore, from tables 5.13, 5.14, and 5.18, these optimum thicknesses correspond to 4.17×10^{-6} MeV to the magnet per MeV in the first wall for SS-B_4C and 1.85×10^{-7} MeV per MeV for the lead-B_4C. Hence the lead B_4C mixture is cheaper to use and the optimum thickness corresponds to better attenuation.

In the above optimization, the operating cost of the refrigerators was ignored. However, for the optimum shield of the lead-B_4C mixture, the power required to run the refrigerators is only about 0.04% of the net power output of the plant (assuming a plant efficiency of about 30% and that a 1000 KW(e) is required for each KW of heat to the magnet). Hence, including the operating cost of the refrigerators will not significantly increase the optimum shield thickness. However, this operating cost can be included in cost optimization of the complete plant.

From the above results we can now find out if the attenuation obtained with the optimum shield is sufficient to satisfy the requirements of the stabilizer and superinsulation. Figure 5.19 shows the response rates for atomic displacement in the stabilizer (copper), dose in superinsulation (mylar), and energy leakage as a function of the shield thickness for a shielding mixture consisting of 35% Pb plus 35% SS plus 30% B_4C. At the optimum thickness (73.8 cm) for this mixture, the dose in mylar facing the shield is about 1.76×10^9 ergs per gram per year for a neutron wall leading of 0.5 MW/m^2. From studies [109] on the effect of radiation on magnet insulations, the mylar can operate under such level of radiation for 20 years without severe deterioration in its

dielectric and mechanical properties. A neutron wall loading as high as 2.0 MW/m^2 is also acceptable. Figure 5.19 shows that the maximum displacement rate in copper at the optimum shield thickness is about 1.3×10^{-5} displacements per atom per year. It is beyond the scope of this study to investigate the radiation damage effects on superconducting and stabilizing materials. However, from the results of a study by Boom [104] it can be concluded that the stabilizer can be designed to accept levels of radiation about two times higher than that of figure 5.19 for 20 years of operation.

5.6 A Proposed Design of a Blanket and Shield

Figure 5.20 shows a schematic of a proposed blanket and shield design. The design can certainly be improved upon and some of the choices can be altered. However, this design represents an adequate and promising model according to the results of the present study. The characteristics of this design are briefly summarized below. The calculated responses for this system are given in detail and they can serve as important input for further studies in areas of heat transfer, decay heat, tritium removal, radiation damage, and general system analysis. The neutronics and photonics transport calculations were carried out in one-dimensional geometry using the S_8-P_3 approximation. The plasma wall radii, r_p and r_w, were taken as 400 and 450 cm. Since the neutronics and photonics results are given below per unit current ($1\ n/cm^2 \cdot sec$) and per unit neutron wall loading to the first wall these results are not appreciably affected by the choice of r_p and r_w as dis-

cussed earlier in this chapter. The material chosen for first wall and blanket structure is vanadium. As discussed in section 5.5 no one material emerges as the best choice but vanadium and niobium has many important and desirable properties. In this proposed design, vanadium was chosen because of lower afterheat and radioactivity and lower heating rate in the first wall than in niobium. The lithium blanket thickness of 40 cm was chosen to give a high tritium breeding ratio of 1.46 in one-dimensional calculations. For practicle systems, feed pipes, divertor, and several access regions need to be employed. In such case, the actual tritium breeding ratio in three-dimensional calculations will be somewhere between 1.2 to 1.3. This is adequate for obtaining a short doubling time of roughly 100 days [101] with reasonable assumptions about the tritium removal system. For the second generation of fusion reactors a much longer doubling time will be required and the lithium region need to be thinned and other materials with high energy multiplication should be employed. The reflector region (zone 7) is stainless steel. The merits of this choice over other alternatives, such as graphite, were discussed in section 5.5. Zone 8 consists of 5 cm 95% Li plus 5% V and provides for cooling the reflector and the blanket structural wall (zone 9). This 5 cm lithium can be rearranged within the reflector region to provide maximum cooling efficiency.

Zone 10 is a 1 cm vacuum gap and it serves as a thermal barrier between the high temperature blanket region and low temperature shield. Zones 11 through 20 comprise the magnet shield. As shown in the pre-

vious section, for the materials investigated, an optimum shield, from a cost point of view, consists of a homogeneous mixture of 70% Pb plus 30% B_4C. An additional gain in energy attenuation is obtained using the heterogeneous arrangement of lead and B_4C shown in figure 5.20. An amount of structural steel was added for structural support. Zones, 11, 14 and 17 are for helium cooling of the shield. Zone 20 serves as the dewar and for further attenuation of the nuclear radiation. Zone 21 is thermal insulation for the magnet and cryogenic systems. The magnet region (zone 22) is essentially that given by Young and Boom [105] and is homogenized for neutronics and photonics calculations. All percentages in figure 5.20, as everywhere in this thesis, are by volume. The nuclei densities used in the calculations accounted for thermal expansion and are given in table 5.25.

Spatial distribution of neutron, gamma, and total heating rates in the blanket and reflector region in the proposed design are given in figure 5.21 . The design is given the identification number 777. From figure 5.21, the total heating rate in the first wall is about 5 watts/cm^3 for 1 MW/m^2 neutron wall loading (note that all the results vary linearly with the wall loading). The maximum volumetric heating rate in the blanket is about 4 watts/cm^3. From figure 5.21 the ratio of the neutron to gamma heating can be clearly seen. In vanadium and stainless steel regions the gamma heating is much larger than the neutron heating but the reverse is true for the lithium regions.

Neutron heating is given by material and zone in table 5.21 . Neutron and gamma heating and gamma energy production by zone are given in table 5.22 in units of MeV per source neutron. Several ob-

servations are in order. The gamma heating is only about 27% of the total nuclear heating in the blanket and shield. The neutron heating in lithium alone contributes about 67% of the total nuclear heating in the system. The nuclear heating rate in the shield (zones 11 through 20) is about 2.5% of the total nuclear heating rate or about 2% of the total thermal power of the plant (including 3.5 MeV per alpha particle). Extracting this amount of energy at high efficiency is therefore not crucial from total plant economics point of view. However, it is necessary to remove this energy in order to ensure the physical integrity of the shield. Table 5.22 compares also the gamma energy production with the gamma heating by zone. The former is larger than the latter in the first few zones of the blanket. However, the total gamma heating in the first wall, blanket and reflector regions is roughly equal to the sum of the gamma energy production in these regions. Hence, the gamma energy leakage from the blanket is small and the gamma heating in the shield results from photons produced locally by neutron interactions rather than from photons transported from the blanket into the shield. This latter remark is quite helpful in performing photonics sensitivity studies of the shield.

Table 5.22 shows that the total nuclear heating is 16.43 MeV per source neutron. Hence, the net energy per fusion reaction is 19.93 MeV, which is lower than the values reported earlier in literature. However, these results are not explained on the basis of simply having different systems. They result rather because the kerma factors and gamma production dat derived in the present work are thorough and self-consistent.

Table 5.23 gives the tritium production in lithium by zone. As discussed above the tritium breeding ratio is high and is about 1.46. The spatial distribution of tritium production in Li^6, Li^7, and total is given in figure 5.22. The $Li^7(n,n'\alpha)t$ reaction rate decreases monotonically with distance from the first wall as the spectrum becomes relatively softer. The $Li^6(n,\alpha)t$ reaction decreases with distance from first wall then increases again near the lithium-reflector interface. The stainless steel reflector slows the neutron down strongly and a good fraction of these low energy neutrons are reflected into the lithium region.

The spatial distribution of helium and hydrogen production in vanadium are given in figure 5.23 in units of atomic parts per million (appm) per year for a neutron wall loading of 1 MW/m^2. Figure 5.24 shows the spatial distribution of the atomic displacements in vanadium in units of dpa per second per unit neutron current (1 $n/cm^2 \cdot sec$) to the first wall and also in units of dpa per year for 1 MW/m^2. From this figure, each atom in the first wall is displaced about 14.5 times per year if the neutron wall loading is 1 MW/m^2.

Table 5.24 shows the tritium production in boron by zone in the shield. For each 10^5 source neutrons, about 3.6 tritium atoms are produced in the shield. The presence of tritium in the shield is undesirable and the implication of this result should be investigated in future studies.

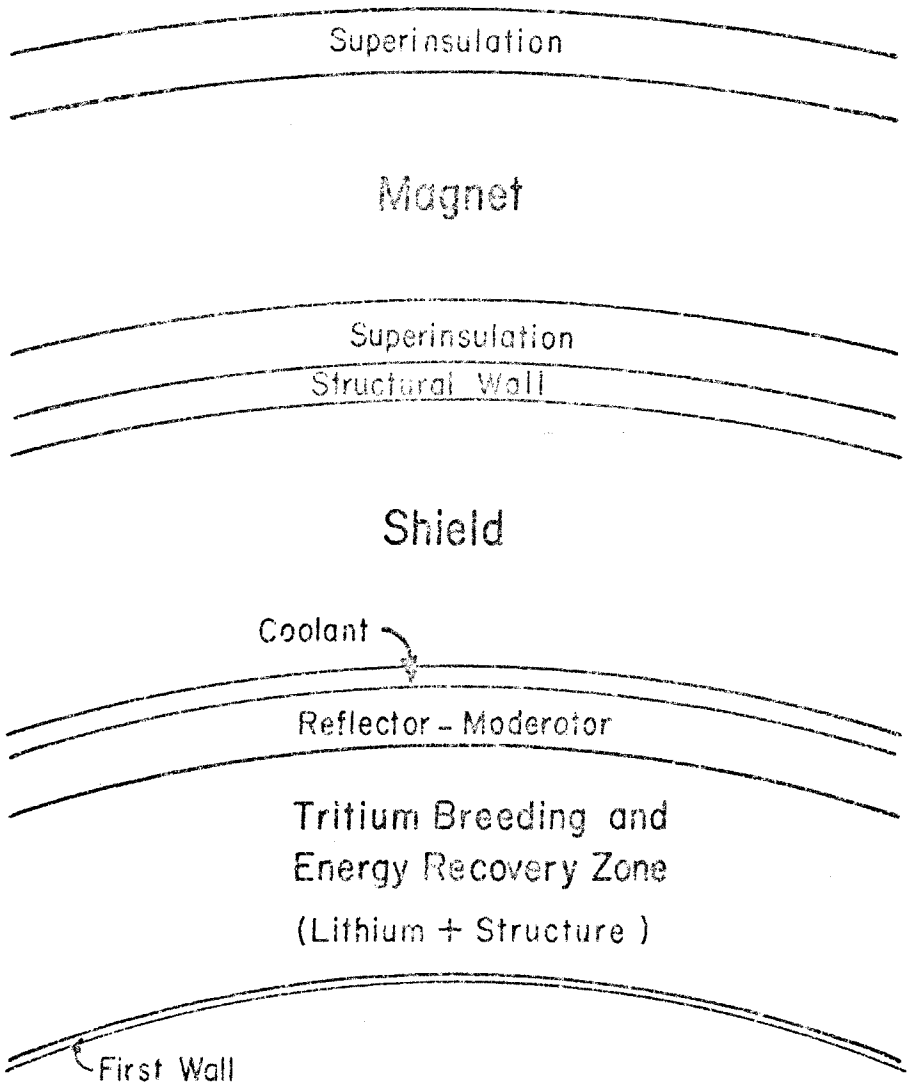

SCHEMATIC OF BLANKET AND SHIELD REGIONS

FIGURE 5.1

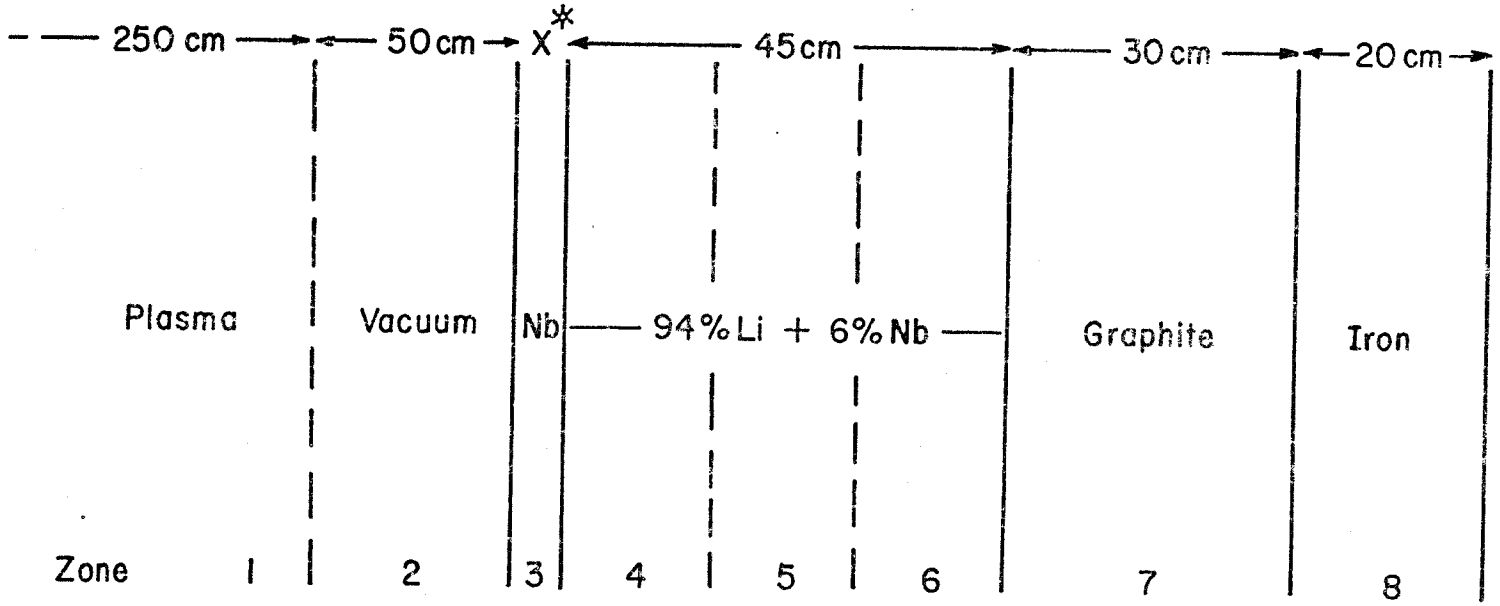

* X is a variable in this series of calculations.

FIG. 5.2 Reference Blanket Design for Investigating the Effect of Varying the First Wall Thickness

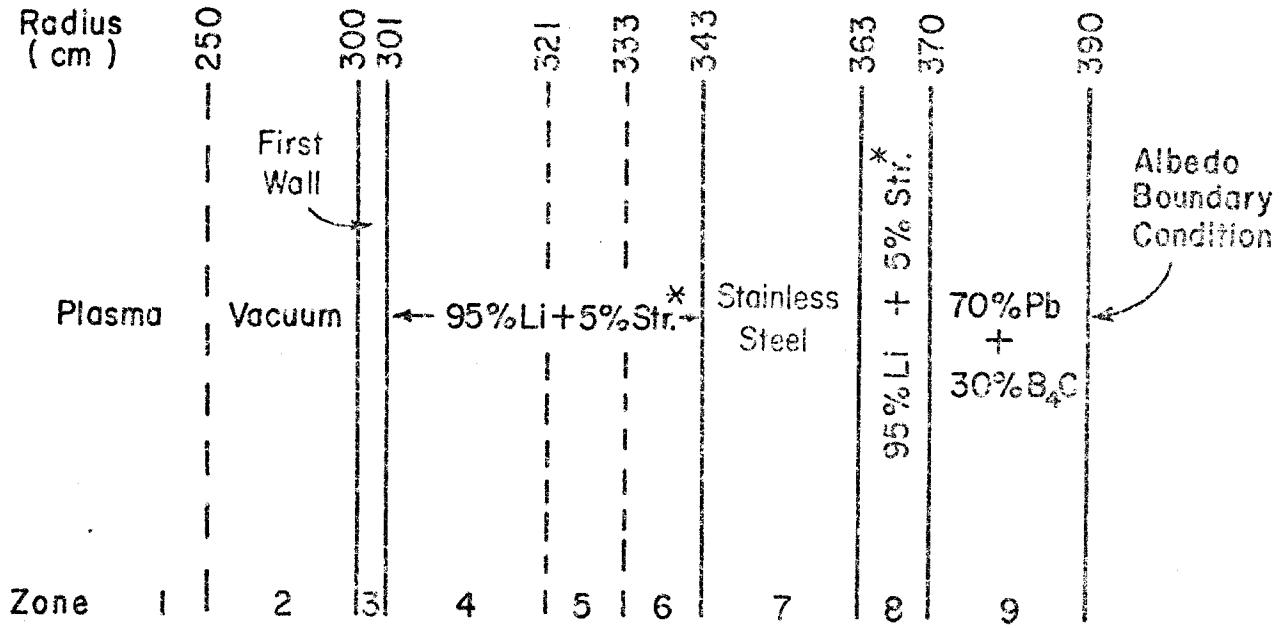

* Materials for first wall and structure are as follows:

Design 301: Niobium, Design 302: Vanadium, Design 303: Stainless Steel

Figure 5.3 Reference Design for Comparison of the performance of several materials for first wall and structure

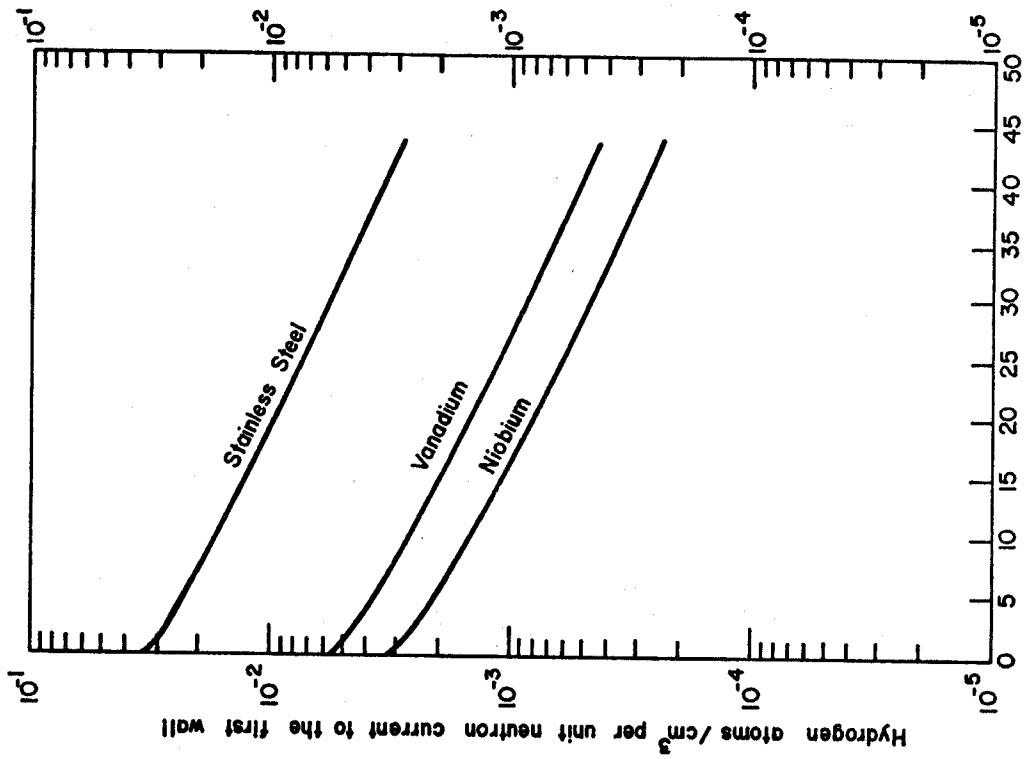

FIG. 5.5 Comparison of Hydrogen Production in Vanadium, Niobium and Stainless Steel

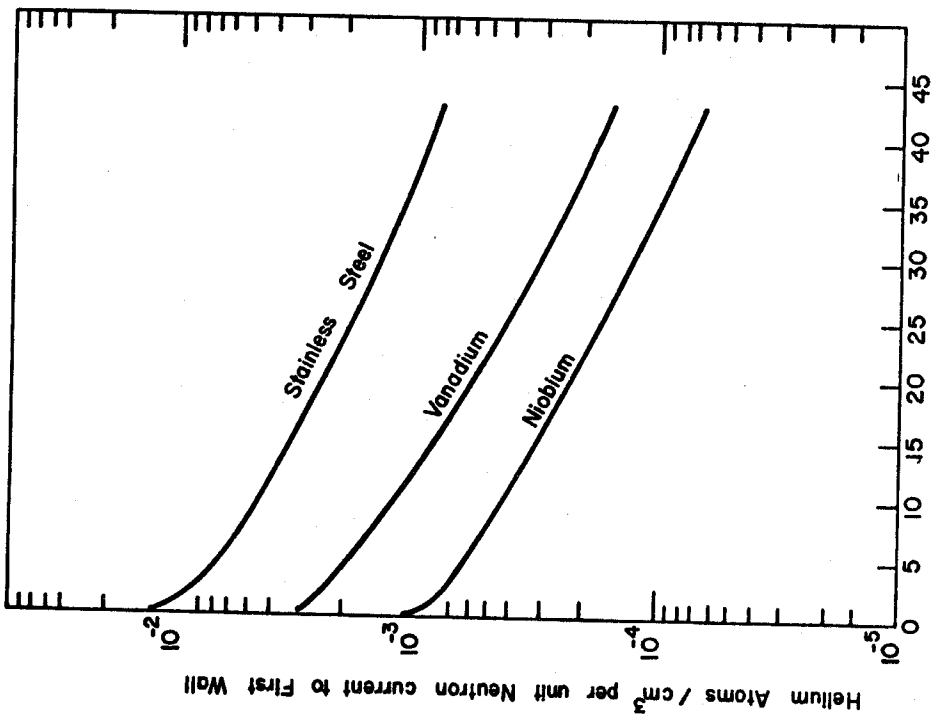

FIG. 5.4 Comparison of Hellium Production in Vanadium, Niobium & Stainless Steel

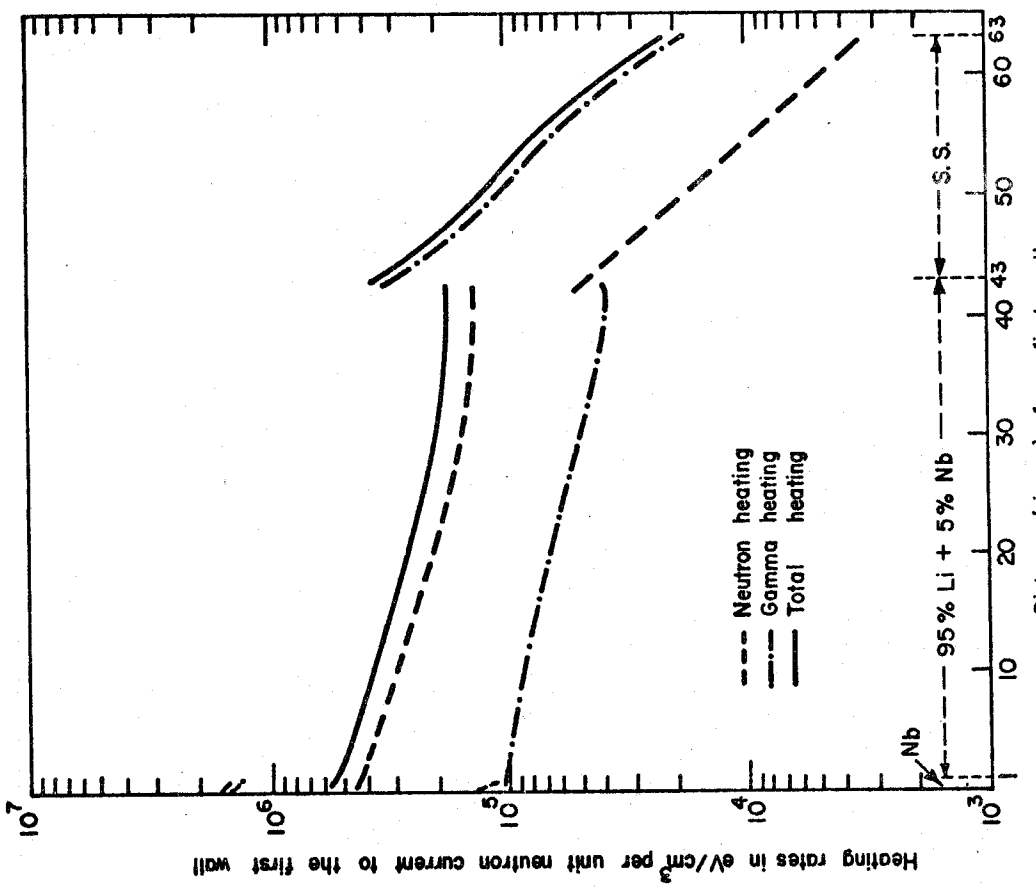

FIGURE 5.7 Spatial Dependence of Neutron, Gamma and Total Heating for Design 301 (Niobium Structure)

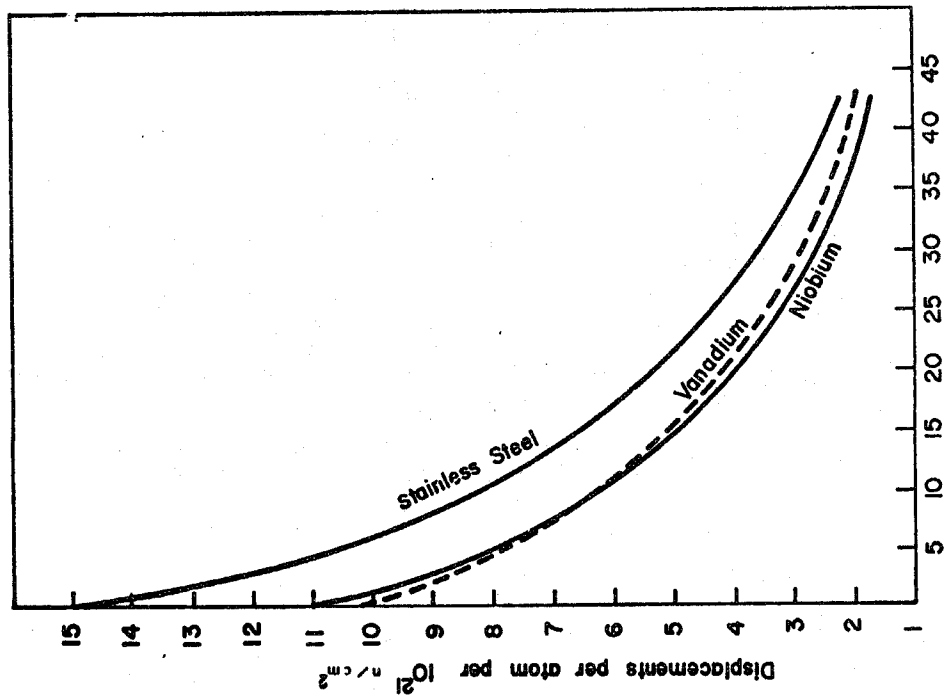

FIG. 5.6 Comparison of Atomic Displacement for Vanadium, Niobium & Stainless Steel

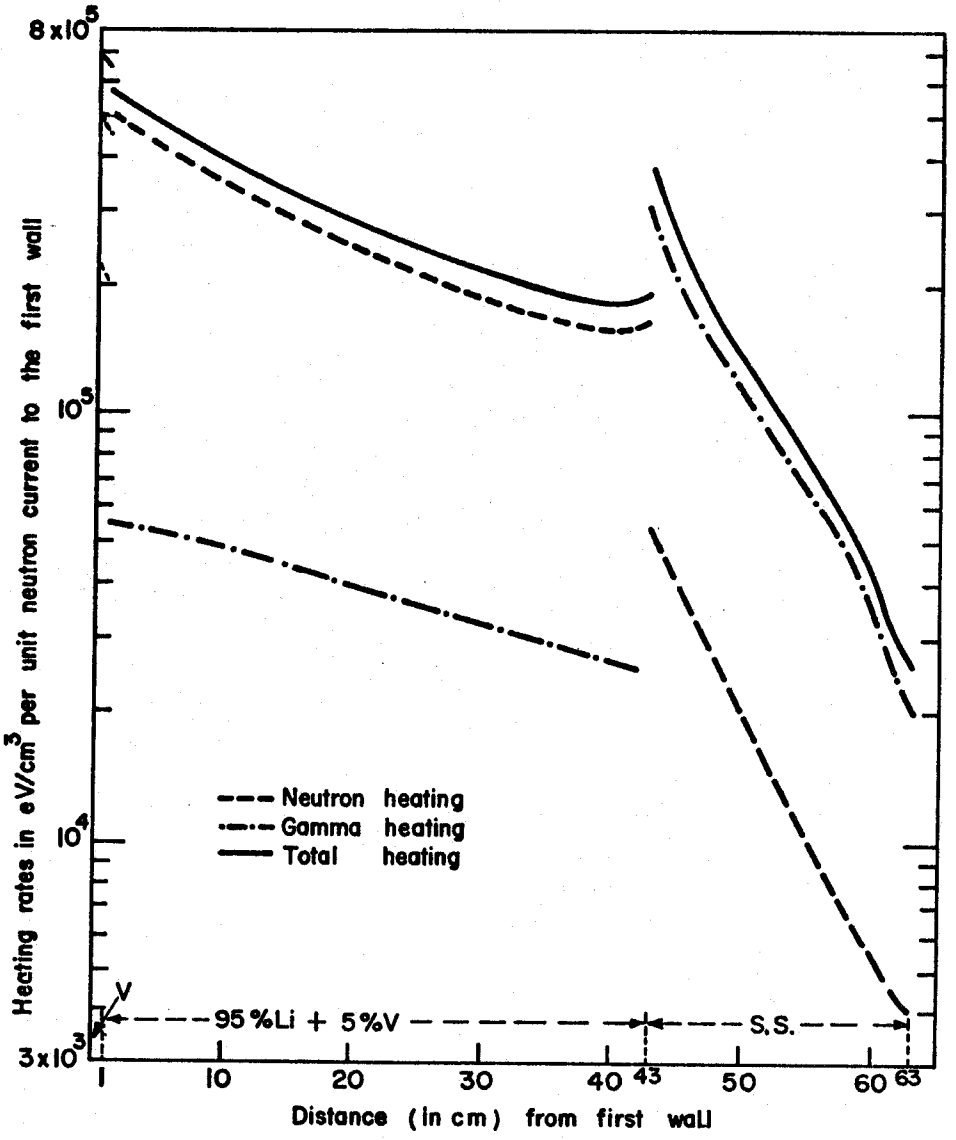

FIG. 5.8 Spatial Dependence of Neutron, Gamma and Total Heating for Design 302 (Vanadium Structure)

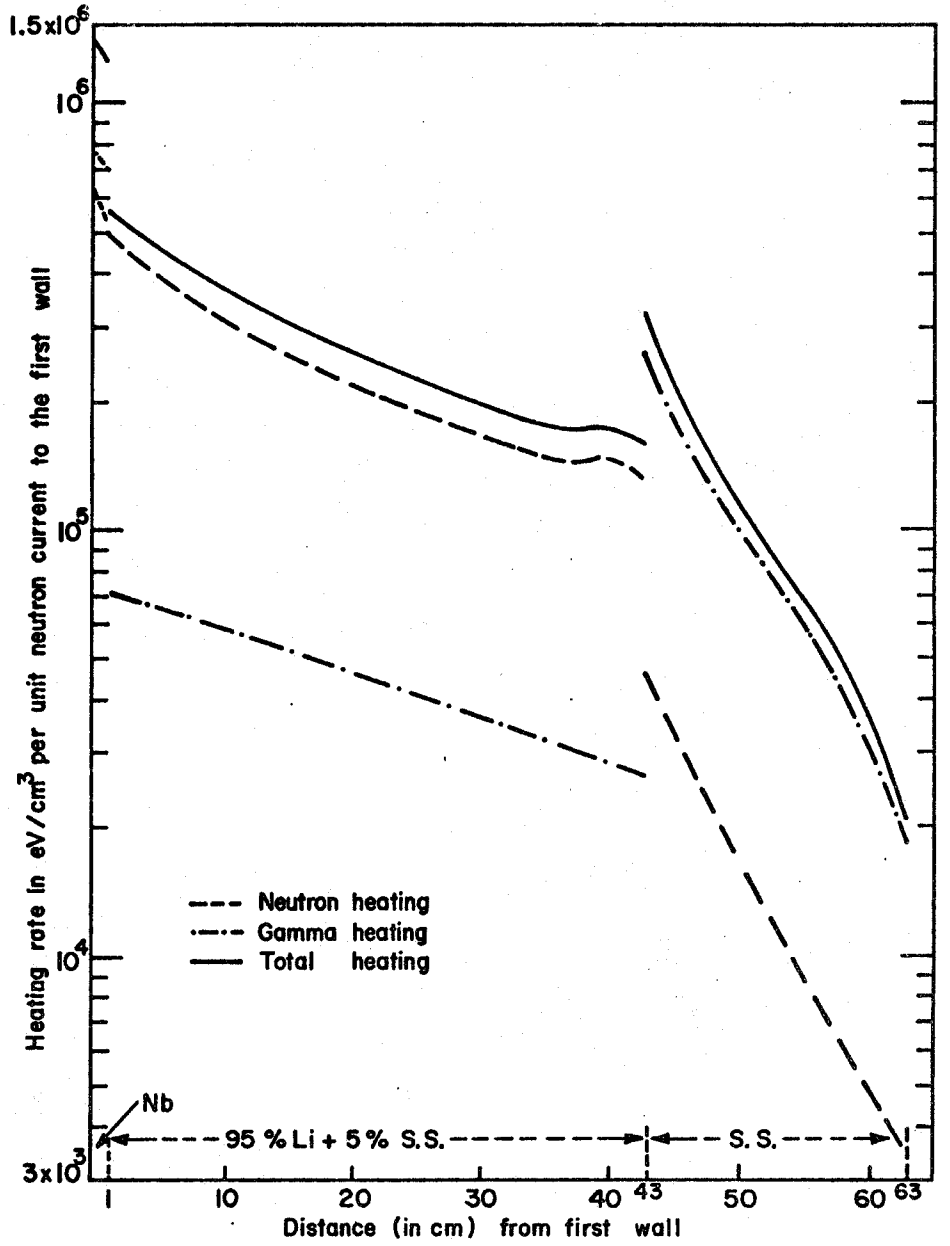

FIG. 5.9 Spatial Dependence of Neutron, Gamma & Total Heating for Design 303 (Stainless Steel Structure)

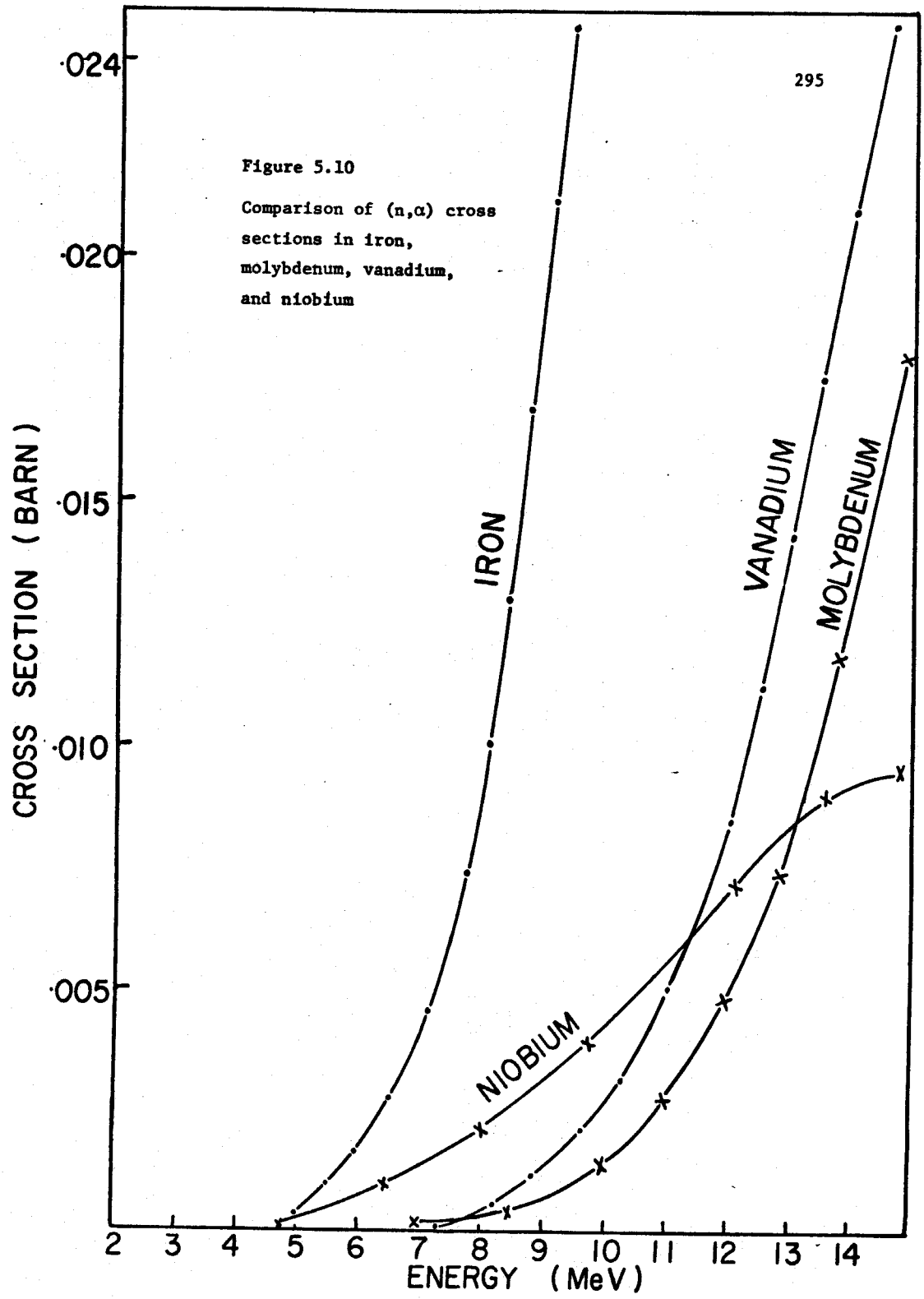

Figure 5.10

Comparison of (n,α) cross sections in iron, molybdenum, vanadium, and niobium

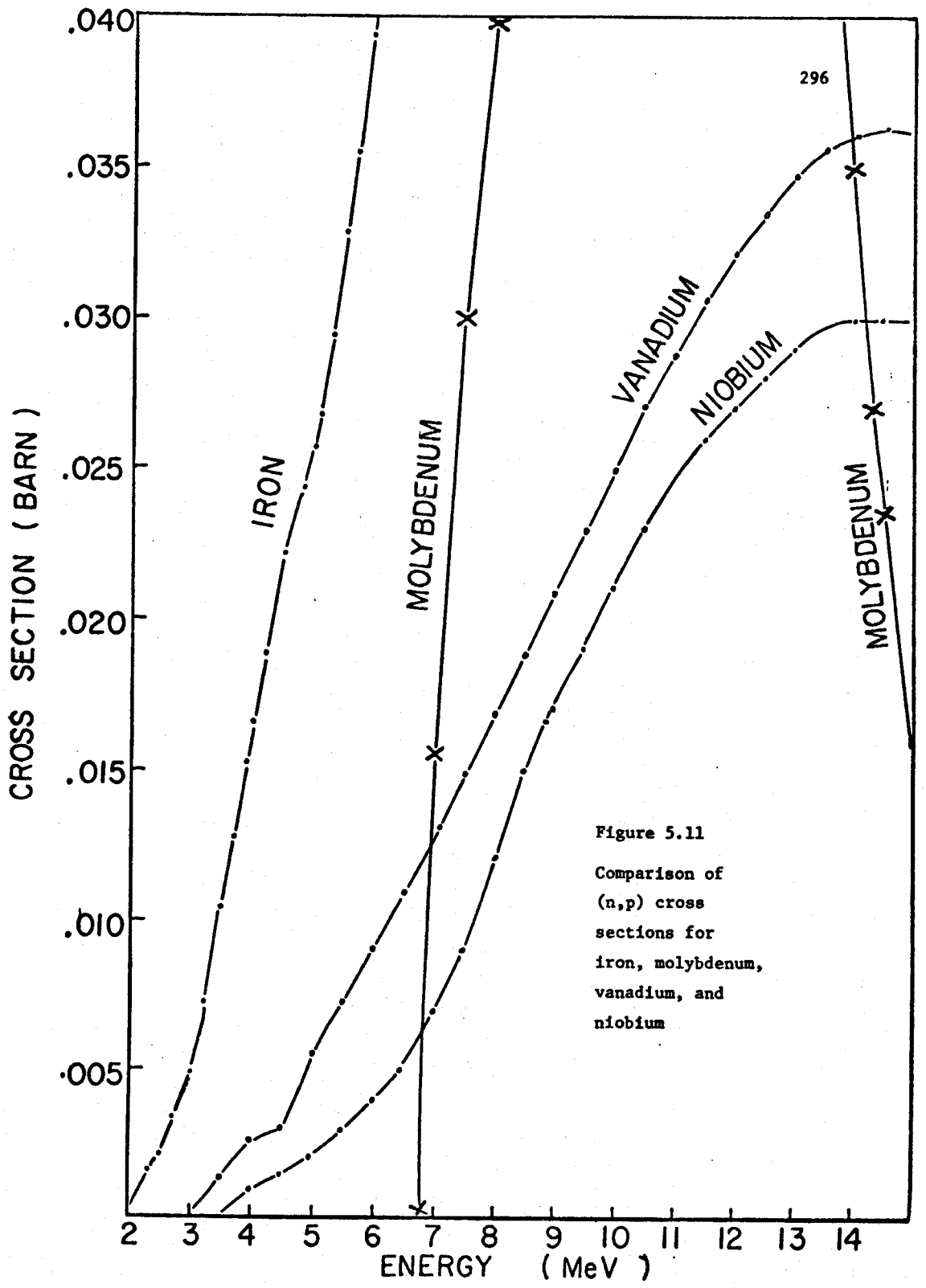

Figure 5.11

Comparison of (n,p) cross sections for iron, molybdenum, vanadium, and niobium

Figure 5.12

Comparison of (n,2n) cross sections
in iron, molybdenum, vanadium, and niobium

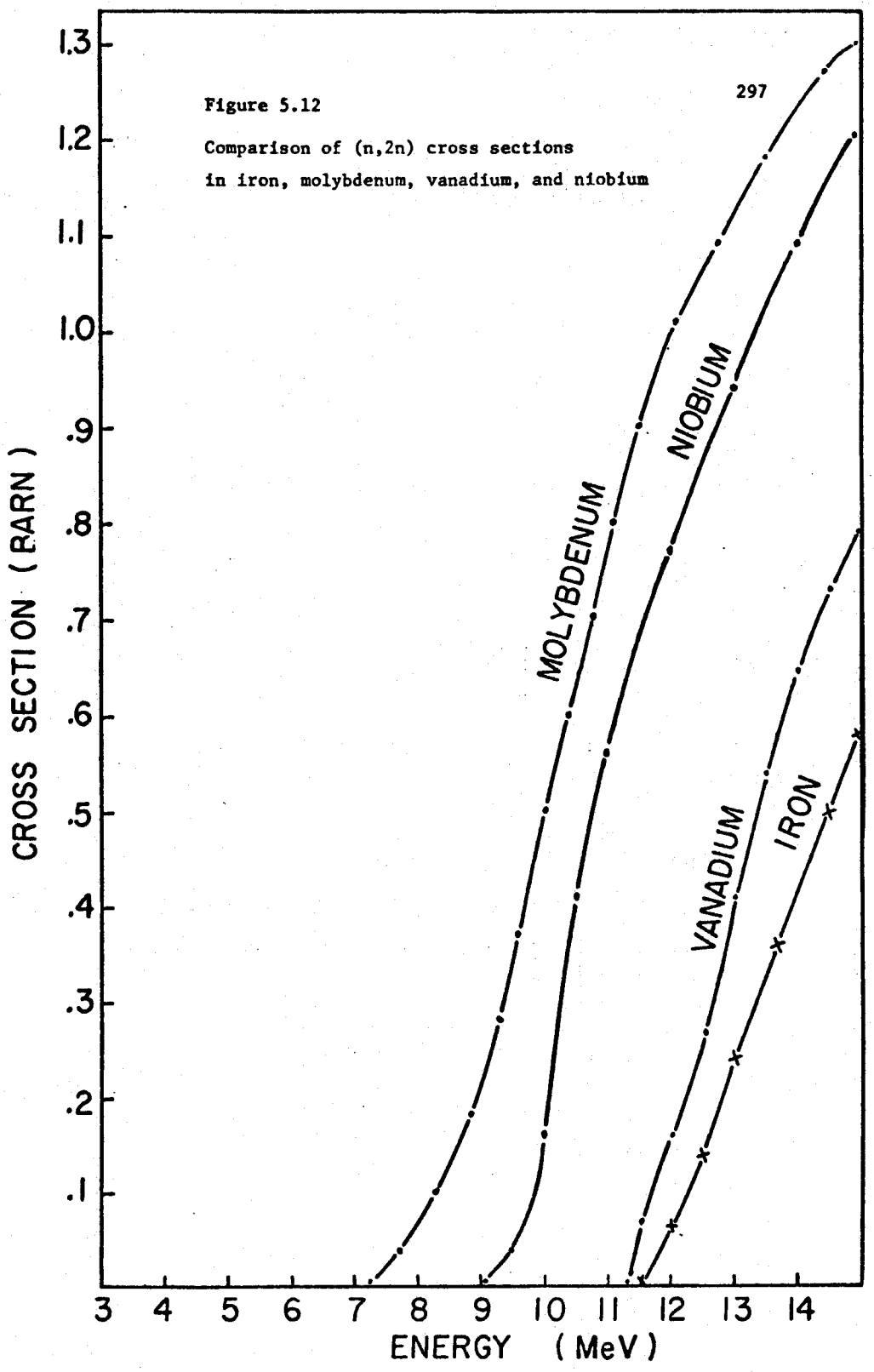

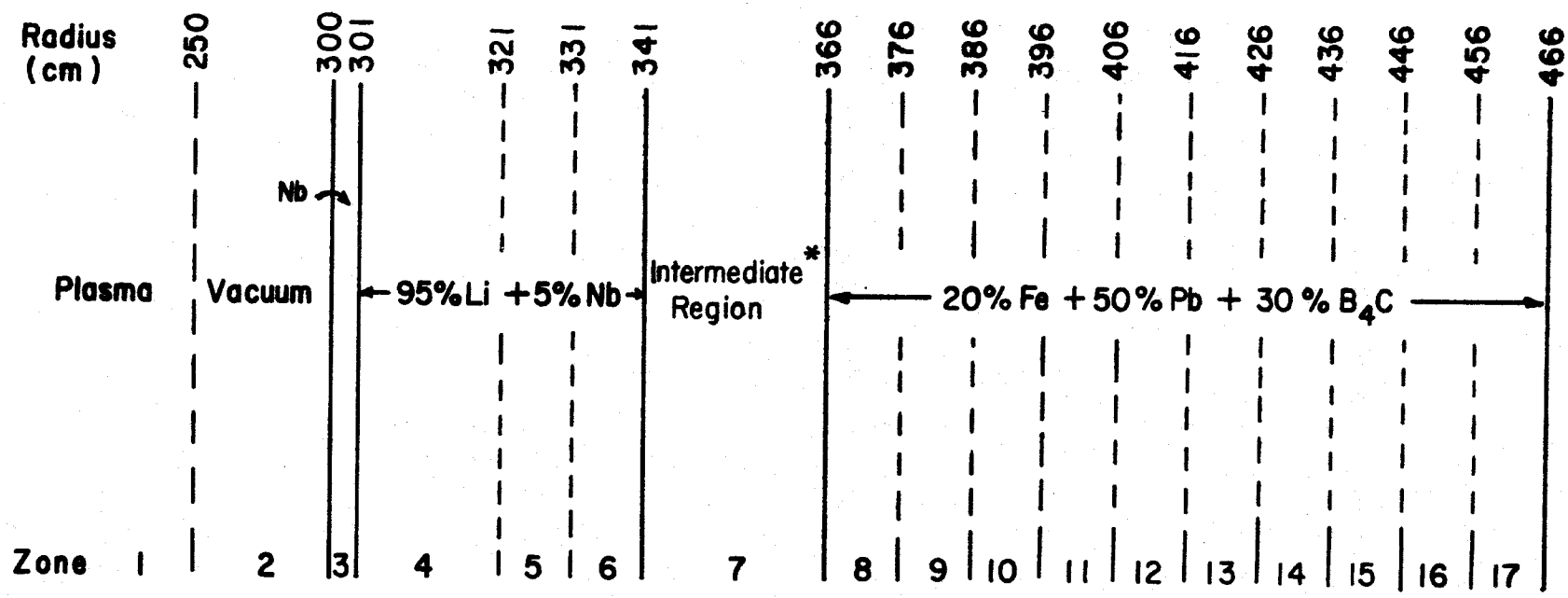

* The material composition in the intermediate region was varied as follows:

Design 110: Graphite

Design 111: 20% Fe + 50% Pb + 30% B_4C

Design 112: Iron

Figure 5.13 Reference Design for comparing the performance of various materials in the intermediate region

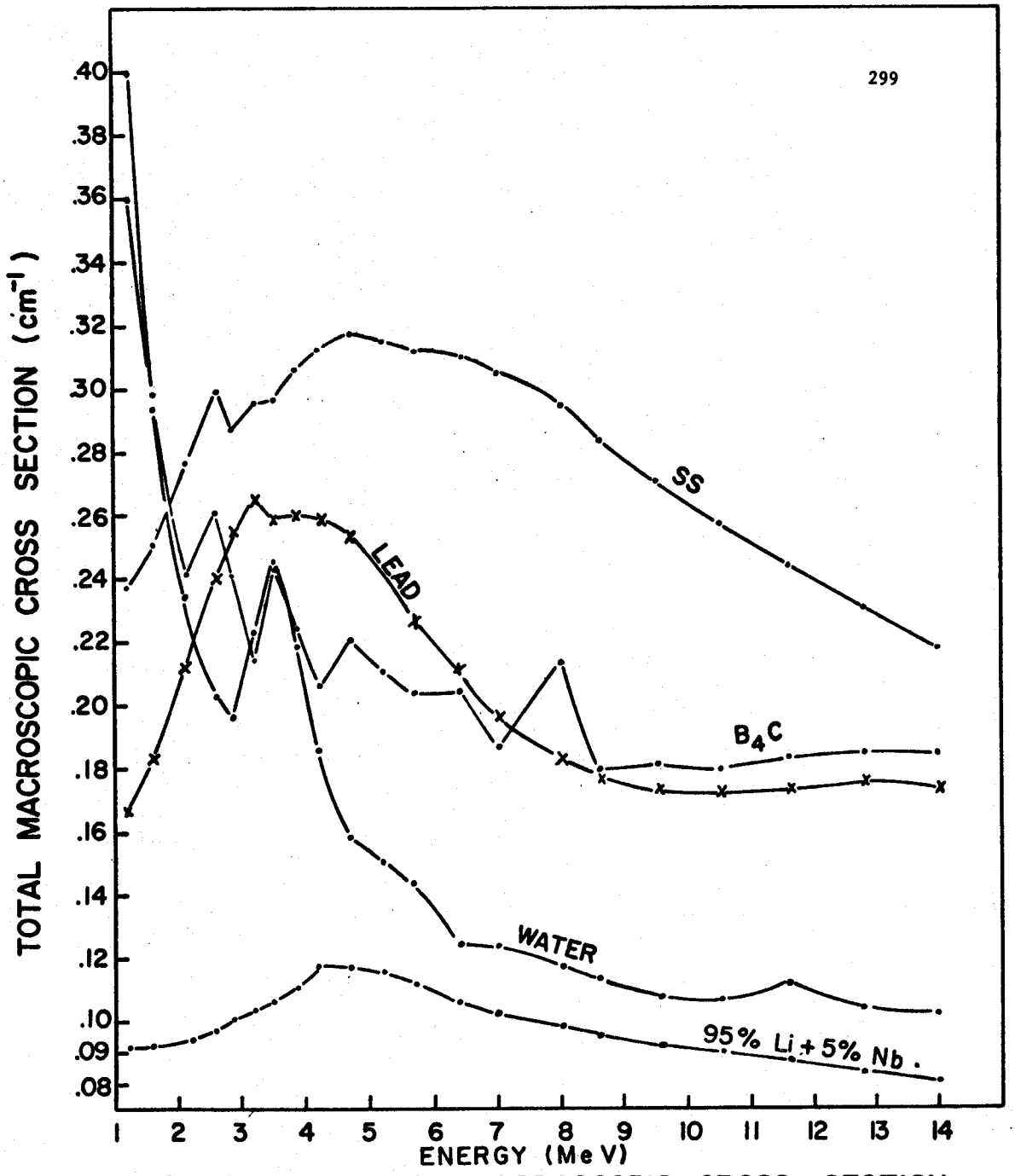

FIGURE 5.14_A TOTAL MACROSCOPIC CROSS SECTION FOR SEVERAL SHIELDING MATERIALS

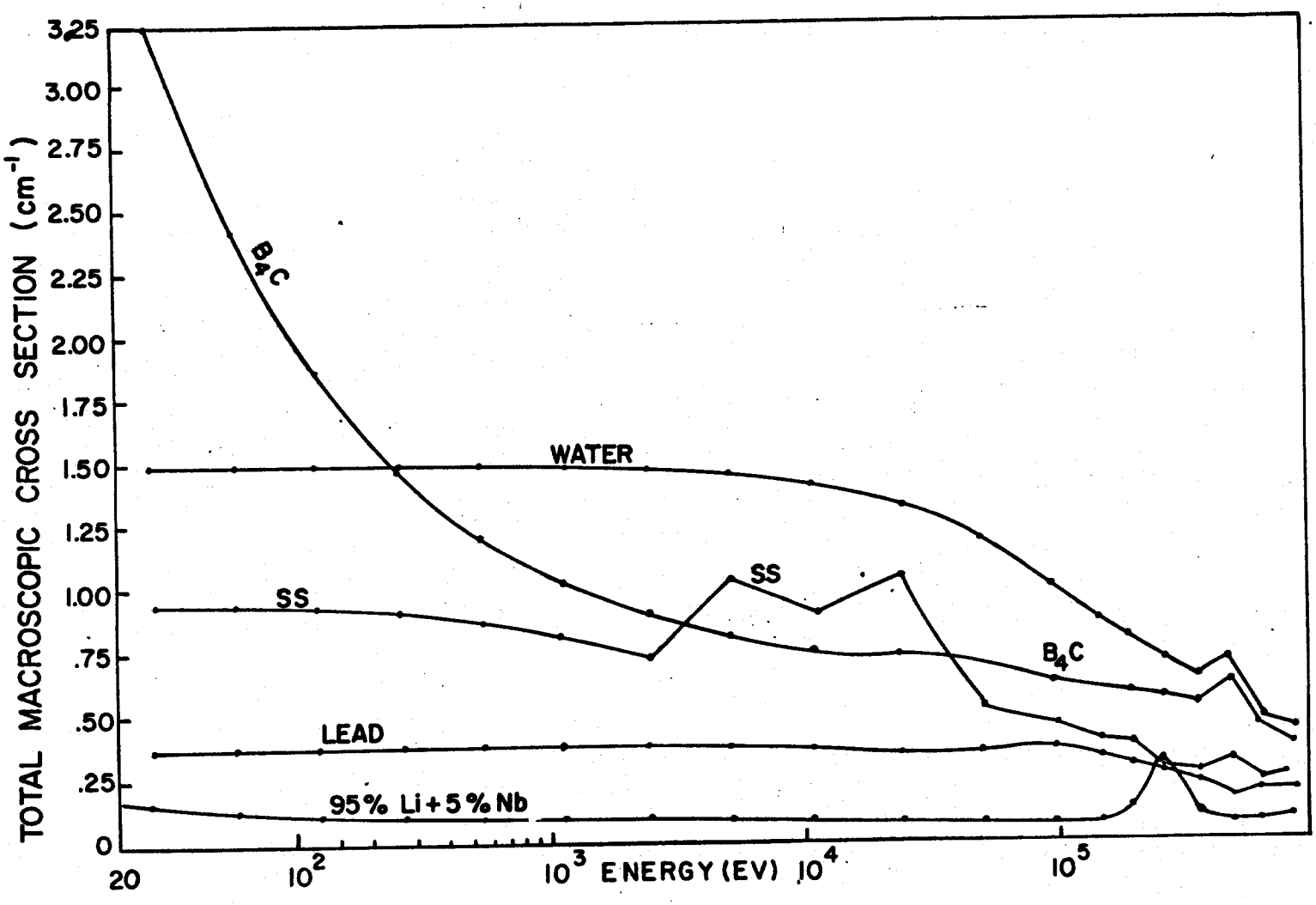

FIGURE 5.14_B TOTAL MACROSCOPIC CROSS SECTION FOR SEVERAL SHIELDING MATERIALS

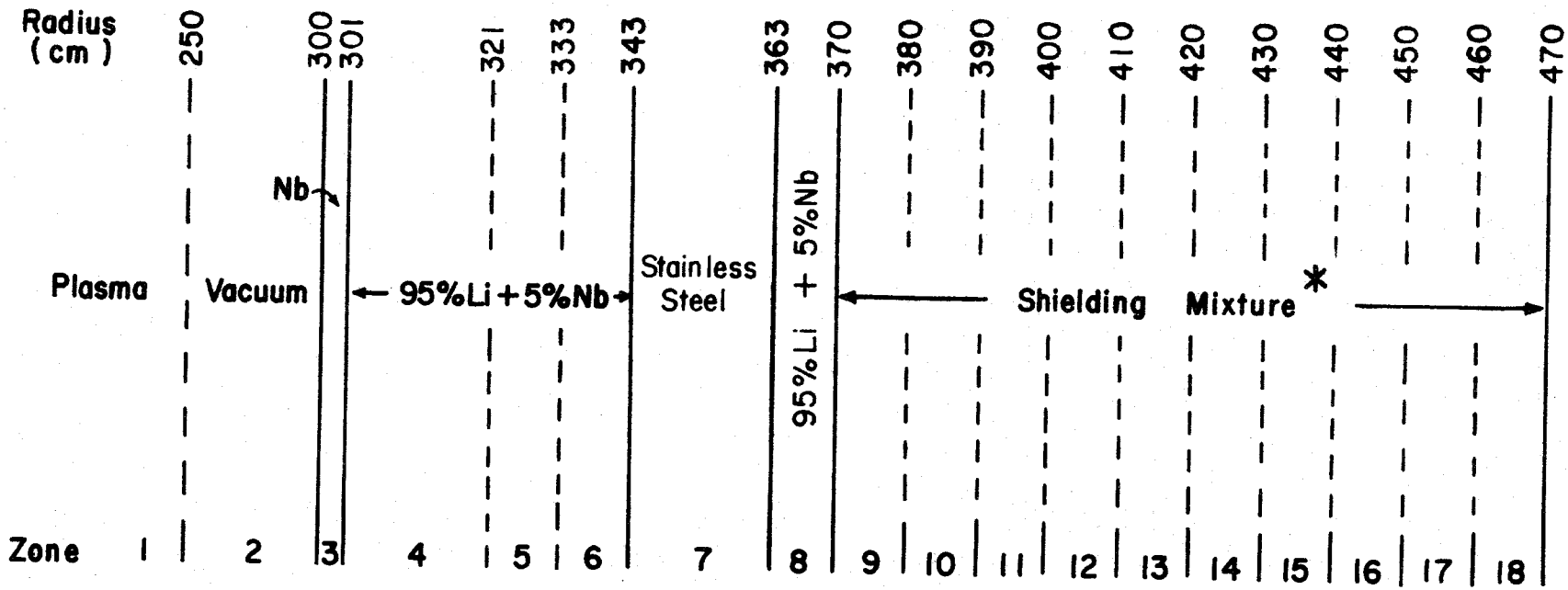

* Shielding mixture varies in this series of designs as follows:

Design 114: 70% SS + 30% B_4C, Design 115: 70% Pb + 30% B_4C, Design 116: 35% SS + 35% Pb + 30% B_4C,

Design 117: 100% SS

Figure 5.15 Reference Design for Shield Calculations

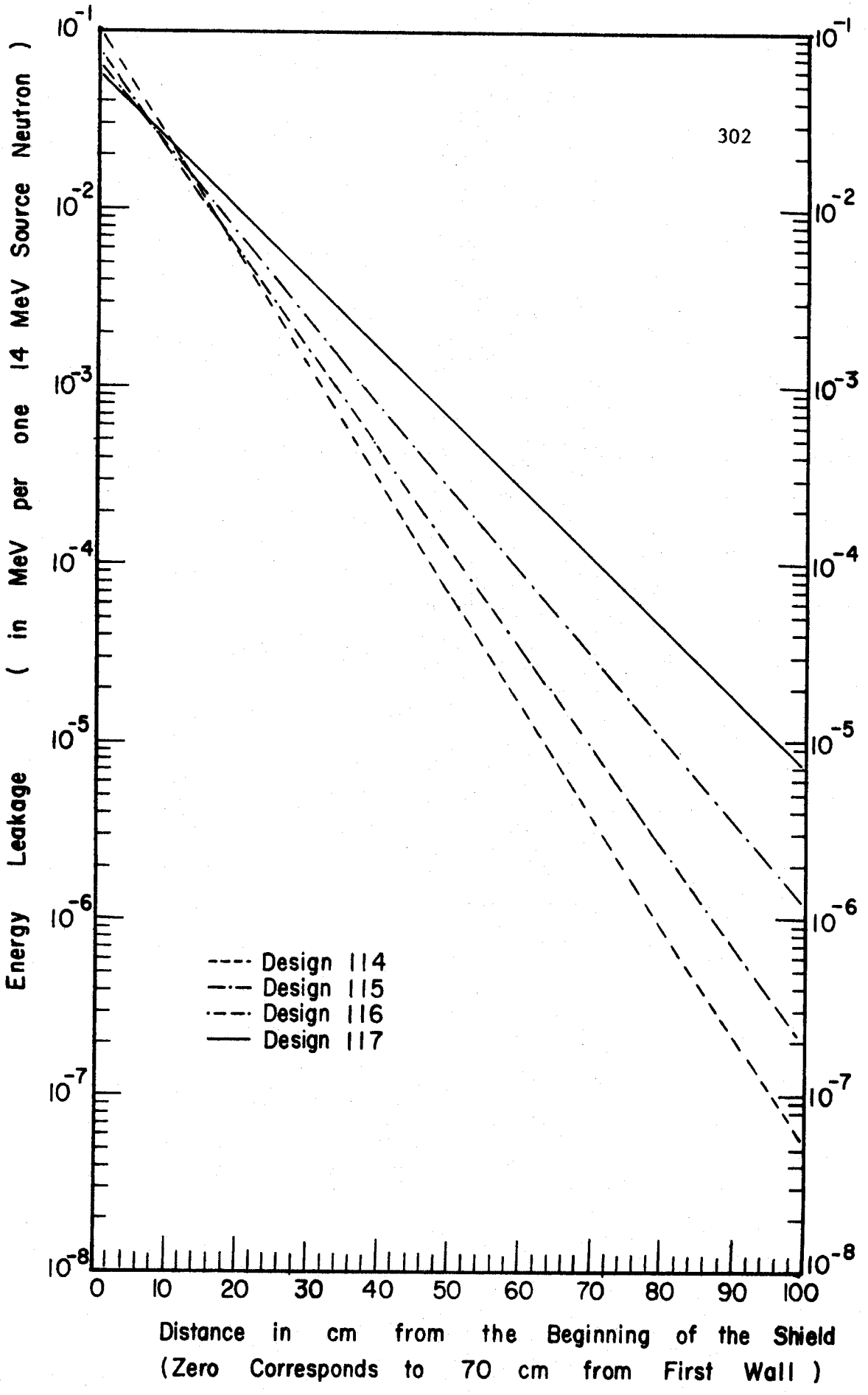
Energy Leakage (in MeV per one 14 MeV Source Neutron)
10^{-1}
10^{-2}
10^{-3}
10^{-4}
10^{-5}
10^{-6}
10^{-7}
10^{-8}
0 10 20 30 40 50 60 70 80 90 100
Distance in cm from the Beginning of the Shield
(Zero Corresponds to 70 cm from First Wall)
---- Design 114
—·— Design 115
-·-·- Design 116
—— Design 117

FIGURE 5.16

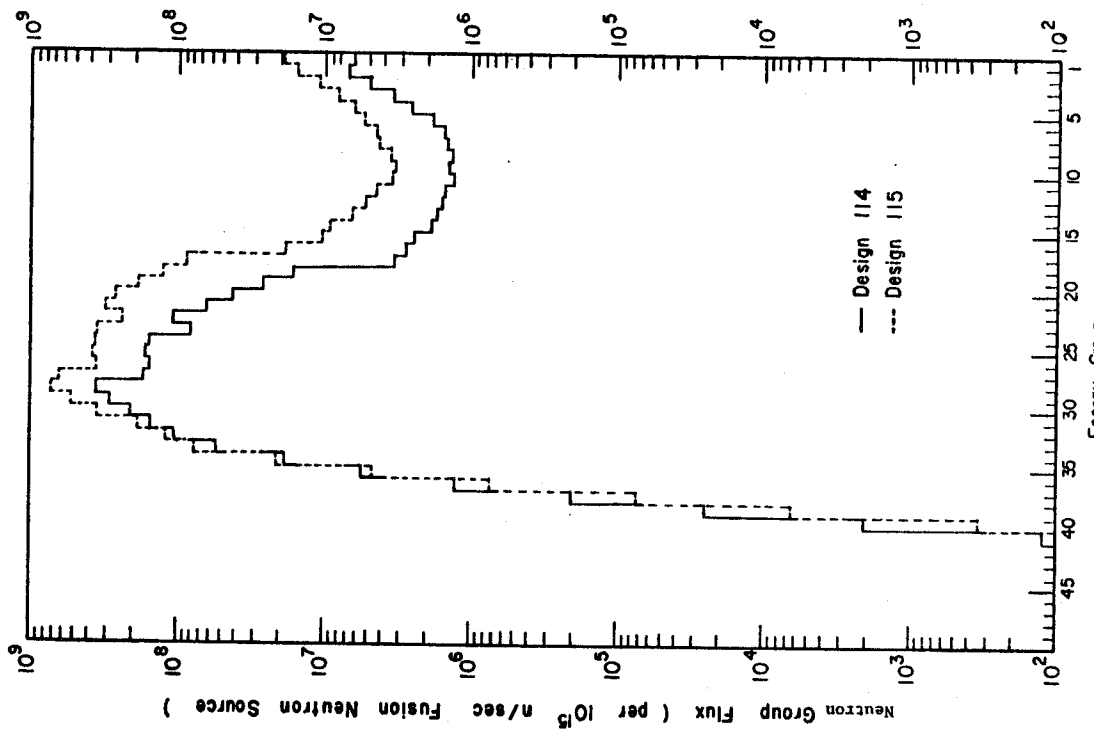

Comparison of Group Flux at 99 cm from the First Wall for Designs 114 and 115

FIGURE 5.17

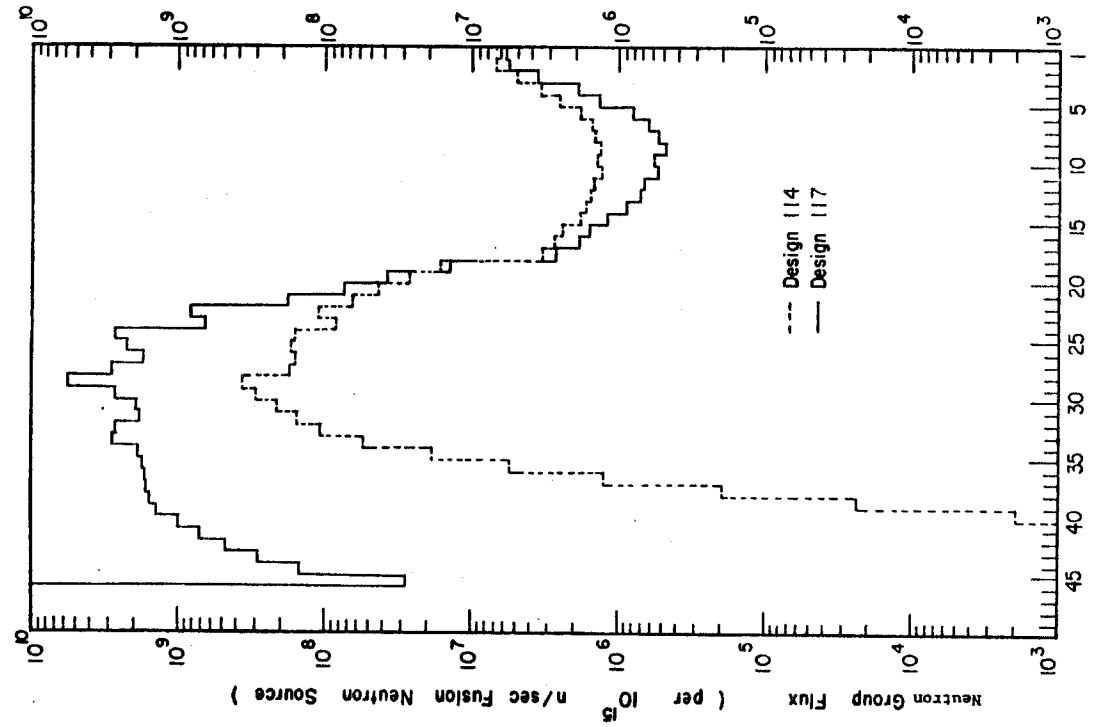

Comparison of Group Flux at 99 cm from the First Wall for Designs 114 and 117

FIGURE 5.18

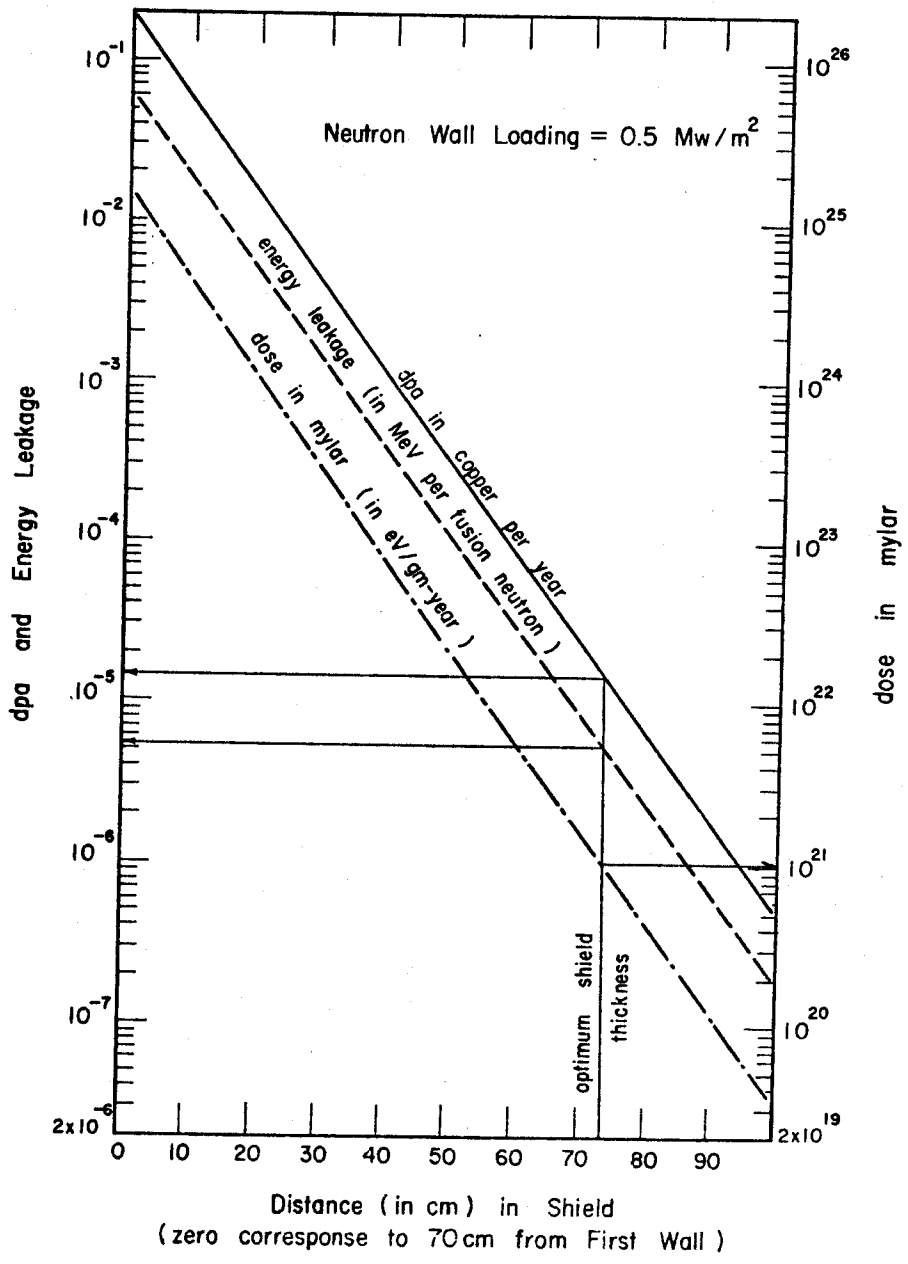

FIG. 5.19 Comparison of Atomic Displacement in Magnet Stabilizer (Copper) dose in Superinsulation (mylar) & Energy Leakage in a Typical Shield (35% Pb + 35% S.S. + 30% B_4C)

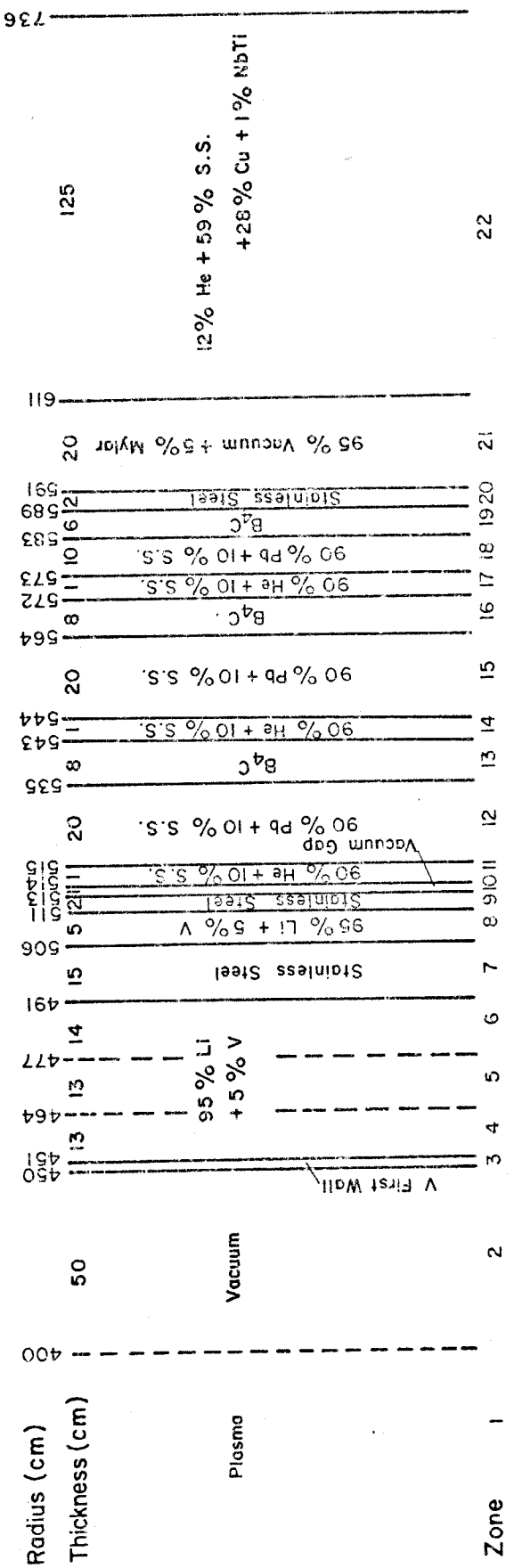

Figure 5.20 A Proposed Design of Blanket and Shield (Design 777)

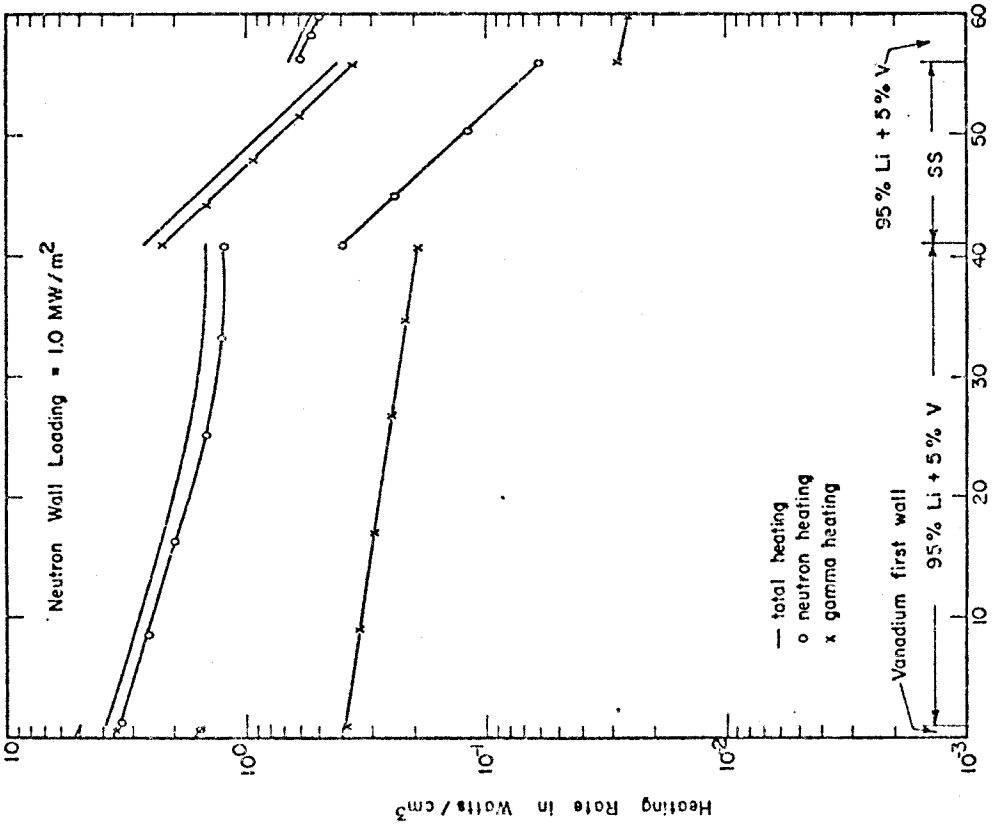

Figure 5.21 Spatial Distribution of Heating Rates in Blanket and Reflector Regions in Design 777.

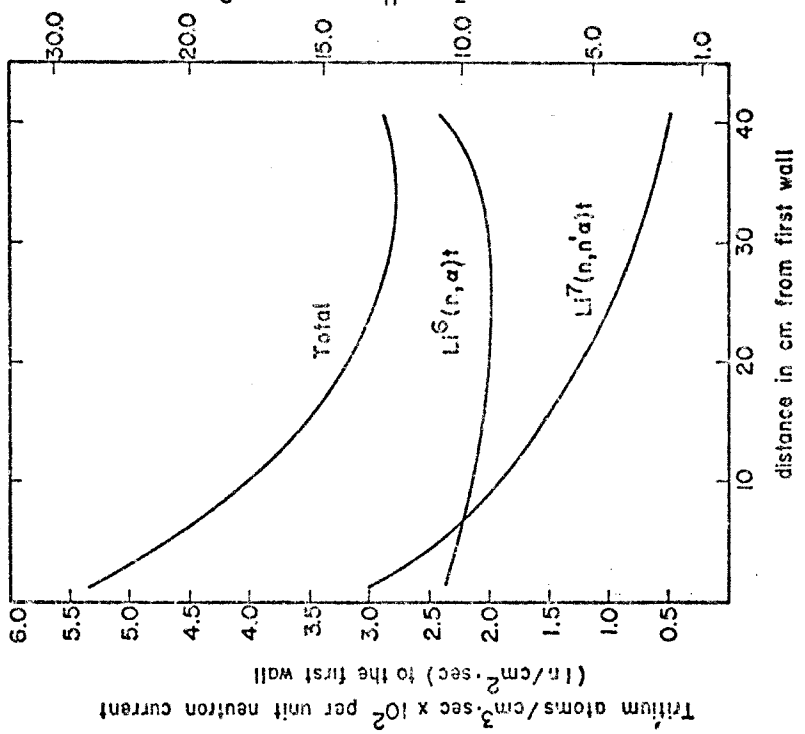

Figure 5.22 Spatial Distribution of Tritium Production in Design 777.

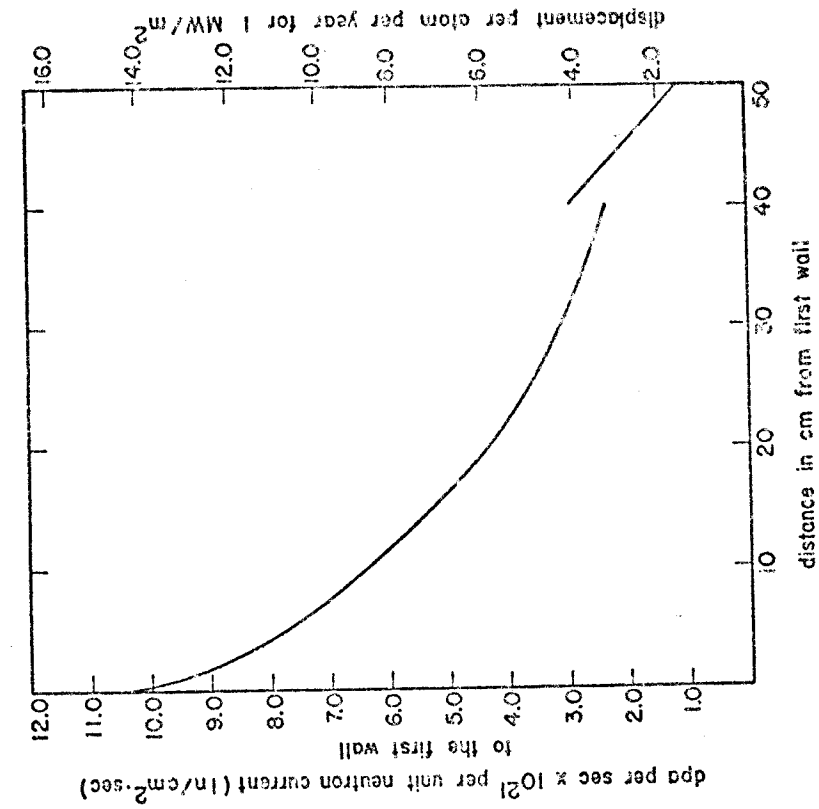

Figure 5.24 Spatial Distribution of Atomic Displacements in Vanadium and Stainless Steel in Design 777.

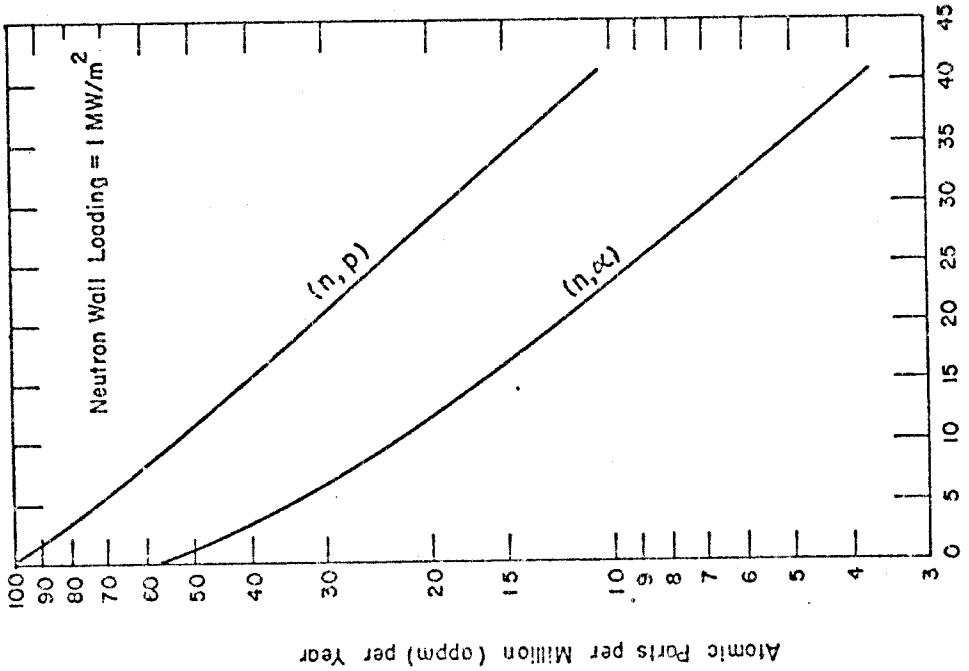

FIG. 5.23 Spatial Distribution of Helium & Hydrogen Production in Vanadium for Design 777

Table 5.1 Neutron 46 Energy Group Structure in eV

Group	Group Limits E(Top)	E(Low)	E(Mid-Point)
1	1.4918 (+7)	1.3499 (+7)	1.4208 (+7)
2	1.3499 (+7)	1.2214 (+7)	1.2856 (+7)
3	1.2214 (+7)	1.1052 (+7)	1.1633 (+7)
4	1.1052 (+7)	1.0000 (+7)	1.0526 (+7)
5	1.0000 (+7)	9.0484 (+6)	9.5242 (+6)
6	9.0484 (+6)	8.1873 (+6)	8.6178 (+6)
7	8.1873 (+6)	7.4082 (+6)	7.7977 (+6)
8	7.4082 (+6)	6.7032 (+6)	7.0557 (+6)
9	6.7032 (+6)	6.0653 (+6)	6.3843 (+6)
10	6.0653 (+6)	5.4881 (+6)	5.7767 (+6)
11	5.4881 (+6)	4.9659 (+6)	5.2270 (+6)
12	4.9659 (+6)	4.4933 (+6)	4.7296 (+6)
13	4.4933 (+6)	4.0657 (+6)	4.2795 (+6)
14	4.0657 (+6)	3.6788 (+6)	3.8722 (+6)
15	3.6788 (+6)	3.3287 (+6)	3.5038 (+6)
16	3.3287 (+6)	3.0119 (+6)	3.1703 (+6)
17	3.0119 (+6)	2.7253 (+6)	2.8686 (+6)
18	2.7253 (+6)	2.4660 (+6)	2.5956 (+6)
19	2.4660 (+6)	1.8268 (+6)	2.1464 (+6)
20	1.8268 (+6)	1.3534 (+6)	1.5901 (+6)
21	1.3534 (+6)	1.0026 (+6)	1.1780 (+6)
22	1.0026 (+6)	7.4274 (+5)	8.726 (+5)
23	7.4274 (+5)	5.5023 (+5)	6.4648 (+5)
24	5.5023 (+5)	4.0762 (+5)	4.7892 (+5)
25	4.0762 (+5)	3.0197 (+5)	3.5480 (+5)
26	3.0197 (+5)	2.2371 (+5)	2.6284 (+5)
27	2.2371 (+5)	1.6573 (+5)	1.9472 (+5)
28	1.6573 (+5)	1.2277 (+5)	1.4425 (+5)
29	1.2277 (+5)	6.7379 (+4)	9.508 (+4)
30	6.7379 (+4)	3.1828 (+4)	4.9604 (+4)

Table 5.1 (cont.)

Group	Group Limits E(Top)	E(Low)	E(Mid-Point)
31	3.1828 (+4)	1.5034 (+4)	2.3431 (+4)
32	1.5034 (+4)	7.1017 (+3)	1.1068 (+4)
33	7.1017 (+3)	3.3546 (+3)	5.2281 (+3)
34	3.3546 (+3)	1.5846 (+3)	2.4696 (+3)
35	1.5846 (+3)	7.4852 (+2)	1.1666 (+3)
36	7.4852 (+2)	3.5358 (+2)	5.5105 (+2)
37	3.5358 (+2)	1.6702 (+2)	2.6030 (+2)
38	1.6702 (+2)	7.8893 (+1)	1.2296 (+2)
39	7.8893 (+1)	3.7267 (+1)	5.8080 (+1)
40	3.7267 (+1)	1.7603 (+1)	2.7435 (+1)
41	1.7603 (+1)	8.3153 (+0)	1.2959 (+1)
42	8.3153 (+0)	3.9279 (+0)	6.1216 (+0)
43	3.9279 (+0)	1.8554 (+0)	2.8917 (+0)
44	1.8554 (+0)	8.7643 (-1)	1.3659 (+0)
45	8.7643 (-1)	4.1399 (-1)	6.4521 (-1)
46	4.1399 (-1)	2.2000 (-2)	2.1800 (-1)

Table 5.2 Effect of Thickness of First Wall

(Results normalized to one fusion (14 MeV) neutron)

Cylinder, S_6, P_3

Design thickness of first wall		101 0.5 cm.	102 1.0 cm.	103 2.0 cm.
Response	Zone			
Nb(n,2n)	3	5.2897	9.8506	17.3833
$\times 10^2$	4	5.2154	4.6861	3.8342
	5	1.9844	1.8340	1.5716
	6	0.8643	0.8037	0.6957
	Total	13.3538	17.1743	23.4847
Nb(n,p)	3	1.5610	2.8655	4.9596
$\times 10^3$	4	1.6606	1.4832	1.2051
	5	0.7047	0.6475	0.5501
	6	0.3309	0.3061	0.2629
	Total	4.2573	5.3022	6.9777
$Li^6(n,\alpha)t$	4	0.2411	0.2484	0.2590
	5	0.2252	0.2283	0.2318
	6	0.3421	0.3427	0.3411
	T_6	0.8084	0.8193	0.8320
$Li^7(n,n'\alpha)t$	4	0.3173	0.2812	0.2263
	5	0.1522	0.1388	0.1167
	6	0.0771	0.0709	0.0604
	T_7	0.5467	0.4909	0.4034
$T_6 + T_7$	T	1.3551	1.3102	1.2354
Neutron Heating for Nb	Total	0.1755	0.2194	0.2947
Li^6	Total	4.5673	4.5685	4.5457
Li^7	Total	5.8782	5.3838	4.5806
C^{12}	Total	0.8335	0.7733	0.6692

Table 5.3-a Neutron Heating (in MeV per one fusion neutron) by Material and Zone for Design 301

Zone	Outer Radius (cm.)	Material	Li^6	Li^7	Nb	Fe	Cr	Ni	sum by zone
3	301	Niobium	------	------	0.1275	------	------	------	0.1275
4	321	95% Li	2.1832	3.8884	0.0650	-----	-----	-----	6.1366
5	333	+	1.0849	1.0169	0.0162	------	------	------	2.1180
6	343	5% Nb	0.9084	0.5148	0.0083	------	------	------	1.4315
7	363	SS	-----	-----	-----	0.2121	0.0489	0.0720	0.3330
8	370	95% Li + 5% Nb	0.1401	0.0210	0.0004	-----	-----	-----	0.1615
sum by material			4.3166	5.4411	0.2174	0.2121	0.0489	0.0720	10.308

Table 5.3-b Neutron and Gamma Heating*

for Design 301

Zone	Outer Radius (cm.)	Material	Neutron Heating	Gamma Heating	Total Heating
3	301	Niobium	0.1275	1.5361	1.6635
4	321	95% Li	6.1366	1.7399	7.8765
5	333	+	2.1180	0.6781	2.7961
6	343	5% Nb	1.4315	0.4247	1.8562
7	363	SS	0.3330	2.1933	2.5263
8	370	95% Li + 5% Nb	0.1615	0.0120	0.1735
Sum over zones 3 through 8			10.3081	6.5841	16.8921

* in MeV per (14 MeV) fusion neutron

Table 5.4-a Neutron Heating (in MeV per one fusion neutron)

by Material and Zone for Design 302

Zone	Outer Radius (cm.)	Material	Li^6	Li^7	V	Fe	Cr	Ni	Sum by Zone
3	301	Vanadium	------	------	0.2208	------	------	------	0.2208
4	321	95% Li	2.5343	4.2939	0.1205	------	------	------	6.9487
5	333	+	1.2618	1.1397	0.0337	------	------	------	2.4352
6	343	5% V	1.0448	0.5806	0.0191	------	------	------	1.6445
7	363	SS	------	------	------	0.2340	0.0538	0.0801	0.2958
8	370	95% Li + 5% V	0.1557	0.0235	0.0013	------	------	------	0.1805
Sum by Material			4.9966	6.0376	0.3953	0.2340	0.0538	10.0801	11.797

Table 5.4-b Neutron and Gamma Heating* for Design 302

Zone	Outer Radius (cm.)	Material	Neutron Heating*	Gamma Heating*	Total Heating*
3	301	Vanadium	.2208	0.4881	0.7089
4	321	95% Li	6.9487	0.9494	7.8981
5	333	+	2.4352	0.4135	2.8487
6	343	5% V	1.6445	0.2766	1.9211
7	363	SS	0.2958	2.0718	2.3676
8	370	95% Li + 5% V	0.1805	0.0093	0.1898
Sum over aones 3 through 8			11.7255	4.2087	15.9342

* in MeV per one (14 MeV) fusion neutron

Table 5.5-a Neutron Heating (in MeV per one fusion neutron) by Material and Zone for Design 303

Zone	Outer Radius (cm.)	Material	Li^6	Li^7	Fe	Cr	Ni	Sum by Zone
3	301	SS	------	------	0.3858	0.0836	0.1322	0.6016
4	321	95% Li	2.2932	3.8189	0.1825	0.0398	0.0659	6.4003
5	333	+	1.1276	0.9961	0.0411	0.0091	0.0156	2.1895
6	343	5% SS	0.9406	0.5013	0.0197	0.0044	0.0074	1.4734
7	363	SS	------	------	0.2039	0.0469	0.0696	0.3204
8	370	95% Li + 5% SS	0.1397	0.0202	0.0006	0.0001	0.0002	0.1608
Sum by Material			4.5010	5.3364	0.8336	0.1840	0.2908	11.1458

Table 5.5-b Neutron and Gamma Heating* for Design 303

Zone	Outer Radius (cm)	Material	Neutron Heating	Gamma Heating	Total Heating
3	301	SS	o.6016	0.7732	1.3748
4	321	95% Li	6.4003	1.2061	7.6064
5	333	+	2.1895	0.4809	2.6704
6	343	5% SS	1.4734	0.3058	1.7792
7	363	SS	0.3204	1.8749	2.1953
8	370	95% Li + 5% SS	0.1608	0.0023	0.1631
Sum over zones 3 through 8			11.1458	4.6432	15.7890

* in MeV per one (14 MeV) fusion neutron

Table 5.6 Comparison of Radiation Damage Parameters, Tritium Production, and Nuclear Heating for Various Structural Materials (Designs 301, 302 & 303)

Design ID		301	302	303
First Wall & Structure		Niobium	Vanadium	Stainless Steel
Response	Zone			
(n,α) in strucural material (reactions per one fusion neutron)×10^4	3	9.4470	28.9301	124.0960
	4	4.3312	12.3060	55.1620
	5	0.9119	2.2741	10.3739
	6	0.4181	1.0062	4.6977
	7	------	------	------
	8	0.0084	0.0020	0.1019
	S_z^*	15.1166	44.5364	194.4315
displacements per atom per 10^{21} fusion neutron	3	10.6349	9.9863	14.3119
(n,p) in structural material (reactions per one fusion neutron)×10^3	3	3.1985	5.4179	25.0850
	4	1.5423	2.7168	12.0252
	5	0.3440	0.6203	2.6478
	6	0.1601	0.2915	1.7909
	7	------	------	------
	8	0.0032	0.0058	0.0361
	S_z^*	5.2482	9.0522	41.5850
(n,2n) in structural material	3	0.1099	0.0858	0.0523
	4	0.0478	0.0351	0.0199
	5	0.0094	0.0061	0.0033
	6	0.0042	0.0026	0.0033
	7	------	------	------
	8	0.0001	0.0001	≈0.0
	S_z^*	0.1715	0.1296	0.0760
Li^6 (n,α) t	4	0.3671	0.4329	0.3927
	5	0.2016	0.2362	0.2114
	6	0.1763	0.2035	0.1836
	T_6	0.7734	0.9042	0.8161
Li^7(n,n'α)t	4	0.3566	0.4009	0.3598
	5	0.0910	0.1033	0.0908
	6	0.0434	0.0496	0.0429
	T_7	0.4918	0.5547	0.4944

(continued on next page)

Table 5.6 (continued)
Comparison of Radiation Damage Parameters, Tritium Production, and Nuclear Heating for Various Structural Materials (Designs 301, 302 & 303)

Design ID		301	302	303
First Wall & Structure		Niobium	Vanadium	Stainless Steel
Response	Zone			
Tritium Breeding Ratio	T	1.2652	1.4589	1.3105
Neutron Heating in MeV per one fusion neutron	3	0.1275	0.2208	0.6016
	4	6.1366	6.9487	6.4003
	5	2.1180	2.4352	2.1895
	6	1.4315	1.6445	1.4734
	7	0.3330	0.2958	0.3204
	8	0.1615	0.1805	0.1608
	S_z^*	10.3081	11.7255	11.1458
Gamma Heating in MeV per one fusion neutron	3	1.5361	0.4881	0.7732
	4	1.7399	0.9494	1.2061
	5	0.6781	0.4135	0.4809
	6	0.4247	0.2766	0.3058
	7	2.1933	2.0718	1.8749
	8	0.0120	0.0093	0.0023
	S_z^*	6.5841	4.2087	4.6432
Total Heating in MeV per one neutron fusion	3	1.6635	0.7089	1.3748
	4	7.8765	7.8981	7.6064
	5	2.7961	2.8487	2.6704
	6	1.8562	1.9211	1.7792
	7	2.5263	2.3676	2.1953
	8	0.1735	0.1898	0.1631
	S_z^*	16.8921	15.9342	15.7890
Net Energy† Leakage from Zone 8				
neutrons----------		0.0672	0.0754	0.0649
gammas----------		0.0367	0.0404	0.0324

(continued on next page)

Table 5.6 (continued)
Comparison of Radiation Damage Parameters, Tritium Production, and Nuclear Heating for Various Structural Materials (Designs 301, 302 & 303)

Design ID		301	302	303
First Wall & Structure		Niobium	Vanadium	Stainless Steel
Response	Zone			
Secondary Gamma Production in MeV per one fusion neutron	3	2.4370	0.7903	1.2514
	4	1.8610	1.1724	1.3190
	5	0.4686	0.3311	0.3555
	6	0.2341	0.1758	0.1819
	7	1.6147	1.7700	1.5683
	8	0.0078	0.0075	0.0020
	S_z^*	6.6232	4.2471	4.6781

† in MeV per source neutron

* sum over Zones 3 through 8

(end Table 5.6)

Table 5.7

Comparison of Helium and Hydrogen Production (in units of appm per year for 1 MW/m^2) in Niobium, Vanadium, and Stainless Steel First Walls

Material	Hydrogen Production*	Helium Production
Niobium (design 301)	80.40	23.65
Vanadium (design 302)	105.00	72.50
SS (design 303)	412.00	203.00

* in units of atomic parts per million per year for a neutron wall loading of 1 MW/m^2

Table 5.8 Effect of enriching lithium in Li^6 on Energy Multiplication in the blanket

Design ID	401	402	403	404
% of Li^6 in Lithium	7.42 (natural)	15.0	30.0	50.0
Neutron Heating* in Li^6	4.9966	6.1338	7.6839	9.3943
Li^7	6.0376	5.4082	4.3270	2.9924
V	0.3953	0.3750	0.3590	0.3481
Fe	0.2340	0.2278	0.2208	0.2153
Ni	0.0801	0.0785	0.0765	0.0749
Cr	0.0538	0.0521	0.0502	0.0487
H_n = SUM	11.7974	12.2754	12.7174	13.0737
$S_{E\gamma}$ = Total Gamma Energy	4.2533	3.7893	3.3851	3.0627
$H_n + S_{E\gamma}$	16.0507	16.0647	16.1025	16.1364

* in MeV per one fusion neutron

Table 5.9 Effect of enriching Lithium in Li^6 on energy multiplication in lithium

(all reactions are in units of reactions per one fusion neutron)

	401	403		Increase
% of Li^6 in lithium	7.42 (natural)	30.0	Reaction Q-value	in energy Mult.
	A	B	Q(MeV)	(B - A)·Q
Li^6				
$Li^6(n,2n)\alpha$	5.51566(-3)	2.37665(-2)	-3.696	-6.7455(-2)
$Li^6(n,n')d$	6.96003(-2)	2.90917(-1)	-1.471	-3.25557(-1)
$Li^6(n,\gamma)$	3.58759(-5)	3.63008(-5)	+7.252	+3.272(-6)
$Li^6(n,p)$	1.51516(-3)	6.30972(-3)	-2.733	-1.31035(-2)
$Li^6(n,\alpha)$	9.0420(-1)	1.05291(+0)	+4.786	+7.11728(-1)
Decay Term for (n,p)	1.51516(-3)	6.30972(-3)	+1.560	+7.4795(-3)
Sum for Li^6				+0.31309
Li^7				
(n,2n)	2.32303(-2)	1.73536(-2)	-7.252	+4.26178(-2)
$(n,2n)\alpha$	2.91689(-2)	2.19858(-2)	-8.723	+6.2658(-2)
$(n,n')\alpha t$	5.54716(-1)	4.05156(-1)	-2.466	+3.6881(-1)
(n,γ)	4.88074(-4)	8.48159(-5)	+2.032	-8.1942(-4)
(n,d)	9.30694(-3)	6.99788(-3)	-7.760	+1.7918(-2)
Decay Term for (n,γ)	4.88074(-4)	8.48159(-5)	+9.310	-3.7542(-3)
Decay Term for (n,d)	9.30694(-3)	6.99788(-3)	+1.560	-3.60207(-3)
Sum for Li^7				+0.48383
Vanadium				
(n,2n)	1.29632(-1)	1.2974(-1)	-11.04	-0.01192(-1)
(n,γ)	2.16129(-2)	4.60876(-3)	+7.304	-1.24198(-1)
(n,p)	9.05218(-3)	8.93991(-3)	-1.683	0.18895(-3)
(n,α)	4.45364(-3)	4.44678(-3)	-2.042	0.014(-3)

(Table 5.9 continued on next page)

Table 5.9 (continued) Effect of enriching in Li^6 on energy multiplication in lithium

(all reactions are in units of reactions per one fusion neutron)

	401	403		Increase
% of Li^6 in lithium	7.42 (natural)	30.0	Reaction Q-value	in energy Mult.
	A	B	Q(MeV)	(B - A)·Q
Vanadium				
(n,γ) decay	2.16129(-2)	4.60876(-3)	+1.070	-1.8194(-2)
(n,p) decay	9.05218(-3)	8.93991(-3)	+0.9340	-0.10486(-3)
(n,α) decay	4.45364(-3)	4.44678(-3)	+0.2100	-0.00144(-3)
Net gain in energy multiplication in vanadium				-1.4348735(-1)
Iron				
(n,2n)	1.2884(-2)	1.31215(-2)	-11.20	-0.266(-2)
(n,γ)	6.54436(-2)	2.44105(-2)	+7.803	-3.201813(-1)
(n,p)	8.16713(-3)	8.09318(-3)	-2.731	0.2019(-3)
(n,α)	3.92790(-3)	3.94955(-3)	-3.926	-0.08499(-3)
(n,p) decay	8.16713(-3)	8.09318(-3)	0.731	-0.05405(-3)
Net gain in energy multiplication in iron				-3.22778(-1)

Table 5.10 Effect of adding Beryllium on Energy Multiplication in the blanket

Design	401	405	406
Thickness of Beryllium	0.0	4.0 cm.	10.0 cm.
Reactions†			
Li (n,α)	0.9042	1.2361	1.5803
Li (n,n')αt	0.5547	0.4410	0.3249
Li Tritium Breeding ratio	1.4589	1.6771	1.9052
Be (n,2n)	0.0	0.3301	0.6627
Be (n,t)	0.0	0.0055	0.0104
Be (n,α)	0.0	0.0303	0.0628
Neutron Heating*			
in Li^6	4.9966	6.4462	7.9520
Li^7	6.0376	4.7795	3.5067
V	0.3953	0.3756	0.3528
Fe	0.2340	0.1507	0.0774
Ni	0.0801	0.0519	0.0269
Cr	0.0538	0.0347	0.0179
Be	0.0	2.2193	4.3891
H_n = Total Neutron Heating*	11.7974	14.0579	16.3497
Gamma Energy* Production = $S_{E\gamma}$	4.2533	3.4891	2.6623
$H_n + S_{E\gamma}$	16.0507	17.5470	19.0120
% increase in energy	0.0	9.322	18.450

† reactions per one fusion neutron

* in MeV per one fusion neutron

Table 5.11-a Effect of Various Materials in the Reflector region on Neutron Heating†

Zone	zone outer radius (cm.)	Material	Design 110	Design 111	Design 112
3	301	Niobium	0.1274	0.1275	0.1276
4	321	95% Li	6.0430	5.9499	6.2626
5	331	+	1.7998	1.6554	1.8810
6	341	5% Nb	1.8821	1.2048	1.5525
7	366	Reflector*	0.8136	1.7209	0.3553
Sum over zones 3 through 7			10.6659	10.6585	10.1790

* The reflector material was varied as follows
Design 110: Graphite
Design 111: 20% Fe + 50% Pb + 30% B_4C
Design 112: Iron

Table 5.11-b Effect of Various Material in the Reflector region on Gamma Heating†

Zone	outer radius (cm.)	Material	Design 110	Design 111	Design 112
3	301	Niobium	1.5233	1.5228	1.5400
4	321	95% Li	1.7091	1.7081	1.7472
5	331	+	0.5538	0.5525	0.5852
6	341	5% Nb	0.4033	0.3937	0.4537
7	366	Reflector*	0.6411	1.4717	2.4680
Sum over zones 3 thru 7			4.8306	5.6488	6.7941

† in MeV per one fusion neutron

Table 5.11-c Effect of Various Materials in the Reflector region on Secondary Gamma Energy† Production

zone	outer radius (cm.)	Material	Design 110	Design 111	Design 112
3	301	Niobium	2.4334	2.4334	2.4409
4	321	95% Li	1.8587	1.8579	1.8655
5	331	+	0.4081	0.4064	0.4105
6	341	5% Nb	0.2615	0.2568	0.2600
7	366	Reflector*	0.2097	0.7035	1.8448
Sum over zones 3 thru 7			5.1714	5.6580	6.8217

Table 5.11-d Effect of Various Materials in the Reflector Region on Total Nuclear Heating†

zone	outer radius (cm.)	Material	Design 110	Design 111	Design 112
3	301	Niobium	1.6507	1.6503	1.6676
4	321	95% Li	7.7521	7.6580	8.0098
5	331	+	2.3536	2.2079	2.4662
6	341	5% Nb	2.2854	1.5985	2.0062
7	366	Reflector*	1.4547	3.1926	2.8233
Sum over zones 3 thru 7			15.4965	16.3073	16.9731

* The reflector material was varied as follows
Design 110: Graphite, Design 111: 20% Fe + 50% Pb + 30% B_4C,
Design 112: Iron

† in MeV per one fusion neutron

Table 5.12 Comparison of Various Materials in the Relector Region

Design	110	111	112
Reflector Material	Graphite	20% Fe + 50% Pb + 30% B_4C	Iron
Neutron Heating*	10.6659	10.6585	10.1790
Gamma Energy Production*	5.1714	5.6580	6.8217
Gamma Heating*	4.8306	5.6481	6.794
Total Heating	15.4965	16.3073	16.9731
Neutron Energy Leakage* from reflector	0.2794	0.0914	0.0616
Gamma Energy Leakage* from reflector	0.3399	0.0025	0.0257
Total Energy Leakage*	0.6193	0.0939	0.0873
$Li^6(n,\alpha)t$	0.7707	0.5808	0.7645
$Li^7(n,n'\alpha)t$	0.4877	0.4850	0.4836
Tritium Breeding Ratio	1.2584	1.0658	1.2481

* in MeV per one fusion (14.06 MeV) neutron

Table 5.13 Neutron and Gamma Energy Leakage by Zone

(in MeV per one fusion neutron)

for Design 114

Zone	Outer Radius (cm.)	Material	$\bar{E}_n$	$\bar{E}_\gamma$	L_{nE}	$L_{\gamma E}$	$L_{nE} + L_{\gamma E}$
1	250	plasma	14.21	3.985	14.208	0.0	14.208
2	300	vacuum	14.21	3.726	14.208	0.0	14.208
3	301	Niobium	11.03	9.314	11.507	8.989(-1)	12.4059
4	321	95% Li	6.187	5.214	4.26	1.019(+0)	5.286
5	333	+	5.245	5.42	2.430	8.09(-1)	3.239
6	343	5% Nb	5.877	7.516	1.518	6.19(-1)	2.137
7	363	SS	0.803	2.319	1.007(-1)	3.63(-2)	1.37(-1)
8	370	95% Li + 5% Nb	0.762	2.580	6.89(-2)	2.94(-2)	9.83(-2)
9	380	70% SS	1.024	2.356	1.59(-2)	6.80(-3)	2.27(-2)
10	390	+	1.140	2.268	3.74(-3)	1.55(-3)	5.29(-3)
11	400	30% B_4C	1.212	2.186	8.85(-4)	3.51(-4)	12.36(-4)
12	410		1.256	2.120	2.10(-4)	7.98(-5)	2.898(-4)
13	420		1.279	2.071	4.99(-5)	1.82(-5)	6.81(-5)
14	430		1.286	2.034	1.19(-5)	4.21(-6)	1.611(-5)
15	440		1.281	2.008	2.82(-6)	9.78(-7)	3.798(-6)
16	450		1.268	1.991	6.68(-7)	2.29(-7)	8.97(-7)
17	460		1.232	1.980	1.587(-7)	5.44(-8)	2.131(-7)
18	470		0.896	1.594	4.110(-8)	1.47(-8)	5.58(-8)

Table 5.14 Neutron and Gamma Energy Leakage by zone

(in MeV per one fusion neutron)

for Design 115

Zone	Outer Radius (cm.)	Material	$\bar{E}_n$	$\bar{E}_\gamma$	L_{nE}	$L_{\gamma E}$	$L_{nE}+L_{\gamma E}$
1	250	plasma	14.21	-----	14.208	-----	14.208
2	300	vacuum	14.21	-----	14.208	-----	14.208
3	301	Niobium	11.035	9.315	11.507	8.989(-1)	12.4059
4	321	95% Li	6.188	5.212	4.267	1.019(+0)	5.286
5	333	+	5.248	5.420	2.430	8.097(-1)	3.2397
6	343	5% Nb	5.885	7.512	1.518	6.189(-1)	2.2369
7	363	SS	0.7931	2.203	9.988(-2)	4.094(-2)	14.082(-2)
8	370	95% Li + 5% Nb	0.7239	2.053	6.722(-2)	3.672(-2)	10.394(-2)
9	380	70% Lead	1.011	2.487	2.146(-2)	8.872(-4)	2.2347(-2)
10	390	+	1.173	2.010	6.975(-3)	1.037(-4)	7.0787(-3)
11	400	30% B_4C	1.285	1.915	2.292(-3)	2.854(-5)	2.3205(-3)
12	410		1.330	1.887	7.561(-4)	9.103(-6)	7.652(-4)
13	420		1.321	1.874	2.494(-4)	2.953(-6)	2.5235(-4)
14	430		1.281	1.868	8.208(-5)	9.601(-7)	8.304(-5)
15	440		1.230	1.867	2.691(-5)	3.120(-7)	2.7222(-5)
16	450		1.174	1.869	8.791(-6)	1.013(-7)	8.892(-6)
17	460		1.094	1.875	2.890(-6)	3.325(-8)	2.923(-6)
18	470		0.834	1.655	1.083(-6)	2.397(-8)	1.107(-6)

Table 5.15 Neutron and Gamma Energy Leakage by zone

(in MeV per one fusion neutron)

for Design 116

Zone	Outer Radius (cm.)	Material	$\bar{E}_n$	$\bar{E}_\gamma$	L_{nE}	$L_{\gamma E}$	$L_{nE} + L_{\gamma E}$
1	250	plasma	14.208	2.738	14.208	0.0	14.208
2	300	vacuum	14.208	2.908	14.208	0.0	14.208
3	301	Niobium	11.035	9.315	11.508	8.98(-1)	12.406
4	321	95% Li	6.188	5.212	4.267	1.019	5.286
5	333	+	5.246	5.420	2.430	8.09(-1)	3.239
6	343	5% Nb	5.881	7.512	1.518	6.19(-1)	2.137
7	363	SS	7.987(-1)	2.207	1.004(-1)	3.92(-2)	1.396(-1)
8	370	95% Li + 5% Nb	7.457(-1)	2.054	6.822(-2)	3.42(-2)	1.0242(-1)
9	380	35% Pb	1.027(+0)	2.620	1.846(-2)	2.49(-3)	2.095(-2)
10	390	+	1.172	2.265	5.083(-3)	3.80(-4)	5.463(-3)
11	400	35% SS	1.264(+0)	2.111	1.410(-3)	8.29(-5)	1.492(-3)
12	410	+	1.304(+0)	2.050	3.925(-4)	2.12(-5)	4.137(-4)
13	420	30% B_4C	1.308(+0)	2.026	1.092(-4)	5.73(-6)	1.149(-4)
14	430		1.289(+0)	2.015	3.035(-5)	1.58(-6)	3.193(-5)
15	440		1.259(+0)	2.012	8.412(-6)	4.39(-7)	8.851(-6)
16	450		1.224(+0)	2.013	2.325(-6)	1.22(-7)	2.447(-6)
17	460		1.165(+0)	2.023	6.440(-7)	3.46(-8)	6.786(-7)
18	470		8.617(-1)	1.774	1.985(-7)	1.521(-8)	2.137(-7)

Table 5.16 Neutron and Gamma Energy Leakage by Zone

(in MeV per one fusion neutron)

for Design 117

Zone	Outer Radius (cm.)	Material	$\bar{E}_n$	$\bar{E}_\gamma$	L_{nE}	$L_{\gamma E}$	$L_{nE} + L_{\gamma E}$
1	250	plasma	1.421(+1)	2.763	1.4208(+1)	≈0.0	14.208
2	300	vacuum	1.421(+1)	3.321	1.4208(+1)	≈0.0	14.208
3	301	Niobium	1.104(+1)	9.319	1.151(+1)	8.98(-1)	12.408
4	321	95% Li	6.204	5.215	4.267(+0)	1.018	5.285
5	333	+	5.288	5.427	2.430	8.081(-1)	3.238
6	343	5% Nb	6.042	7.552	1.518	6.166(-1)	2.134
7	363	SS	8.65(-1)	2.284	9.896(-2)	3.31(-2)	13.206(-2)
8	370	95% Li + 5% Nb	1.229	2.494	6.469(-2)	2.23(-2)	8.699(-2)
9	380	SS	5.989(-1)	2.439	1.761(-2)	6.803(-3)	2.441(-2)
10	390	SS	3.914(-1)	2.772	5.322(-3)	3.90(-3)	9.222(-3)
11	400	SS	2.952(-1)	2.925	1.752(-3)	1.92(-3)	3.672(-3)
12	410	SS	2.396(-1)	2.989	6.133(-4)	8.51(-4)	14.643(-4)
13	420	SS	2.029(-1)	3.019	2.217(-4)	3.69(-4)	5.907(-4)
14	430	SS	1.769(-1)	3.037	8.071(-5)	1.60(-4)	2.4071(-4)
15	440	SS	1.576(-1)	3.049	2.9161(-5)	6.9(-5)	9.816(-5)
16	450	SS	1.426(-1)	3.059	1.042(-5)	2.95(-5)	3.992(-5)
17	460	SS	1.281(-1)	3.069	3.805(-6)	1.29(-5)	1.67(-5)
18	470	SS	1.088(-1)	2.582	1.88(-6)	5.17(-6)	7.05(-6)

Table 5.17 Comparison of Gamma Energy Production by Zone in MeV per one fusion neutron For Designs 114, 115, 116, and 117

Zone	Outer Radius (cm.)	Design 114	Design 115	Design 116	Design 117
1	250	0.0	0.0	0.0	0.0
2	300	0.0	0.0	0.0	0.0
3	301	2.437	2.437	2.437	2.437
4	321	1.861	1.861	1.861	1.861
5	333	0.469	0.469	0.469	0.469
6	343	0.234	0.234	0.234	0.234
7	363	1.616	1.615	1.615	1.690
8	370	7.634(-3)	7.784(-3)	7.700(-3)	8.48(-3)
9	380	4.157(-2)	1.369(-2)	2.846(-2)	1.501(-1)
10	390	8.796(-3)	4.449(-3)	7.221(-3)	8.276(-2)
11	400	2.019(-3)	1.453(-3)	1.942(-3)	3.784(-2)
12	410	4.743(-4)	4.757(-4)	5.331(-4)	1.628(-2)
13	420	1.125(-4)	1.558(-4)	1.479(-4)	6.972(-3)
14	430	2.679(-5)	5.095(-5)	4.120(-5)	2.986(-3)
15	440	6.397(-6)	1.662(-5)	1.149(-5)	1.260(-3)
16	450	1.529(-6)	5.403(-6)	3.201(-6)	5.162(-4)
17	460	3.648(-7)	1.747(-6)	8.876(-7)	1.990(-4)
18	470	8.307(-8)	5.432(-7)	2.337(-7)	5.649(-5)
Sum over all zones		6.6771	6.6435	6.6621	6.9989

Table 5.18 Neutron, Gamma, and Total Energy Attenuation Coefficients* for Various Shield Compositions

Design	114	115	116	117
Shield composition	70% SS + 30% B_4C	70% Pb + 30% B_4C	35% Pb + 35% SS + 30% B_4C	100% SS
Neutron Energy attenuation coefficient, μ_n (cm^{-1})	0.1438	0.1113	0.1282	0.1022
Gamma energy attenuation coefficient, μ_γ (cm^{-1})	0.1466	0.1160	0.1320	0.0828
Total energy attenuation coefficient, μ (cm^{-1})	0.1445	0.1113	0.1283	0.0902

* obtained by fitting the energy attenuation leakage curve to exponentials (see equations 5.11)

Table 5.19 Values of Optimum Shield Thickness for several values of the Parameters in equations 5.13 through 5.21 for an energy attenuation coefficient of 0.1447 in the shield

(corresponding to 70% SS + 30% B_4C)

parameter / Case No.	r_w (cm)	r_b (cm)	W_n watts/cm^2	m	a_s^* \$/cm^3	a_m \$/cm	a_r \$/cm	t_{so} (cm)
1	400	470	100	1	0.088	18.96	5.312(+5)	57.60
2	400	470	1000	1	0.088	18.96	2.115(+6)	73.19
3	400	470	50	1	0.088	18.96	3.504(+5)	52.90
4	400	470	100	2	0.088	0.03386	5.312(+5)	57.00
5	400	470	100	1	0.0352	18.96	5.312(+5)	66.97
6	200	270	100	1	0.0352	18.96	3.504(+5)	66.65
7	200	270	100	1	0.088	18.96	3.504(+5)	57.87
8	200	270	100	2	0.088	0.03386	3.504(+5)	57.69
9	200	270	50	1	0.088	18.96	9.204(+5)	68.65

* a_s of 0.088 corresponds to \$6.4/lb for a density of 6.26 gm/cm^3 and 0.0352 corresponds to \$2.55/lb for a density of 6.26 gm/cm^3

Table 5.20 Values of Optimum Shield Thickness for several values of the Parameters in equations 5.13-5.21 for an energy attenuation coefficient of 0.1113 cm^{-1} in the shield

(corresponding to 70% Pb + 30% B_4C)

Parameter / Case No.	r_w (cm)	r_b (cm)	W_n $\frac{watt}{cm^2}$	m	a_s^* $/cm^3	a_m $/cm	a_r $/cm	t_{so} (cm)
1	400	470	100	1	0.0176	18.96	5.312(+5)	91.06
2	400	470	1000	1	0.0176	18.96	2.115(+6)	111.3
3	400	470	50	1	0.0176	18.96	3.504(+5)	84.96
4	400	470	100	2	0.0176	0.03386	5.312(+5)	87.98
5	200	270	100	1	0.0176	18.96	3.504(+5)	89.65
7	200	270	100	2	0.0176	0.03386	3.504(+5)	88.38

* a_s of 0.0176 corresponds to 0.92 $/lb for 70% Pb + 30% B_4C

Table 5.21

Neutron Heating by Material and Zone for Design 777
(in units of MeV per source neutron)

zone	composition	Li^6	Li^7	V	Fe	Cr	→
1	plasma						→
2	vacuum						→
3	Vanadium	-----	-----	0.219	-----	-----	→
4	95% Li + 5% V	1.735	3.142	0.091	-----	-----	→
5	95% Li + 5% V	1.492	1.711	0.050	-----	-----	→
6	95% Li + 5% V	1.486	0.989	0.032	-----	-----	→
7	Stainless Steel	-----	-----	-----	0.255	0.059	→
8	95% Li + 5% V	0.342	0.039	0.002	-----	-----	→
9	SS	-----	-----	-----	8.04(-3)	1.96(-3)	→
10	vacuum	-----	-----	-----	-----	-----	→
11	90% He + 10% SS	-----	-----	-----	3.57(-4)	8.75(-5)	→
12	90% Pb + 10% SS	-----	-----	-----	3.67(-3)	9.11(-4)	→
13	B_4C	-----	-----	-----	-----	-----	→
14	90% He + 10% SS	-----	-----	-----	1.75(-5)	4.24(-6)	→
15	90% Pb + 10% SS	-----	-----	-----	1.82(-4)	4.53(-5)	→
16	B_4C	-----	-----	-----	-----	-----	→
17	90% He + 10% SS	-----	-----	-----	8.18(-7)	2.00(-7)	→
18	90% Pb + 10% SS	-----	-----	-----	5.51(-6)	1.36(-6)	→
19	B_4C	-----	-----	-----	-----	-----	→
20	SS	-----	-----	-----	1.95(-6)	4.71(-7)	→
sum by material		5.055	5.880	0.394	0.268	0.062	→

note: this table is continued on the next page in a cross ways direction as indicated by the arrows in the right hand column

Table 5.21 (continued)

Ni	B-10	B-11	C-12	Pb	sum by zone	zone
					0.0	1
					o.o	2
-----	-----	-----	-----	-----	0.219	3
-----	-----	-----	-----	-----	4.968	4
-----	-----	-----	-----	-----	3.253	5
-----	-----	-----	-----	-----	2.507	6
0.088	-----	-----	-----	-----	0.402	7
-----	-----	-----	-----	-----	0.383	8
2.43(-3)	-----	-----	-----	-----	1.243(-2)	9
-----	-----	-----	-----	-----	0.0	10
1.05(-4)	-----	-----	-----	-----	5.49(-4)	11
1.01(-3)	-----	-----	-----	7.58(-3)	1.32(-2)	12
-----	2.02(-1)	1.04(-2)	3.18(-3)	-----	2.13(-1)	13
5.30(-6)	-----	-----	-----	-----	2.70(-5)	14
5.03(-5)	-----	-----	-----	3.93(-4)	6.71(-4)	15
-----	9.23(-3)	5.45(-4)	1.65(-4)	-----	9.94(-3)	16
2.45(-7)	-----	-----	-----	-----	1.26(-6)	17
1.56(-6)	-----	-----	-----	1.16(-5)	2.85(-5)	18
-----	6.84(-4)	4.42(-5)	1.35(-5)	-----	7.42(-4)	19
6.07(-7)	-----	-----	-----	-----	3.03(-6)	20
0.091	0.212	0.011	0.003	0.008	11.976	sum by material

note: the above is an extension of the rows of table 5.21 on the preceding page.

Table 5.22

Neutron and Gamma Heating and Gamma Energy Production (in MeV per source neutron) by Zone for Design 777

zone	composition	neutron heating	gamma energy production	gamma heating	total heating
1	plasma	0.0	0.0	0.0	0.0
2	vacuum	0.0	0.0	0.0	0.0
3	vanadium	0.219	0.778	0.499	0.718
4	95% Li + 5% V	4.968	0.859	0.649	5.617
5	95% Li + 5% V	3.253	0.492	0.514	3.767
6	95% Li + 5% V	2.507	0.298	0.414	2.921
7	Stainless Steel	0.402	1.836	2.125	2.527
8	95% Li + 5% V	0.383	0.014	0.019	0.402
9	Stainless Steel	1.243(-2)	7.44(-2)	7.16(-2)	8.40(-2)
10	vacuum	0.0	0.0	0.0	0.0
11	90% He + 10% SS	5.49(-4)	3.39(-3)	2.44(-3)	2.99(-3)
12	90% Pb + 10% SS	1.32(-2)	9.12(-2)	1.52(-1)	1.65(-1)
13	B_4C	2.13(-1)	6.45(-4)	8.18(-4)	2.13(-1)
14	90% He + 10% SS	2.70(-5)	1.22(-4)	3.92(-5)	6.62(-5)
15	90% Pb + 10% SS	6.71(-4)	3.91(-3)	4.51(-3)	5.18(-3)
16	B_4C	9.94(-3)	2.95(-5)	3.70(-5)	9.98(-3)
17	90% He + 10% SS	1.26(-6)	5.77(-6)	1.77(-6)	3.03(-6)
18	90% Pb + 10% SS	2.85(-5)	1.21(-4)	1.53(-4)	1.82(-4)
19	B_4C	7.42(-4)	3.36(-6)	7.88(-6)	7.50(-5)
20	SS	3.03(-6)	2.64(-5)	1.78(-5)	2.08(-5)
sum for system		11.976	4.450	4.45	16.43

Table 5.23

Tritium Production (in atoms per souce neutron) for Design 777

zone	$Li^6(n,\alpha)t$	$Li^7(n,n'\alpha)t$	sum by zone
4	o.2926	0.2934	0.586
5	0.2717	0.1582	0.430
6	0.2859	0.0869	0.373
8	0.0699	0.0016	0.072
sum	0.9202	0.5401	1.4603

Table 5.24

Tritium Production in Boron in the Shield for Design 777 (in atoms per source neutron)

zone	$B^{10}(n,t)$	$B^{11}(n,t)$	sum by zone
13	3.054(-5)	3.187(-6)	3.372(-5)
16	1.497(-6)	1.275(-7)	1.625(-6)
19	1.637(-7)	1.284(-8)	1.765(-7)
sum	3.220(-5)	3.327(-6)	3.553(-5)

Table 5.25

Nuclide Densities
(used in design 777)

Material/Nuclide	Nuclide density ($atoms/cm^3 \times 10^{-24}$)
Vanadium	0.072
95% Li + 5% V	
Li^6	0.0031
Li^7	0.0419
V	0.0035
Stainless Steel	
Fe	0.0600
Cr	0.0143
Ni	0.0091
Boron Carbide	
B-10	0.0185
B-11	0.0748
C-12	0.0233
90% Pb + 10% SS	
Pb	0.0287
Fe	0.0060
Cr	0.0014
Ni	0.0009

Chapter 6

GENERAL CONCLUSIONS AND RECOMMENDATIONS

Chapter 6

GENERAL CONCLUSIONS AND RECOMMENDATIONS

6.1 Summary and General Conclusions

This research was devoted to investigating some of the theoretical and calculational problems involved in the neutronics and photonics analysis of fusion reactor blankets and shields. The study has dealt with three distinct subjects: a - calculational methods for nuclear heating (with emphasis on fusion systems), b - flux calculations in CTR systems, and c - neutronics and photonics design for CTR blankets and shields. The following points serve as a brief summary of the results and conclusions.

A. Kerma Factors

1 - A theoretical model was developed for calculating fluence-to-kerma factors from basic nuclear data. No major simplifying assumtions were introduced and the accuracy of the calculated kerma factors depends only on the availability and accuracy of the basic nuclear data. (chapter 2 section 2).

2 - A computational algorithm was developed for calculating kerma factors from nuclear data in ENDF format. Based on this algorithm, a computer program, called MACK, was written. MACK processes all reactions significant to energy deposition. The flexibility of the input for the program allows generating pointwise and group parameters appropriate for

any desired application. (chapter 2 section 3)

3 - Calculation of other response functions such as for helium and hydrogen production was automated for multigroup representation by integrating the required processing with the computational capability developed for kerma factors.

4 - A library of kerma factors and group cross sections was generated with MACK for all materials of interest for CTR using a weighting function appropriate for fusion ractors. (section 3.2)

5 - Two algorithms were devised for investigating the validity of the kerma factor results using a pointwise and an overall energy balance. (section 3.4)

6 - The validity of the theoretical model and the correctness of the computation of the kerma factors obtained in the present work were verified using both algorithms. (section 3.4)

7 - Comparison of the kerma factor results obtained in the present work with previous work showed that the present work provides a very considerable improvement in kerma factor calculations. (section 3.4.4)

8 - Application of the overall and pointwise balances (sections 3.4.2 and 3.4.3) showed that gamma production data currently available for many materials suffer from very large uncertainties, particularly the data for Li^6, Li^7, Nb, and C^{12}.

9 - A sensitivity study of neutron energy deposition to nuclear data was carried out (section 3.5). This study showed that: a - The (n, charged particles) reactions contribute, in general, about 30 to 50 % of the neutron heating for typical fusion spectra. b - A change

in the average secondary neutron energy, $\overline{E}_{n',\ell}$, of the $Li^7(n,n'\alpha)t$ reaction results in a relative change in the neutron heating in Li^7 which is approximately one-third of that in $\overline{E}_{n'\ell}$. c - The relative change in the neutron heating by elastic scattering due to a change in the angular distribution is larger than the relative change in $\overline{\cos\theta}_{c.m.}$. Ignoring the anisotropy of scattering can result in severly overestimated kerma factors. d - The local energy deposition by radioactive decay is about 2% or less in most materials in typical CTR spectra.

B. Flux Calculations for CTR Systems

1 - The accuracy of the various approximations in a discrete-ordinates one-dimensional transport model was determined.

2 - The cylindrical geometry should be used in one-dimensional calculations.

3 - The neutronics and photonics results are relatively insensitive to the exact neutron source distribution so that simple forms can be used.

4 - For neutron and gamma discrete-ordinates transport calculations, the approximations S_8 and P_3 are adequate and have an accuracy of better than 5% everywhere.

C. Neutronics and Photonics Design of CTR Blankets and Shields

With the developments and conclusions summarized above the neutronics and photonics analysis of CTR systems became feasible. The study of the nuclear design of blankets and shield showed the following.

1 - No neutronically unacceptable effects arise from using a first

wall thickness somewhere between 0.0 and 4.0 cm.

2 - Among the materials investigated in this study, no one material emerges as the best choice for the first wall and structure. a - Helium and hydrogen production are highest in stainless steel, lower in vanadium, and the lowest in niobium. b - For 1 MW/m^2 neutron wall loading each atom is displaced about 15 times each year in niobium and vanadium and about 20 times each year in stainless steel. c - The total heating rate in niobium is about 2.3 times that in a vanadium and 1.2 times that in a stainless steel first wall. d - Using niobium for first wall and blanket structure increases the useful power by about 1.1 MeV per fusion reaction over a stainless steel and 1.0 MeV over a vanadium system.

3 - Tritium breeding ratios for the systems investigated are so high that it seems very unlikely that any uncertainty in nuclear data will cause CTR systems to be unable to produce excess tritium required for reasonable doubling times.

4 - The energy per fusion reaction was found to be about 20 MeV or less for most of the CTR systems investigated. This is about 2 MeV or more lower than one often sees in literature for similar systems. The difference arises as a consequence of the improved calculational methods and careful treatment of all available data in the present work.

5 - Since the energy produced per fusion reaction is low (compared with fission reaction, for example) it is necessary to find out methods for improving the energy production per fusion reaction. Two

concepts were investigated. a - Adding 4 cm of beryllium increases the power output by about 10% which is large enough to offset the high cost of beryllium. b - Increasing the isotopic ratio of Li^6 in the lithium blanket does not improve the economy of the system.

6 - The study of the possible shielding material showed that a mixture of stainless steel and boron carbide provides the required attenuation with a minimal thickness.

7 - The optimum shielding composition from cost point of view is a mixture of lead and B_4C. However, an amount of structural steel is necessary for structural reasons.

8 - Nuclear heating in the magnet, rather than radiation damage to a - superinsulation, b - copper stabilizer, and c - superconductor, is the limiting factor.

6.2 Recommendations

Many remarks were made throughout this thesis suggesting areas in which more work should be undertaken. The following is a summary of the most important areas for future studies.

1 - More information about nuclear data for (n,charged particles) and (n;n' charged particles) are needed. Although these reactions do not significantly affect neutron transport in most cases it was shown in this work that they generally contribute a significant fraction to the neutron heating. An accurate assessment of charged particle production is also essential to radiation damage studies. The data needed for these reactions are: a - reaction total cross sections, b - excitation function to various levels, c - energy distribution of charged particles and neutrons emitted particularly in the incident neutron energy range for which the residual nucleus is left in the continuum region.

2 - The lack of information about gamma production data, particularly for the most important CTR materials, was pointed out in several places of this work. More data about gamma production cross sections are required for accurate calculation of local energy deposition (for both neutron and gamma heating) and gamma energy leakage to the CTR magnets.

3 - It was shown in this work that available neutron and gamma production data do not preserve the energy in some instances. Consequently, kerma factor and gamma production sets independently derived from this data lead to calculated heating rates which violate

the energy conservation law. Hence, it is strongly suggested that: a - neutron and gamma data in ENDF/B and similar data libraries be checked to ensure that the energy conservation law is not violated. and b - gamma production cross sections be derived concurrently with the neutron kerma factors. In calculating the neutron kerma factors from the neutron data in END/B, the MACK program currently calculates a matrix of the total energy production as a function of the incident neutron energy. This matrix can be used to fix the normalization of the gamma production cross sections. It seems logical at present that the MACK program should be extended to process gamma production cross sections from the gamma files in ENDF/B. This can ensure deriving consistent and energy preserving sets of neutron kerma factors and gamma production cross sections.

4 - The energy per fusion, calculated in this work to be of about 20 MeV, in currently proposed CTR designs seems to be low from an economics point of view. Hence, additional studies aimed at increasing the energy multiplication should be conducted to evaluate materials and configurations not yet treated.

5 - As indicated earlier, the part of this work on magnet shield is a first quantitative look at the nuclear aspects of the shield design. More work is needed to evaluate materials and configurations not considered in this thesis. Cost optimization of the shield should be integrated into a scheme for optimizing the cost of the complete fusion reactor to allow for inclusion of more variable parameters.

BIBLIOGRAPHY

1. a. Radiation Quantities and Units, compiled by Commission on Radiological Units and Measurements (ICRU), National Bureau of Standard Handbook 84 (ICRU report 10a), November 1962.

   b. D. K. Trubey, "Use of ICRU-Defined Quantities and Units in Shielding," ORNL-RSIC-16 (October 1968).

2. Protection Against Neutron Radiation up to 30 Million Electron Volts, compiled by the Subcommittee on Heavy Particles (Neutrons, Protons, and Heavier), National Bureau of Standards Handbook 63 (November 1957).

3. B. J. Henderson, Conversion of Neutron or Gamma Ray Flux to Absorbed Dose Rate, XDC 59-8-179, General Electric Company (August 1959).

4. J. A. Auxier and W. S. Snyder, The Calculation of Kerma as a Function of Neutron Energy, Oak Ridge National Laboratory, ORNL-4168 (1967).

5. R. L. Bach and R. S. Caswell, "Energy Transfer to Matter by Neutrons," Radiation Res., 35, 1 (1968).

6. J. J. Ritts, M. Solomito, and P. N. Stevens, "Calculation of Neutron Fluence-to-Kerma Factors for the Human Body," Nucl. Applic. and Tech., 7(1), 89-99 (July 1969).

7. J. J. Ritts, M. Solomito, and D. Steiner, "Kerma Factors and Secondary Gamma-Ray Sources for Some Elements of Interest in Thermonuclear Blanket Assemblies," ORNL-TM-2564 (June 1970).

8. MUG; A Program for Generating Multigroup Photon Cross Sections," J. R. Knight and F. R. Mynatt, CTC-17 (January 1970).

9. M. J. Stanley, "Klein-Nishina Photon Cross Sections (Program GAMMA)," APEX-487, General Electric Company (May 1959).

10. M. K. Drake, Editor "Data Formats and Procedures for the ENDF Neutron Cross Section Library," BNL-50279 (October 1970).

11. W. W. Engle, Jr., "A Users Manual for ANISN" K-1693, Oak Ridge Gaseous Diffusion Plant, March 1967.

12. R. D. Evans, "The Atomic Nucleus," McGraw Hill Book Co., Inc. (1955).

13. R. B. Leighton, "Principles of Modern Physics," McGraw Hill Book Company, Inc. (1959).

14. C. M. Lederer, J. M. Hollander, and I. Perlman, "Table of Isotopes," 6th edition, John Wiley and Sons, New York (1967).

15. Odelli Ozer, Editor, "Description of the ENDF/B Processing Codes and Retrieval Subroutines," BNL 50300 (Revised June 1971).

16. R. Q. Wright, N. M. Greene, J. L. Lucius, and C. W. Craven, Jr., "SUPERTOG: A Program to Generate Fine Group Constants and P_n Scattering Matrices from ENDF/B," ORNL-TM-2679 (1969).

17. K. Gregson, M. F. James, and D. S. Norton, "MLBW - A Multilevel Breit-Wigner Computer Programme," UKAEA Report AEEW-M-517, March 1965.

18. J. M. Otter, "Comment on the Calculation of the Scattering Cross Section for Multiple Resonances," Technical Note, Nucl. Sci. Eng. 28 (1967).

19. K. Gregson and M. F. James, "TEMPO - A General Doppler Broadening Programme for Neutron Cross-Sections," UKAEA Report AEEW-M-518, February 1965.

20. B. J. Toppel, A. L. Rago, and D. M. O'Shea, "MC^2: A Code to Calculate Multigroup Cross Sections, USAEC Report ANL-7318 (June 1967).

21. R. E. Schenter, J. L. Baker, and R. B. Kidman, "ETOX: A Code to Calculate Group Constants for Nuclear Reactor Calculations," USAEC Report BNWL-1002 (ENDF-127) (May 1969).

22. P. F. Zweifel and H. Hurwitz, Jr., J. Appli. Phys. 25, 1241 (1954).

23. H. Amster, J. Appl. Phys. 29, 623 (1958).

24. J. E. Lynn, "The Theory of Neutron Resonance Reactions," Claredon Press (1968).

25. G. I. Bell and S. Glasstone, "Nucleus Reactor Theory," Van Nostrand R. Comp. (1970).

26. R. N. Hwang, "Doppler Effect Calculations with Interference Corrections," Nucl. Sci. Eng. 21, 523 (1965).

27. S. K. Penny and L. W. Owen, "A Re-Evaluation of Vanadium Neutron and Gamma-Ray Production Cross Sections," ORNL-TM-4007 (November 1972).

28. W. E. Alley and R. M. Lessler, "Semiemperical Neutron-Induced Reaction Cross Sections," UCRL-50484 Rev. 1 (August 1972).

29. D. W. Muir, Los Alamos Scientific Laboratory, Private Communication (December 1972).

30. W. Kohler et al., Proceedings Texas Symposium on Technology of Controlled Fusion Experiments and the Engineering Aspects of Fusion Reactors, Austin, Texas (November 1972).

31. R. Q. Wright and R. W. Roussin, "DLG 2/100G Neutron Transport Code Cross Section Data Generated by SUPERTOG from ENDF/B3," (July 1972). This library can be obtained through the Radiation Shielding Information Center (RSIC) at Oak Ridge Nation Laboratory.

32. R. Q. Wright, ORNL (private communication).

33. A. J. Impink, Jr. "Neutron Economy in Fusion Reactor Blanket Assemblies," Technical report No. 435, M. I. T. Research Laboratory of Electronics, Cambridge, Mass. (1965).

34. L. Rosen and L. Stewart, "The Neutron-Induced Disintegration of Li^6 and Li^7 by 5 to 14 MeV incident Neutrons," LA-2643 (1961).

35. J. T. Kriese, ORNL (private communication).

36. C. W. Maynard and M. A. Abdou, "Neutron and Gamma Physics Problems in Fusion Reactors," Conference on New Developments in Reactor Physics and Shielding, CONF-720901, Book 2 (September 1972).

37. M. N. Rosenbluth, R. D. Hazeltine and F. L. Hinton, "Plasma Transport in Toroidal Confinement Systems," Phy. Fluids 15, 116 (1972).

38. S. Blow, V. Crocker, and B. Wade, "Neutronics Calculations for Blanket Assemblies of a Fusion Reactor. Paper 5.5 in reference 60 below.

39. J. D. Lee, "Tritium Breeding and Energy Generation in Liquid Lithium Blankets," Paper 5.3 in reference 60 below.

40. D. Steiner, "The Nuclear Performance of Fusion Reactor Blankets, Nuclear App. and Tech. 9, 83(1970).

41. D. K. Trubey, and Betty F. Maskewitz, "A Review of the Discrete Ordinates S_n Method for Radiation Transport Calculations," ORNL-RSIC-19 (1968).

42. "Proceedings of The International Working Sessions on Fusion Reactor Technology," Oak Ridge National Laboratory, CONF-710624 (June 28-July 2, 1971).

43. R. Q. Wright et al., "UKAEA to ENDF/B Translation ....," ORNL-TM-2880; also ENDF-134.

44. J. Blatt and V. Weisskopf, "Theoretical Nuclear Physics," J. Wiley and Sons, Inc., New York (1940).

45. B. Nicolaenko, "Energy-Dependent Baltzman Equation in the Fast Domain," J. Math. Physics, 11, 174 (1970).

46. J. J. Ritts -- TVA (private communication — May 1973).

47. L. Spitzer, Jr., D. J. Grove, W. E. Johnson, L. Tonks, and W. G. Westendorp, NYO 5047 (1954).

48. E. P. Johnson, NYO 7900 (1957).

49. P. R. Bell and others, ORNL 2457 (1958).

50. N. C. Christofilos, N. W. Cook, W. B. Myers, C. E. Taylor, and W. Wells TID 7558, Suppl. 1 (1960).

51. D. J. Rose and M. Clark, Jr., Plasma and Controlled Fusion, 2nd revised printing, M.I.T. Press, Cambridge, Mass. (1965) Chapter 13.

52. A. J. Impink, Jr., Neutron Economy in Fusion Reactor Blanket Assemblies, Technical report No. 434, M.I.T. Research Laboratory of Electronics, Cambridge, Mass. (1965).

53. W. G. Homeyer, Thermal and Chemical Aspects of the Thermonuclear Blanket Problem, Technical report No. 435, M.I.T. Laboratory of Electronics, Cambridge, Mass. (1965).

54. L. N. Lontai, Study of a Thermonuclear Reactor Blanket with Fissile Nuclides, Technical Report No. 436, M.I.T. Laboratory of Electronics, Cambridge, Mass. (1965).

55. P. S. Spangler, Fusion Reactor Blanket Experiment, Technical Report 437, M.I.T. Research Laboratory of Electronics, Cambridge, Mass. (1965).

56. L. M. Petrie, Jr., Gamma-Ray Spectra In Fusion Blanket Mock-Ups, Technical Report 438, M.I.T. Research Laboratory of Electronics, Cambridge, Mass. (1965).

57. D. J. Rose, "On the Feasibility of Power by Nuclear Fusion," ORNL-TM-2204, Oak Ridge National Laboratory (1968).

58. D. Steiner, "Neutronic Calculations and Cost Estimates For Fusion Reactor Blanket Assemblies," ORNL-TM-2360 (1968).

59. A. Fraas, Parameters for a Series of Reference Designs of Thermonuclear Reactors, Appendix III, reference (11).

60. Proceedings of B. N. E. S. Nuclear Fusion Reactor Conference Culham (1969).

61. Blow, S., Crocker, V. S. and Wade, B. O., Neutronics calculations for Blanket Assemblies of a fusion reactor, Proceedings of B. N. E. S. Nuclear Fusion Reactor Conference, Culham (1969) Paper 5.5.

62. D. Steiner, Neutronic Behavior of Two Fusion Reactor Blanket Designs, Proceedings of B. N. E. S. Nuclear Fusion Reactor Conference, Culham (1969) 483.

63. J. D. Lee, Tritium Breeding and Energy Generation in Liquid Lithium Blankets, Proceedings of B. N. E. S. Nuclear Fusion Conference, Culham (1969) Paper 5.3.

64. R. W. Werner, Module Approach to Blanket Design-A Vacuum Wall Free Blanket Using Heat Pipes, Proceedings of B. N. E. S. Conference, Culham (1969) Paper 6.2.

65. G. R. Hopkins and G. Melese-d' Hospital, Direct Helium Cooling Cycle for a Fusion Reactor, Proceedings of B. N. E. S. Nuclear Fusion Reactor Conference, Culham (1969) Paper 6.1.

66. R. W. Werner, B. Meyers, P. B. Mohr, J. D. Lee, and N. C. Christofilos, Preliminary Design Consideration for an Astron Power Reactor System, Proceedings of B. N. E. S. Nuclear Fusion Reactor Conference, Culham (1969) Paper 5.2.

67. E. F. Johnson, Overall Tritium Balances in Fusion Reactors, Proceedings of B. N. E. S. Nuclear Fusion Reactor Conference, Culham (1069) Paper 5.1.

68. A. P. Fraas, Conceptual Design of a Fusion Power Plant to Meet the Total Energy Requirements of an Urban Complex, Proceedings of B. N. E. S. Nuclear Fusion Reactor Conference, Culham (1969) 1.

69. D. Steiner, The Nuclear Performance of Fusion Reactor Blankets, Nuclear App. and Tech. 9, 83 (1970).

70. A. P. Fraas and H. Postma, Preliminary Appraisal of the Hazards Problems of a D-T Fusion Reactor Power Plant, ORNL-TM-2822 (Revised) (1970).

71. A. P. Fraas, Conceptual Design of the Blanket and Shield Region of a Full-Scale Fusion Reactor, ORNL-TM-3096 (1970).

72. D. Steiner, "The Neutron-Induced Activity and Decay Power of the Niobium Structure of a D-T Fusion Reactor Blanket, ORNL-TM-3094 (1970).

73. Proceedings of IAEA Fourth Conference on Plasma Physics and Controlled Nuclear Fusion Research, Madison, Wisconsin (June 1971).

74. Reference 42 above.

75. H. Borgwaldt, W. H. Kohler, and K. E. Schroeter, Neutronic Thermal Design Aspects of Thermonuclear Fusion Reactor Blankets, Reference (27), Paper CN-28/K-12 (Revised).

76. D. Steiner, Emergency Cooling and Radioactive Waste-Disposal Requirements for Fusion Reactors, Reference (27), Paper CN-28/K-11.

77. Th. Bohn, and S. Forster, Blanket Cooling Concepts and Heat Conversion Cycles for Controlled Thermonuclear Reactors Reference (27), Paper CN-28/K-13.

78. A. P. Fraas, A Diffusion Process For Removing Tritium From The Blanket of A Thermonuclear Reactor, ORNL-TM-2358 (1968).

79. M. A. Abdou and C. W. Maynard, "Computational Techniques for Fusion Reactor Neutronics and Photonics," University of Wisconsin Fusion Design Memo 3 (1971).

80. M. A. Abdou, A Revised Manual For ANISN-1108 University of Wisconsin Report PLP-429.

81. W. E. Ford III, ORNL (private communication).

82. D. J. Dudziak, R. E. Seamon, and D. V. Susca "LAPHANO: A P Multigroup Photon-Production Matrix and Source Code for ENDF," LA-4750-MS (ENDF-156) (January 1972).

83. W. E. Ford III, "POPOP4: A Code for Converting Gamma-Ray Spectra to Secondary Gamma-Ray Production Cross Sections," USAEC report CTC-12 (May 1969).

84. W. E. Ford III, "POPOP4 Library of Neutron-Induced Secondary Gamma-Ray Yield and Cross Section Data," USAEC Report CTC-42.

85. J. D. Jenkins, "RICE: A Program To Calculate Primary Recoil Atom Spectra from ENDF/B Data," ORNL-TM-2706 (February 1970).

86. W. F. Sheely, "Correlation of Radiation Damage to Steel with Neutron Spectrum," Nucl. Sci. Eng., 29, 165 (1967).

87. R. E. Dahl and H. H. Yoskikawa, "Neutron Exposure Correlation for Radiation Damage Studies," Nucl. Sci. Eng., 21, 312 (1965).

88. D. G. Doran, "Neutron Displacement Cross Sections for Stainless Steel and Tantalum Based on a Linhard Model," Nucl. Sci. Eng. 49, 130 (1972).

89. S. Blow, "The Effect of the Neutron Energy Spectrum on Neutron Displacement Damage in Niobium," J. Phys. D: Appl. Phys., 1971, Vol. 4.

90. D. G. Martin, "Radiation Damage Effects in the Containment Vessel of a Thermonuclear Reactor," United Kingdom Atomic Energy Authority Report CLM-R 103 (March 1970).

91. Doran, Kulcinski, and Abdou, "Gaseous Products and Transmutation Effects in CTR Materials," University of Wisconsin Fusion Design Memo (February 1973).

92. D. K. Sze and W. E. Stewart, "Lithium Cooling for a Low-β Tokamak Reactor," Proc. Texas Symp. Technology of Controlled Thermonuclear Fusion Experiments and the Engineering Aspects of Fusion Reactors (November 1972).

93. M. A. Hoffman, and G. A. Carlson, "Calculation Techniques for Estimating the Pressure Losses For Conducting Fluid Flows in Magnetic Fields," Lawrence Radiation Laboratory, TID-4500, UC-20.

94. S. J. Leverette, "An Investigation of The Temperature Distribution in the Lithium Blanket of a Fusion Reactor," ORNL-TM-3701 (1973).

95. M. A. Abdou et al., "Preliminary Conceptual Design of a Tokamak Reactor," Proc. Texas Symp. Technology of Controlled Thermonuclear Fusion Experiments and the Engineering Aspects of Fusion Reactors (November 1972).

96. M. V. Davis, "Selected Properties of Materials with Application to CTR Design," ANL/CTR-72-01 (Revised December 1972).

97. W. F. Vogelsang, University of Wisconsin Fusion Design Group, (private communication).

98. D. J. Dudziak, "A Technical Note on D-T Fusion Reactor After-heat," Nuclear Technology 10, 391 (March 1971).

99. A. P. Fraas, "Conceptual Design of the Blanket and Shield Region of a Full Scale Toroidal Fusion Reactor," to be published (1973).

100. "An Assessment of Fusion Power," Wash-1239.

101. W. F. Vogelsang, "Breeding Ratio, Inventory, and Doubling Time in a D-T Reactor," Trans. Am. Nucl. Soc., 14, 33 (1972).

102. J. R. Weir, J. O. Stiegler, and E. E. Bloom, "Irradiation Behavior of Cladding and Structural Materials," USAEC Report ORNL-TM-2258 (September 1968).

103. "Proceedings of The Conference on Continuum Aspects of Graphite Design," Catlinburg, Tennessee, CONF-701105 (November 1970).

104. R. W. Boom and Phillip A. Sanger (private communication), University of Wisconsin Fusion Design Group.

105. W. C. Young and R. W. Boom, "Materials and Cost Analysis of Constant-Tension Magnet Windings For Tokamak Reactors," 4th International Conference, Brookhaven (September 1972).

106. M. S. Lubell et al., "Economics of Large Superconducting Toroidal Magnets For Fusion Reactors," ORNL-TM-3927 (1972) and I. E. E. E. Conf. Record, I. E. E. E. Cat. No. 72 CHO 682-5 TABSC.

107. R. Harrington and R. Giberson, "Chemical and Physical Changes in Gamma-Irradiated Plastics," Mod. Plastics (1958).

108. Proceedings of the 1968 Summer Study on Superconducting Devices and Accelerators, Brookhaven National Laboratory (June 10 - July 19, 1968).

109. H. Brechna, "Effect of Nuclear Radiation on Organic Materials; Specifically Magnet Insulations in High-Energy Accelerators," SLAC-40; also UC-28 (March 1965).

110. T. W. Evans, "The Effects of Irradiation on Boron Carbide," BNWL-679 (February 1968).

111. W. M. Mueller, et al "Metal Hydrides," Academic Press (1968).

112. T. R. England, "An Investigation of Fission Product Behavior and Decay Heating in Nuclear Reactors," Ph.D. Thesis, Univ. of Wisconsin (August 1969).

113. H. K. Forsen and D. G. McAlees, "Neutron Wall Current and Energy Considerations for Alternate Fusion Fuel Cycles," UW - FDM - 9 (February 1972).

Notes For Appendices

In this thesis reference was made to the following appendices:

Appendix A: A User's Manual For MACK

Appendix B: Resonance Region Treatment

Appendix C: Average β-particle Kinetic Energy

Appendix D: Response Library

Because of the size of these appendices, their utility as an integral part of this thesis was questionable. Therefore, the appendices are eliminated and their contents will be published in separate reports. The contents of appendices A, B, and C can be found in the following document: M. A. Abdou et al, "MACK: A computer Program To Calculate Neutron Energy Release Parameters and Multigroup Neutron Reaction Cross Sections From Nuclear Data in ENDF Format," ORNL - TM - 3994, Oak Ridge National Laboratory (July 1973). The material of appendix D will be published as a University of Wisconsin Fusion Design Memo.